Studies on Single Wall Carbon Nanotubes and Polymer
Composite Films and Fibers

A Thesis
Presented to
The Academic Faculty

By

Xiefei Zhang

In Partial Fulfillment
of the Requirements for the Degree
Doctor of Philosophy in the
School of Polymer, Textile and Engineering

Georgia Institute of Technology
August 2004

Studies on Single Wall Carbon Nanotubes and Polymer
Composite Films and Fibers

Approved by:

Dr. Satish Kumar, Advisor

Dr. Anselm Griffin

Dr. David M. Collard

Dr. Hamid Garmestani

Dr. Peter J. Ludovice

Dr. Samuel Graham

August 9, 2004

ACKNOWLEDGMENTS

This work could have not been finished without the support and sacrifice of many people I had met over the last couple of years. They are the group of intelligent and nice people I would like to be with in my lifetime.

To begin, I would like to thank deeply my advisor Dr. Satish Kumar for his help and insight resolving many of the problems encountered throughout this work. Dr. Kumar has advised and mentored me right from my start at Georgia Tech. He has given me the freedom to work on problems and approaches of most interest to me. He has been a great source of ideas, invaluable feedback, and endless support and encouragement through all stages of my Ph.D. program.

Secondly, I wish to thank the members of the reading committee, Dr. Anselm Griffin, Dr. David Collard, Dr. Hamid Garmestani, Dr. Pete Ludovice, and Dr. Sam Graham for their part in guiding this research. Also, I wish to appreciate the help from Dr. Tao Liu, Dr. Veedu Sreekumar, Dr. Young-Bin Park and all the other members of our research group for their help during this work.

Finally, I would like to express appreciation to my family for their long-standing support and patience in the completion of this work.

TABLE OF CONTENTS

LIST OF TABLES

LIST OF FIGURES

ix

SUMMARY

Single wall carbon nanotubes (SWNT) have been extensively studied over the last decade due to their excellent comprehensive properties for a variety of applications. The novel 1-D nanometer size with high tensile strength and modulus makes SWNTs a good candidate for producing reinforced composite with various matrices. The superior thermal conductivity and relatively high electrical conductivity of SWNTs embeds thermal and electric transport abilities into these composites. Due to the unique electronic properties, nanometer size electronic devices, such as field effect transistor, light emission devices, etc. are realizable. Furthermore, SWNTs can find applications in energy storage devices, for nanostructure templates, as well as for nanosize probes and sensors.

This study is focused on the applications of SWNTs as reinforcement for polymer matrices. Due to van der Waal interactions, SWNTs form bundles of about 30 nm diameters. In order to take full advantage of the SWNT mechanical properties, SWNT must exfoliate or at least disperse in small diameter bundle sizes. Optical microscopy and SEM only give qualitative information of dispersion. Quantitative characterization through TEM or AFM can be time consuming in order to get statistical result. In this study, simple method is developed to quantitatively estimate the size of SWNT bundle in dispersion based on the geometry controlled electrical percolation behavior.

Poly (vinyl alcohol) (PVA) composite films incorporated with well dispersed, poly (vinyl pyrrolidone) (PVP) and sodium dodecyl sulfate (SDS) covered single wall carbon nanotubes (SWNT) exhibit significant improvement in tensile strength and modulus as compared to the control PVA and PVA/PVP/SDS films. The evidence of load transfer to the nanotubes in the composite film has been obtained from the shift in the Raman SWNT D* band peak position.

Single wall carbon nanotubes (SWNT), polyvinyl alcohol (PVA), dimethyl sulfoxide (DMSO) and H_2O homogeneous dispersion has been prepared using stirring and sonication. This dispersion was extruded into fiber via gel spinning. The mechanical performance of PVA / SWNT (3wt%) composite fiber was superior to that of the control PVA gel-spun fiber. The tensile strength of composite fiber increased by 22% compared to the control PVA gel-spun fiber from 0.9 GPa to 1.1 GPa. Also, the Young's modulus increased by 40% from 25.6 GPa to 35.8 GPa. Dynamic mechanical properties and X-ray diffraction studies suggest that the SWNT influenced the properties of both amorphous as well as crystal regions of PVA in the composite fiber.

Single wall carbon nanotube films (*bucky paper)* have been prepared using aqueous dispersions containing 0, 3, 6, and 10 molar nitric acid. With increasing nitric acid concentration, film tensile strength increased from 10 MPa to 74 MPa, tensile modulus from 0.8 GPa to 5.0 GPa, while in plane dc electrical conductivity decreased from 3×10^4 S/m to 1.2×10^4 S/m. In plane storage modulus exhibited no decrease in the measured temperature range (room temperature to 200 °C). Raman spectroscopy shows that nitric acid treatment results in the loss of the small diameter tubes. This is consistent with the X-ray diffraction observation, which shows that with increasing nitric

acid concentration, (10) and (11) SWNT d-spacings increased from 1.23 nm to 1.29 nm and from 0.74 to 0.87 nm, respectively. Morphological changes in the film have been monitored using scanning electron microscopy.

CHAPTER 1

INTRODUCTION

1.1 SWNT History

Significant discussion on nanostructured materials is currently centered around carbon nanotubes (both the multi wall and single wall carbon nanotubes). Carbon is the only element in the periodic table that has isomers from 0 dimension (0D) to 3 dimension (3D). The history of synthetic 2D carbon materials began in the 19th century and the man-made 3D carbon materials (diamond) first emerged in the middle of the 20th century. A new era in carbon materials began with the discovery of buckminsterfullerenes ("buckyballs")[1] in 1985. 1D carbon materials (carbon nanotubes) multi wall carbon nanotubes (MWNT) in 1991[2] and single wall carbon nanotubes (SWNT) in 1993[3, 4] were discovered by Iijima. The history of carbon related materials is listed in Table 1.1. The discovery of these structures ignited world wide research boom that still seems to be growing. Actually, carbon tubes with graphite layer structure have been made decades before Iijima's discovery, but these structures were not recognized as nanotubes.[5]

Numerous investigators have reported remarkable physical and mechanical properties for this new form of carbon, carbon nanotubes. Unique electronic properties, higher thermal conductivity than diamond as well as superior mechanical properties of carbon nanotubes offer tremendous opportunities for the development of

fundamentally new material systems. In particular, the excellent mechanical properties of carbon nanotubes, combined with their low density, offer an opportunity for the development of nanotube-reinforced composite materials. Due to their tiny tip size, carbon nanotubes have been successfully used as scanning probe microscope tips[6]. Also, due to their ability to absorb hydrogen as well as metals, they have potential application for fuel cell.[7]

Table 1.1 Chronicle of discovery of carbon nanotubes[8]

Year	Event	Comments
1960	Production of carbon tubes with graphite layer structure	Arc discharge, 5 μm in diameter Bacon[5]
1970	The C_{60} molecule is suggested[9]	
1985	Discovery of C_{60}[10]	C_{60} is detected in mass spectrum
1990	Fullerene synthesis in large quantities	
1991	Discovery of MWNT[2]	DC arcing of graphite
1993	Discovery of SWNT[3]	Arc process in the presence of Fe
1996	Ropes of SWNT[28]	Large-scale production of SWNT by laser ablation

There are two main types of carbon nanotubes that can have high structural perfection. Single wall carbon nanotubes (SWNTs) consist of a single graphite sheet seamlessly wrapped into a cylindrical tube. Multi wall carbon nanotubes (MWNTs) comprise an array of such nanotubes that are concentrically nested like rings of a tree trunk. Due to the superior mechanical, unique electronic and thermal properties as

well as the smaller size and larger surface area of SWNTs compared to MWNTs, our research interests are focused on SWNTs. So, in the following section, the structure, production, properties and the applications of SWNTs will be addressed in detail.

1.2 SWNT Structure

Carbon based materials are found in a variety of forms, for example, graphite, diamond, carbon fiber, carbon tube, etc. Hybridization of carbon atomic orbital relate to many possible configurations of the electronic states. Each carbon atom has six electrons, which occupy $1s^2$, $2s^2$, and $2p^2$ atomic orbital. The core electrons take the $1s^2$ orbital and they are strongly bonded. The other four valence electrons are weakly bonded. These four valence electrons can readily mix with each other due to the small energy difference of upper 2p and lower 2s energy levels. This process is called hybridization. In carbon, three possible hybridizations are possible: sp, sp^2 and sp^3. The hybridization determines the chemical, physical, and configurationally properties of carbon materials. sp hybridization is observed in acetylene like materials, sp^2 hybridization is observed in ethylene, while sp^3 hybridization is seen in methane like structure. The hybridization and other physical parameters of carbon atom in different dimensional carbon materials are listed in Table 1.2.

The single wall carbon nanotubes can be described as rolling up a graphite sheet in to a one dimensional cylindrical shape. Normally, the diameter of SWNT is in the range of 0.4 to 3 nm, the length is in the range of several hundred nanometers to several microns. The diameter and chirality as well as other physical properties are closely related to the single vector called chiral vector. In order to understand

structure and structure-related properties of SWNT, several parameters are defined on

the un-rolled graphite sheet, as shown in Figure 1.1.

Table 1.2 Parameters of carbon atom in various carbon materials[11]

Dimension	0-D	1-D	2-D	3-D
	C_{60}	Carbon nanotube	Graphite	Diamond
Hybridization	sp^2	sp^2	sp^2 (sp)	sp^3
Density (g/cm^3)	1.72	1.2 – 2.0	2.26	3.515
Bond length (Å)	1.4	1.44	1.42	1.54
Electronic properties	Semiconductor E_g = 1.9 eV	Metal or semiconductor	Semi-metal	Insulator E_g = 5.47 eV
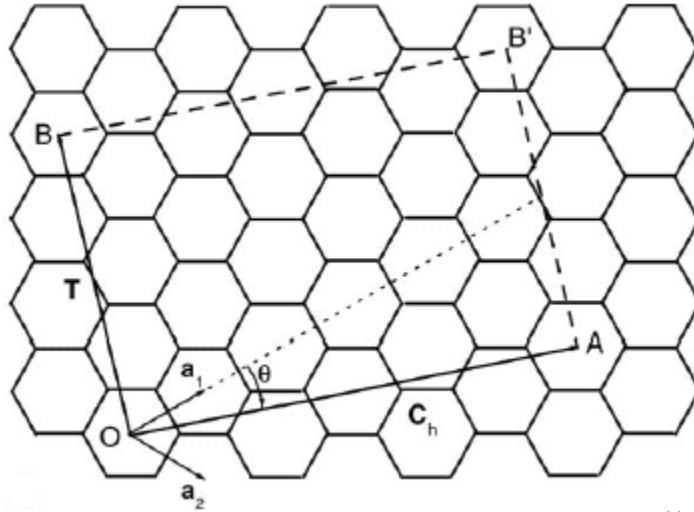
Figure 1.1 The unrolled honeycomb SWNT lattice.[11]

The structure of single wall carbon nanotube is specified by the chiral vector OA, C_h. In Figure 1.1 OB is the direction of nanotube axis and the OA direction corresponds to the nanotubes equator. The a_1 and a_2 in the figure are unit vectors, which are composed of the chiral vector, $C_h = na_1 + ma_2$ ($0 < m < n$). Here n and m are integers. The θ is the angle between chiral vector and one unit vector, which is defined as chiral angle, and is always smaller that 30°. During the formation of SWNT, the graphite sheet rolls up along the chiral vector C_h. The physical parameters related to the SWNT are listed in Table 1.3. Based on the difference between n and m values in the chiral vector, the electronic properties of SWNT can be predicted. If n - m is an integer multiple of three, then the SWNT is metallic tube. Otherwise tube is semiconducting. Also based on the n and m, we can geometrically define three types of SWNT. If n equals to m, then we call it an armchair tube; if m equals to zero, then we call it a zig-zag tube; otherwise, we call the tube a chiral tube (as shown in Figure 1.2). Armchair tube is always a metallic, zig-zag and chiral tubes can be metallic or semiconducting.
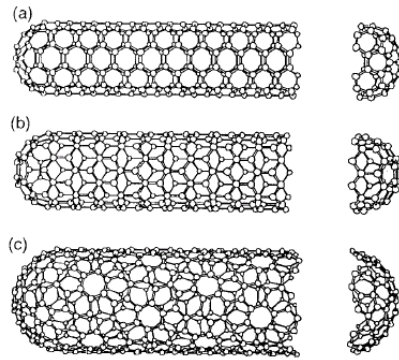
Figure 1.2 Schematic representation of different conformations of SWNT: a) armchair conformation, b) zig-zag configuration, and c) chiral configuration.[11]

Table 1.3 Structural parameters of single wall carbon nanotube[12]

Symbol	Name	Formula	Value
a_{C-C}	carbon-carbon distance		1.421 Å (graphite)
a	length of unit vector	$\sqrt{3}a_{C-C}$	2.46 Å
$\mathbf{a}_1, \mathbf{a}_2$	unit vectors	$\left(\frac{\sqrt{3}}{2}, \frac{1}{2}\right)a, \left(\frac{\sqrt{3}}{2}, -\frac{1}{2}\right)a$	in (x,y) coordinates
$\mathbf{b}_1, \mathbf{b}_2$	reciprocal lattice vectors	$\left(\frac{1}{\sqrt{3}}, 1\right)\frac{2\pi}{a}, \left(\frac{1}{\sqrt{3}}, -1\right)\frac{2\pi}{a}$	in (x,y) coordinates
$\mathbf{C}_h$	chiral vector	$\mathbf{C}_h = n\mathbf{a}_1 + m\mathbf{a}_2 \equiv (n,m)$	n,m: integers
L	circumference of nanotube	$L = |\mathbf{C}_h| = a\sqrt{n^2 + m^2 + nm}$	$0 \leq |m| \leq n$
d_t	diameter of nanotube	$d_t = \dfrac{L}{\pi} = \dfrac{\sqrt{n^2 + m^2 + nm}}{\pi}a$	
θ	chiral angle	$\sin\theta = \dfrac{\sqrt{3}m}{2\sqrt{n^2 + m^2 + nm}}$	$0 \leq |\theta| \leq 30°$
		$\cos\theta = \dfrac{2n + m}{2\sqrt{n^2 + m^2 + nm}}$	
		$\tan\theta = \dfrac{\sqrt{3}m}{2n + m}$	
d	the highest common divisor of (n,m)		
d_R	the highest common divisor of $(2n + m, 2m + n)$	$d_R = \begin{cases} d & \text{if } n - m \text{ not a multiple of } 3d \\ 3d & \text{if } n - m \text{ a multiple of } 3d. \end{cases}$	
$\mathbf{T}$	translational vector of 1D unit cell	$\mathbf{T} = t_1\mathbf{a}_1 + t_2\mathbf{a}_2 \equiv (t_1, t_2)$	t_1, t_2: integers
		$t_1 = \dfrac{2m + n}{d_R}$	
		$t_2 = -\dfrac{2n + m}{d_R}$	
T	length of $\mathbf{T}$	$T = \dfrac{\sqrt{3}L}{d_R}$	
N	number of hexagons per 1D unit cell	$N = \dfrac{2(n^2 + m^2 + nm)}{d_R}$	$2N \equiv n_C/\text{unit cell}$

1.3 SWNT Production

SWNTs are mainly produced by carbon arc discharge, laser ablation of carbon, or chemical vapor deposition (typically on catalytic particles), although there are several other methods to produce nanotubes. The resulting SWNT diameters range from 0.4 to 3 nm.

In the arc discharge method (Figure 1.3 a), electric arc discharge is generated between two graphite electrodes under an inert atmosphere (helium or argon). The high temperature between the two rods during the process allows the sublimation of carbon. In 1993, Iijima reported the arc discharge and catalyst-assisted synthesis of SWNTs. He used arc-discharge chamber filled with a gas mixture of methane and argon. Two vertical thin electrodes were installed in the center of the chamber. The lower electrode, the cathode, had a shallow dip to hold a small piece of iron during the evaporation. DC current between the electrodes generated the arc-discharge. The three components—argon, iron and methane, were critical for the synthesis of SWNTs. The TEM analysis of the obtained specimens revealed the presence of SWNT threads, which were curved and tangled together to form bundles. These nanotubes had diameters in the range of 0.7 to 1.65 nm.

The second technique for producing carbon nanotubes is the laser ablation method (Figure 1.3 b). Graphite target is vaporized by laser irradiation under flowing inert atmosphere. The laser vaporization produces carbon species, which are swept by the flowing gas from the high-temperature zone to a conical water-cooled copper collector. [13] When a small amount of transition metal such as Ni and Co has been added to the carbon target, SWNTs can form. These SWNTs are remarkably uniform in diameter and they form bundles of 5 – 20 nm diameter. These bundles form a two dimensional triangular lattice.

Although the chemical vapor deposition (CVD) method had been used to produce carbon filament and fiber since the 1960s, it had not been applied to make carbon nanotubes until 1993 (Figure 1.3 c).[14] High-quality SWNTs can grow on

silicon wafers patterned with micrometer scale islands of catalytic material by the CVD technique. Methane is the carbon source. High reaction temperature in the range of 850–1000 °C is necessary to form small diameter SWNTs. The optimal choice of a catalyst is a Fe/Mo species.[15] Currently, the SWNT that many researchers depend on is the high pressure carbon monoxide (HiPco) nanotubes from Carbon Nanotechnology (CNI).
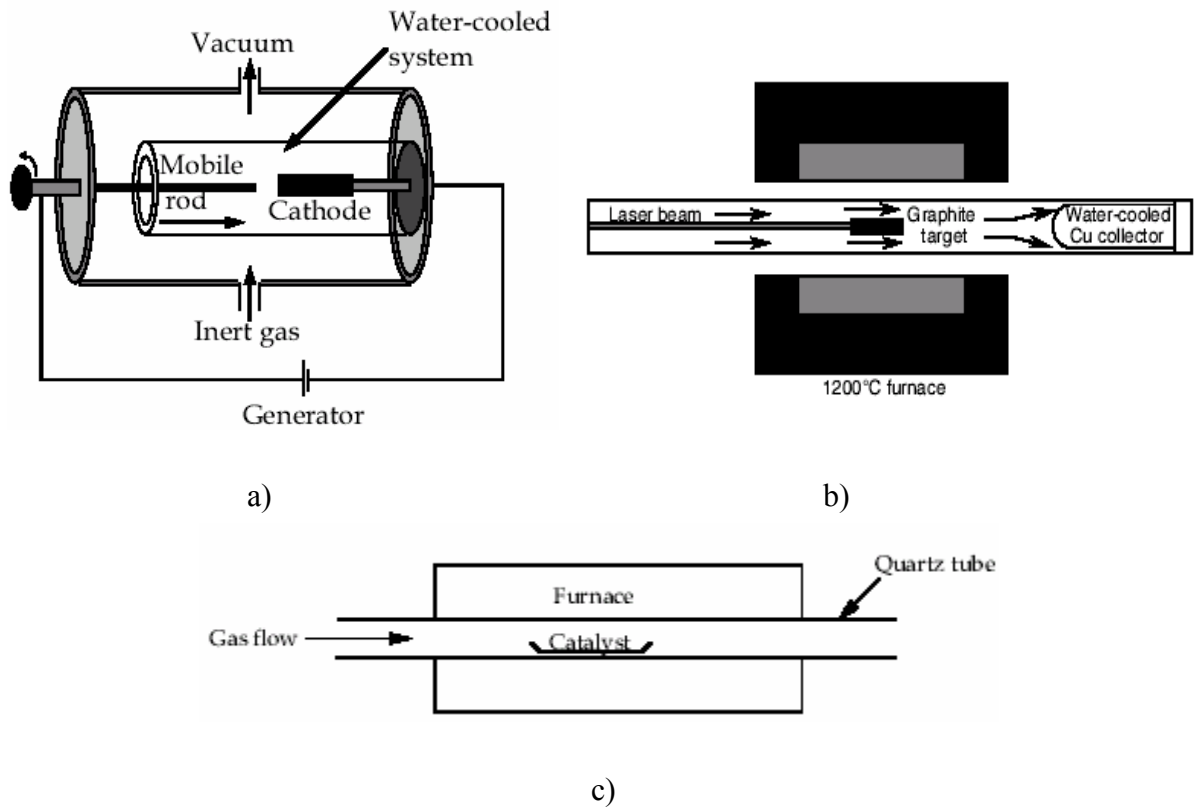
Figure 1.3 Representative schematics of SWNTs production methods a) electric arc discharge, b) laser ablation, c) chemical vapor deposition.[16]

Beside the methods mentioned above, solar energy[17], electrolysis[18] and low-temperature solid pyrolysis[19] can be used to produce carbon nanotubes. The

representative instrument set-ups of different SWNT production methods are shown in the Figure 1.3. Also the technical details of SWNTs made from different methods are listed in Table 1.4.

Table 1.4 The technical details of different SWNT synthesis methods[20]

Method of Synthesis	Catalyst	T (K)	Type of Carbon Deposition	Diameter (Å)
Arc discharge	Ni, NiO	> 2273	SWNT	10 – 16
Arc discharge	La2O3	> 2273	SWNT	18 - 21
Arc discharge	Ni/Y	> 2273	SWNT	12 - 17
Arc discharge	YC2	> 2273	SWNT	11 - 17
Laser ablation	Ph/Pd	> 2273	SWNT	6.8 – 14.3
CVD	Fe	1373- 1473	SWNT	16.9
Laser ablation	Ni/Co	1473	SWNT	13.8 – 20
CVD	Mo/Al2O3	1473	SWNT	10 - 50

1.4 SWNT Purification

Whichever method is used for synthesis, the nanotube samples obtained generally contain large amount of impurities. For example, in the single wall carbon nanotubes samples, catalyst particles as well as amorphous carbon are main impurities. Most applications require the removal of impurities prior to further processing.

In order to remove the amorphous carbon and the catalyst particles, nitric acid oxidation routine has been adopted by many researchers.[21, 22, 23] The acid-treated SWNTs and ropes of SWNTs are covered by decomposition products. Due to the presence of carboxylic acid groups, the debris can be washed away with a basic aqueous solution, leaving in many cases 25%−50% of the starting material. Higher purity can be achieved by an additional filtration step. The final purity of SWNT achieved after such purification process is above 90%. Method of oxidation through nitric acid has the advantage that metal particles and amorphous carbon are almost completely removed. Moreover, it is cheap and capable of purifying large quantities of material. However, there are several studies showing that the SWNTs are at least partially attacked during the acid treatment. The material loss during oxidation is larger than the content of impurities, which implies that some SWNTs are destroyed. Raman investigation on nitric acid oxidized SWNT confirms the damage of the tube.[24] Although nitric-acid-treated samples might also contain intact SWNTs, the extent of chemical modification in oxidized samples should be carefully evaluated in future experiments. Vacuum annealing at 1200 °C is suggested to heal the defects. Beside the nitric acid treatment, hydrogen chloride acid is also used to wash away the metal particle as well as the amorphous carbon.[25]

It is also possible to purify SWNTs by centrifugation assisted by surfactant or similar materials. SWNT content of the sample is raised 40%−70% after multiple centrifugations as assisted by benzalkonium chloride.[26] Also, SWNT can be purified by a single centrifugation step for 30 min of tube and SDS dispersion prepared by

sonication and agitation. Most of the material is collected in the sediment, but very pure tubes remain in low concentration in the supernatant.

Chromatography has also been successfully used to purify SWNT samples.[27] Furthermore, the nanotubes in different fractions show different size distribution. It can be individual tubes or tube bundles, and shows that chromatography supplies well-separated SWNTs. So, in this way highly pure and length-selected SWNTs in aqueous suspension are obtained as observed by AFM.

1.5 SWNT Dispersion

SWNTs have a strong tendency to orient parallel to each other forming bundles due to van der Waals interaction. The SWNTs arrange themselves in a hexagonal structure within the bundle.[28] The binding energy is about 900 meV/nm.[29] They typically exist as ropes or bundles 20-35 nm in diameter and a few micrometers long; the SWNT ropes are entangled together in the solid state to form a complex network structure. These factors, coupled with the fact that these pseudo-1D graphitic cylinders do not have any surface functional groups, make them very difficult to disperse in any media.[30] In addition, they tend to have properties distinctly inferior to those of individual nanotubes. Therefore, in most areas of research, it would be beneficial to have dispersed individual nanotubes, or at least have some control over the bundle size. This is the case not only for fundamental studies where individual SWNTs are essential but for more applied studies such as composites. For example, the electrical percolation threshold will decrease in case of small bundle size as

compared to larger ones. Also, small size bundle will provide large bonding surface area in case of mechanical reinforcement of matrix by SWNT.

SWNT dispersibility using both non-covalent and covalent approaches is an active area of research. Sonication and shear mixing are used in many cases to produce well-dispersed SWNTs. Dispersion is also assisted by surfactant, polymer or by in situ polymerization in various solvent or matrix. Enhanced dispersion in solvent or matrix based on the chemical modification of SWNT can be considered a destructive approach, as it deteriorates the intrinsic properties of SWNT to a certain extent.

Sonication, either probe or bath sonicator, has been used to assist carbon nanotube dispersion since their discovery and is still widely used in current research. However, there is an inherent problem using this technique, as it introduces considerable amount of defects, including buckling, bending, and dislocations in the carbon structures. Prolonged sonication increases the disorder, ultimately leading to the formation of amorphous carbon.[31]

A series of anionic, cationic, and nonionic surfactants and polymers have been studied by Moore et al[32] for their ability to suspend individual single wall carbon nanotubes. The size of the hydrophilic group of nonionic surfactant or polymer is claimed to be the major factor for suspending nanotubes. With higher molecular weights, more SWNT suspension is realized because of enhanced steric stabilization with longer polymeric groups. The SWNT dispersion mechanism has been studied in detail in the sodium dodecylbenzenesulfonate (NaDDBS) and water system. SWNT purification can affect their surface properties. Thus, carbon nanotubes can exhibit

either negative or positive charges on the surface, depending on the pH of the surrounding media. Analysis of the adsorption isotherms of the anionic surfactant on SWNT indicates that the interactions between the surfactant molecules and the nanotube walls are mostly hydrophobic in nature. Only at pH values far from the point of zero charge the Coulombic interaction between the negatively charged head groups of the surfactant and the charged surface of the nanotubes becomes important. The adsorption studies also revealed that each SWNT is covered by a monolayer of surfactant at saturation, in which the molecules rest with the tails oriented vertically on the surface. Therefore, adsorbed surfactant is believed responsible for the effective suspension of the SWNT. The author also drew the conclusion that the formation of micelles in solution is not a requirement for SWNT suspendability. [33]

Transmission electron microscope study shows that SDS is absorbed on the SWNT surface in an extremely ordered manner.[34] Molecular dynamics simulation result suggests that several tens of nanometers thick layer of surfactant can be wrapped around the SWNTs.

Chemical modification can enhance SWNT solubility and dispersibility in various polymer matrices. An H_2SO_4/HNO_3 mixture has been used to chemically modify SWNT. Carboxylic acid and quinone groups were reported at the end ports and defect ports[35]. Carboxyl acid groups were further converted into acyl chloride groups by treatment with thionylchloride. Subsequently, the acylchloride reacted with alkyl-aryl amine, 4-dodecyl-aniline, to give long alkyl tail modified SWNT[36]. Such chemical modification would help SWNT dissolve in common solvents, such as THF, CH_2Cl_2 and CS_2. SWNT can also be first treated with concentrated HCl solution, then

refluxed in thionyl chloride for 24h to convert carboxylic acids to acyl chloride. Lipophilic and hydrophilic dendra, which were terminated with alkyl chains and oligometric PEG (poly (ethylene glycol)), reacted with oxidized SWNT via esterification or amidation. The lipophilic dendron-functionalized SWNT were soluble in hydrocarbon and weakly polar organic solvents, while PEG oligomer functionalized SWNT were soluble in both organic solvents and water.[37] Highly purified single-wall carbon nanotubes can be fluorinated to form "fluorotubes", which are then solvated as individual tubes in various alcohol solvents via ultrasonication.[38] Functionization of SWNT by attaching certain aliphatic or aromatic chain can also improve the dispersion quality in the polymer matrix. Functionalization of the SWNTs was obtained by using an optimized H_2SO_4/70% HNO_3 acid treatment and subsequent fluorination. Epoxy composites containing 1 wt % nanotubes are processed by dissolving the functionalized SWNTs in dimethylformamide and mixing with the epoxy resin thereafter. The functionalized nanotubes were observed to be highly dispersed and well integrated in the epoxy composites.[39]

Enhanced SWNT dispersion can also obtain through in situ polymerization.[40] For example, a solution of 0.325 M aniline dissolved SWNTs in 1 M HCl is stirred at 0–5 °C and then an equal volume of precooled (5 °C) oxidant solution containing 0.125 M ammonium persulfate in 1 M HCl is slowly added dropwise to the well-stirred solution; the mixture was further polymerized for 2 h at 0–5 °C under constant stirring. The SWNT/PANI composite was obtained by filtering and rinsing the reaction mixtures with deionised water followed by drying under vacuum at 80°C for 24 hrs. Interestingly, experiment indicates that SWNTs can be well dispersed in most

solvents such as acetone, THF, DMF, etc., after refluxing in aniline. It was believed that the SWNTs had been completely peeled off and presented as individual tubes or thin bundles. Uniform, well-dispersed single wall carbon nanotube (SWNT)/polyaniline (PANI) composite films Have been prepared by electrochemical polymerization of aniline containing well-dissolved SWNTs.[41] A homogeneous polyimide/SWNT composite has been obtained with low conductive percolation level and enhanced mechanical performance through the in situ polymerizing monomers in the presence of SWNT.[42] The same phenomenon has been observed in case of PMMA/SWNT.[43]

For the reinforcement of polymer/SWNT composite, obviously surfactant is not the best choice, as the surfactant is difficult to be removed. The surfactant molecules left in the composite may deteriorate the reinforcing effect of SWNT. Therefore, polymer assisted dispersion of SWNT would be the ideal option. Indeed, several research groups have reported that the polymer can increase the dispersion quality of SWNT. Smalley group indicates that PVP can wrap around the SWNT rendering SWNTs soluble in aqueous solvent. (Figure 1.4)[44] This PmVP wrapped SWNT can be dissolved in organic solvents. Synthesized hyperbranched polymer, which exhibits an appropriate degree of branching, is found to be more efficient at breaking nanotube bundles than 'mother PmVP'. Introducing a certain degree of branching into the PmVP polymer makes it more rigid and less efficient for wrapping bundles of SWNTs. However, the pockets provided by the hyperbranched polymer offer a better fit for the SWNTs. The outcome is that more single strands of SWNTs
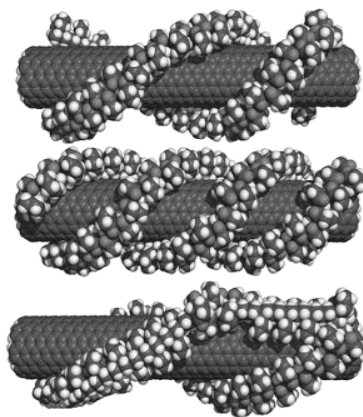
Figure 1.4 PVP wrapped SWNTs.[44]

are observed when branch PmPV is used.[45] Natural polymers[46] such as arabic gum and starch[47] are also helpful in dispersing SWNT in aqueous media. It is found that in the PMMA/SWNT composite films, the distance between the nanotubes in bundles increases because of the intercalation of the polymer.[48]

1.6 SWNT Mechanical Properties

The mechanical behavior of carbon nanotubes is exciting since nanotubes are seen as the "ultimate" carbon fiber ever made. The traditional carbon fibers have about ten times the specific strength (strength/density) of steel and are excellent load-bearing reinforcements in composites. Carbon fibers have been used as reinforcements in high strength, light weight, high performance composites; one can typically find these in a range of products from tennis rackets to spacecraft. Single wall carbon nanotube has even higher tensile strength and Young's modulus than most carbon fibers. Nanotubes should then be ideal candidates for structural applications. Since carbon–carbon covalent bonds are one of the strongest in nature, a

structure based on a perfect arrangement of these bonds oriented along the axis of nanotubes would produce an exceedingly strong material. Significant researches have been done to predict the mechanical performance of individual or bundle of SWNTs.

There are two major categories of molecular simulation methods, which are classical molecular dynamics (MD) and ab initio methods, though tight-binding-based models have also been occasionally used. Ruoff et al.[49] have suggested the use of the elastic modulus of graphite by neglecting the change in the atomic structure when a piece of graphene sheet is rolled into a nanotube. Based on this assumption, the elastic modulus of SWNT is 1.06 TPa and tensile strength is around 20 GPa. Theoretical calculations reported by Krishnan et al. have estimated a wide range of elastic moduli of 0.5–5.5 TPa.[50] Using empirical lattice dynamics model, the Young's modulus and shear modulus of SWNT are predicted to be 1.0 and 0.45 TPa, respectively.[51] By using the ab initio method, Lier has predicted the elastic modulus of higher than 1 TPa.[52] Based on tight binding based model, non-orthogonal tight binding formalism, Goze estimated the Young's modulus of SWNT to be 1.22 TPa.[53] This value is in good agreement with previous studies. More importantly, the calculation predicts that there is little dependence of modulus on tube diameter, but it is noticeable only for the small diameter tube. Natsuki et al. used continuum shell model to predict the Young's modulus and shear modulus of SWNT.[54] In this model SWNT is regarded as discrete molecular structure linked by carbon-to-carbon bonds. The shear modulus was assumed to be half of the Young's modulus. This study predicts rapidly decreasing axial modulus with increase in nanotube diameter (Figure 1.5). Based on this model, the axial and the shear moduli were predicted in the range

17

of 0.61–0.48 TPa and 0.30– 0.27 TPa, respectively. An interesting finding in this study was that the moduli also depended on the SWNT wall thickness.
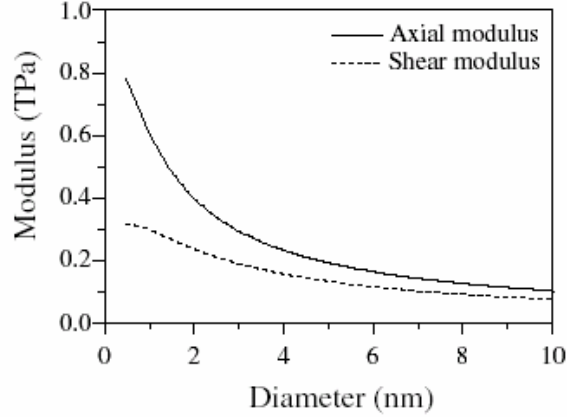
Figure 1.5 Variation of modulus with SWNT diameter.[54]

Although testing of SWNT is challenging and requires specially designed stages and nano-size loading devices, some smart experiments have provided valuable information on the mechanical behavior of SWNT, as well as its modulus and strength. Direct observation on individual single walled carbon nanotube's freestanding room-temperature vibrations in a transmission electron microscope has been used to estimate SWNT stiffness.[50] Twenty-seven nanotubes in the diameter range of 1.0–1.5 nm were measured to yield an average Young's modulus of 1.25 TPa. This value is higher than the currently accepted value of the in-plane modulus of graphite. The SWNTs in bulk always aggregate together, to form bundle of several tens of nanometers. Small size SWNT bundles are often used instead of individual SWNT due to difficulty in exfoliation. So, it is important to know the SWNT small bundle mechanical properties. Atomic Force Microscopy has been used to measure the mechanical properties of SWNT bundles of various diameters.[55] The small

diameter and long ropes elastic and shear modulus are estimated to be 1 TPa and 1 GPa respectively. AFM measurements thus confirm that SWNT ropes are high-modulus fibers but with an unexpectedly low shear modulus. This should be taken into account in the design of SWNT ropes-based composite materials. It would be particularly interesting to cross-link the nanotubes in a rope, for example, by irradiation or chemical methods, to increase the rigidity of suspended portions of the ropes, resulting in high lateral deflections. Applying the similar method, Yu et al[56] obtained the strength and modulus of this small SWNT bundle (15 SWNTs) of 30 GPa and 1 TPa, respectively. It was also found that the elongation to break or strain is about 5.3%. In this study, SWNTs on the perimeter of the bundle were reported to carry most of the load. Walters et al.[57] used AFM to obtain tensile strength of 45 GPa and strain of about 5.8 %. The representative AFM set up is shown in Figure 1.6 and SWNTs deflection is give by following equation.

$$\delta = \delta_B + \delta_S = FL^3/192EI + f_s FL/4GA \tag{1-1}$$
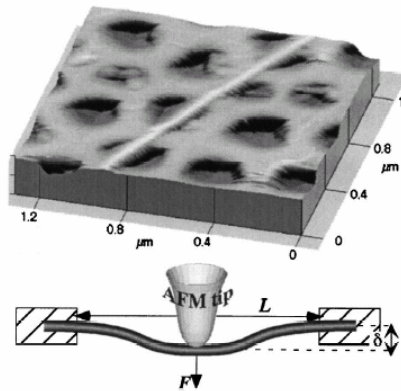
Figure1.6 AFM used for measuring the modulus of SWNT bundle.[57]

Where δ is the sum of the deflections due to bending, δ_B, and to shear, δ_S, L is the suspended length, E is the elastic modulus, f_s is the shape factor (equals to 10/9 for a cylindrical beam), G is the shear modulus, I is the second moment of area of the beam ($I = \pi D^4/64$ for a filled cylinder), and A is the cross-sectional area.

Yakobson has studied the fracture and deformation behavior of SWNT by simulation.[58] Simulations on SWNTs have suggested very interesting deformation behavior; highly deformed nanotubes were seen to switch reversibly into different morphological patterns with abrupt releases of energy. Necking occurs in SWNT through defect migration causing changes in lattice helicity, and plastic deformation. Nanotubes get flattened, twisted and buckled as they deform. They sustain large strains (40%) in tension without showing signs of fracture. Zhang et al.[59] have used tight bonding MD to investigate the plastic deformation of nanotubes. Summary of tensile strength and Young's modulus values reported in literature are listed in Tables 1.5 and 1.6.

Table 1.5 Selected experimental results of SWNT Young's modulus

Structure	Young's Modulus (TPa)	Method of measurement
SWNT	1.3	Monitor the thermal vibration amplitudes
	1.25	Thermal oscillation measured by TEM
	1.2	Bending by AFM tip
	5	Micro-Raman spectroscopy of NT compressed in epoxy matrix
SWNT ropes	0.81	NT deflection by AFM tip
	1.0	Pulling using AFM tip

Table1.6 Selected experimental results of SWNT tensile strength

Structure	Tensile strength (TPa)	Method of measurement
SWNT	3.6 ± 0.4 to 22.2 ± 2.2	From tensile experiment on SWNT ropes
	30	AFM
	45	AFM
SWNT ropes	2.3 – 14.2	Fiber testing machine
	45 ± 7	Pulling using AFM tip

1.7 SWNT Electronic Properties

Depending on the chiral vector (n, m), along which is graphite sheet rolled up, SWNT may be robustly metallic (n = m), weakly metallic (n-m = integral multiple of 3) or semiconducting (all the others). The 1-D structure of SWNT is associated with specific band structure resulting from unusual transport properties. Due to the 1-D nature of their band structure, SWNT exhibits pikes or peaks in its density of state, as shown in Figure 1.7.
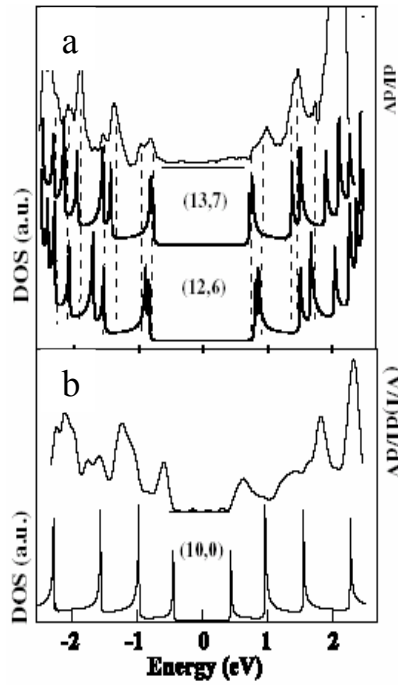
Figure 1.7 Density of state of (a) metallic and (b)semiconducting SWNTs.

Based on the theoretical prediction, $E = k a_{c-c} \gamma_0 / d$, the energy of pair of van Hove singularity can be obtained. Here E is transition energy, a_{c-c} is the nearest-neighbor carbon-carbon distance, 0.144 nm, γ_0 is the nearest-neighbor carbon-carbon interaction energy, 2.9 eV,[60] d is the diameter of SWNT and k is constant. The value

of k is 2, 4 and 8 for 1st, 2nd and 3rd van Hove transitions in semi-conducting tubes and 6, and 12 for 1st and 2nd van Hove transitions in metallic tubes, respectively[61]. The transition energy between the pairs of van Hove singularity can be predicted using tight bonding model. For a semiconducting tube, the first order band gap is given by:

$$E_g = \frac{2\gamma_0 a_{c-c}}{D} \qquad (1\text{-}2)$$

For metallic tube, the first order band gap is give by:

$$E_{met} = \frac{6\gamma_0 a_{c-c}}{D} \qquad (1\text{-}3)$$

where a_{C-C} is the carbon–carbon bond length (1.42 Å) and D is the nanotube diameter. In both cases the distance between consecutive conduction or valence van Hove singularities is given by:

$$\Delta E = \frac{3\gamma_0 a_{c-c}}{D} \qquad (1\text{-}4)$$

γ_0 can be value 2.7 eV for best fitting STS result, it also can be 2.95 eV for best fitting Raman data.

The semi-conducting tubes can be used as nano electronic device, such as light emission device or transistor as described later. The metallic tube is a very unique 1-D nanowire due to its high electrical conductivity. Experimental results show that a SWNT rope has a axial conductivity of 10^6 S/m at 300K.[62] The macroscopic SWNT sample, in the form of randomly oriented nanotubes ropes, forms a pseudo-metal with conductivity of the order of 10^4 - 10^5 S/m.[63] In the case of SWNT mats, the reported conductivity is in the order of 200 S/cm. [64, 65, 66] The length and temperature dependence of SWNT electrical conductivity has also been studied.[67, 68]

1.8 SWNT Thermal Properties

Potential application of carbon nanotube based devices, such as diodes,[69] field-effect transistors[70] and elementary logic circuits[71] depends on the efficiency of the heat removal from the active section of the device. Thermal conductivity is a key factor for heat dissipation. The in-plane thermal conductivity of graphite is very high, second only diamond. The c-axis thermal conductivity of graphite is, as one might expect, very low due to the weakly bound layers, which are attracted to each other only by van der Waals forces. Contribution to a finite in-plane thermal conductivity in graphite at low temperature (<140 K) is thought to be phonon scattering from the edges of the finite crystallites. Even in highly oriented pyrolytic graphite (HOPG), the in-plane coherence length is typically < 100 nm. At low temperatures, the phonon free path is controlled mainly by boundary scattering and at temperatures above 140 K, phonon-phonon (umklapp processes) dominates. Transmission electron microscopy (TEM) images suggest that defect-free tubes exist with lengths exceeding several microns, which is significantly longer than the typical crystallite length present in graphite. So, it is possible that the axial thermal conductivity of carbon nanotubes may be higher than graphite and diamond.

Shi et al. designed micro-device to measure thermal conductance of SWNT bundles. They found that 10 nm and 148 nm diameter bundles have thermal conductance about several hundred and several W/m-K, respectively.[72] J. Hone[73] studied the thermal conductivity of loosely packed, tangled single wall carbon nanotube mats in the 350K to 8 K temperature range. The results showed that the

thermal conductivity is nearly linear in this temperature, in contrast to that of graphite and carbon fiber, which shows the dependence on square of the temperature. The thermal conductivity of densely packed bulk sample is about 36 W/m-k at room temperature. Theoretical calculations suggest that the thermal conductivity for the individual SWNT could be as high as 6000 W/m-k at the room temperature. Based on the difference of Lorenz ratio of electron and phonon, it is believed that phonon scattering is the dominant factor for thermal conduction in SWNT in the above temperature ranges. From the measurement of thermal conductivity, relaxation time is estimated to be about 10^{-11} s, which implies the phonon scattering length is about 100 nm. This length is smaller than the tube length, but larger than inter-tube distance, which suggests that the inter-tube contact may be providing connectivity for scattered phonons.

As heat in SWNT is mostly carried by acoustic phonons, a model was established to calculate the thermal conductivity considering the three-phonon umklapp process and neglecting the electronic component of thermal conductivity.[74] The result shows that the thermal conductivity of an isolated SWNT increases with the increase in temperature at low temperatures, and shows a peaking behavior at about 85 K before falling off at higher temperatures. It is believed that the SWNT thermal conductivity temperature dependence can be attributed to the boundary scattering and the umklapp scattering process. At low temperatures, thermal transport in SWNT is decided by phonon boundary scattering. As temperature increases, umklapp scattering process becomes dominant in heat transfer. Moreover, thermal conductivity is found to be diameter dependent. Relatively higher thermal

conductivity for SWNTs with smaller diameters is found as compared to the tubes with large diameters. The thermal conductivity at 300 K is approximately inversely proportional to the SWNT diameter.

The combination of equilibrium and nonequilibrium molecular dynamics simulations with accurate carbon potential is used to predict the thermal conductivity of single wall carbon nanotubes as well as its dependence on the temperature.[75] Based on this calculation, extremely high thermal conductivity (6600 W/m-K) of SWNT is obtained. This value is much higher than that of planar graphite and diamond. The high conductivity of SWNT is believed coming from the large phonon mean free path in 1-D structure of SWNT. The heat capacity and phonon mean free path govern the temperature dependence of SWNT's thermal conductivity. At low temperatures, phonon mean free path is nearly constant, and the temperature dependence of thermal conductivity follows that of the specific heat. At high temperatures, where the specific heat is constant, conductivity decreases as the phonon mean free path becomes smaller due to umklapp processes. Therefore, the trend is such that the result appears to show that the thermal conductivity increases with the temperature at low temperatures, passes a peak, and then decreases with further increase in temperature.

Thermal conductivity temperature peaking behavior is shown by all types of single wall carbon nanotubes.[76] This peaking behavior is closely associated with the SWNT diameter, but not the chirality. With different size, the SWNT thermal conductivity peak appears at a different temperature. This behavior is attributed to two combined factors: the onset behavior of Umklapp scattering;[77] the heat is carried mainly though radial phonon. Also, this phenomenon allows one to design specific

thermal management device to satisfy the temperature requirement. At room temperature, the thermal conductivity of magnetically aligned SWNT bulk film is measured to be greater than 200 W/m k.[78]

1.9 SWNT Chemistry

Understanding the chemistry of single wall carbon nanotubes is critical to manipulate them and to take advantage of their properties. Chemical modification is essential for the deposition of catalysts and other species onto nanotube surfaces for nanocatalytic and sensor applications. Chemical modification helps SWNT dispersion and solubilization SWNT. From a fundamental scientific perspective, functionalization allows for the exploration of intrinsic molecular nature of these SWNTs and permits interface study between SWNT and bulk material. In general, the chemistry of carbon nanotubes is divided into two categories: the end cap and the side wall chemistry. The end cap chemistry of SWNT initiates at the stress concentrated end caps (five or seven member ring) and at defects by various oxidizating agents. Then further esterification or amidization is carried out. Mawhinney et al[79] used ozone to oxidize single wall nanotubes at room temperature. They found that the reactive sites are located at end caps and at kinks of SWNTs'. The concentrations of functional groups, carbonyl and quinone, first increase with exposure time, then reach equilibrium. The FTIR spectrum of oxidized SWNTs is shown in Figure 1.8. The spectral bands that develop at 1739, 1200, and 1040 cm^{-1} are indicative of the presence of ester groups. The band at 1650 cm^{-1} is assigned to C=O stretching mode of quinone groups, while the band at 1581 cm^{-1} is assigned to C=C double bonds

located near the newly formed oxygenated groups. Upon heating, the oxygen

functional groups begin to disappear, and is totally gone at 873K.
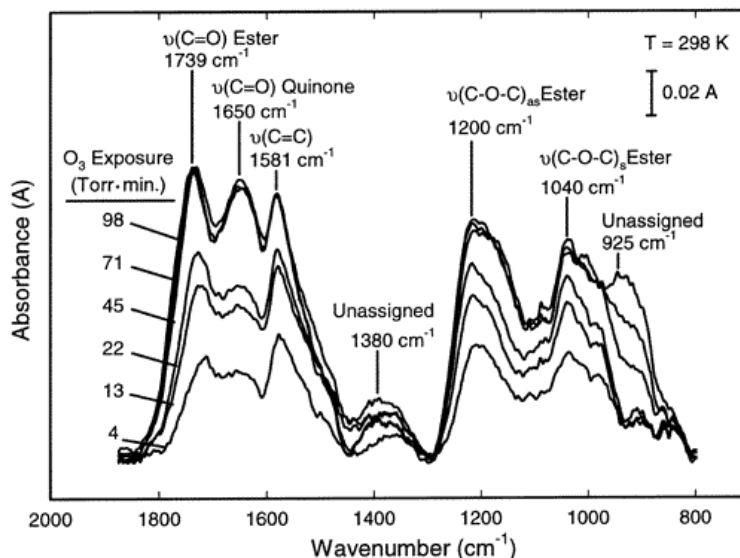
Figure 1.8 Infrared spectra resulting from the ozonation of SWNTs. The background

spectrum of the nanotubes before ozone exposure has been subtracted.[79]

Kuznetsova et al[35] used H_2SO_4/HNO_3 mixture followed by treatment with

H_2SO_4/H_2O_2 to chemically modify SWNTs. Carboxylic acid and quinone groups were

observed at the end ports and at defect ports. Nitric acid was found to suppress the

first and second order van Hove transitions for semi-conducting single wall

nanotubes. But upon thermal or laser annealing, the transitions are recovered.[80] The

intensity of the C=O stretch vibration of -COOH group appeared to increase slightly

upon heating to 280 °C and then decreased on further heating to higher temperature.

The intensity increase was believed the result of further oxidation of -C-OH in phenol

and C=O in quinone. Subsequent intensity decrease was the result of decomposition of COOH group.

Oxidization of single wall carbon nanotubes by $H_2SO_4/30\%H_2O_2$ and neutralization by NaOH was done by Zhao et al[81] The oxidized SWNT was found sensitive to the pH value. It was soluble in the buffers with pH > 3. The solutions were stable over 12 hrs, which was long enough for optical measurements. For pH <3, the sample solution was not stable, and aggregation occurred within minutes. It was thought due to deprotonation, at pH > 3.0 the carboxylic groups acquired charges which resulted in mutual repulsion between the tubes, hydration shells around the tubes, and a consequent solubility of the tubes at pH<3.0, the SWNTs were protonated, and aggregation occurred due to van der Waals forces. Also, the intensity of first interband transition of semi-conducting SWNT decreased with decrease in pH value, while the second interband transition of semi-conducting tube (S_{22}) and first interband transition of metallic tube (M_{11}) were unchanged. This result indicated that the change in the concentration of H^+ and OH^- caused an electronic structure change in semiconducting SWNTs by refilling or depleting their valence band. The intensity change was reversible by changing the pH value of the buffer.

5M nitric acid treated single wall nanotubes and octadecylamine (ODA) mixture was heated at 120-130 °C for 4-8 days. The reacted mixture was then washed with ethanol and sonicated. These tubes were soluble (0.5 mg/ml) in tetrahydrofuran and 1,2-dichlorobenzene. The length of most of the SWNT was longer than 1 micrometer.[82] The SWNT and ODA followed the normal acid-base reaction forming a SWNT-carboxylate zwitterions. The ionic functionalization gave high yield of

soluble long SWNT, which were ready for ion exchange for adjusting the surface properties. The ion was compatible with biomelecules for further application in Biochemistry.
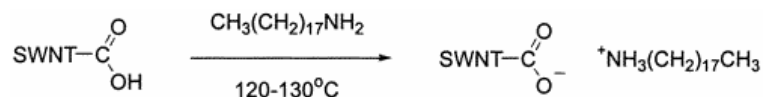
Bower et al immersed SWNT mat into 70% nitric acid and observed the increased intertube spacing, and the spacing reversed back on heat-treatment at 500 K as observed by X-ray diffraction.[83] They attributed this to the intercalation of HNO_3 molecules between nanotubes. But the intertube spacing increase can also be the result of presence of carbonyl, carboxyl or phenol group produced during nitric acid oxidation and the reversibility of intertube spacing by heating is due to the decomposition of functional groups. A similar routine was adopted by Liu et al[84]. In their process, cysteamine, $(NH_2CH_2CH_2SH)$ was chosen to react with carboxyl acid terminated SWNT. Assisted by the interaction between S and Au, these modified SWNTs self-assembled as a monolayer on a gold surface.

HNO_3 or HNO_3/H_2SO_4 has been used to oxidize SWNT[85]. XPS detected three types of oxygen in functional groups, which were described as phenol (532.5 eV), carbonyl (530.95 eV) and carboxyl (533.76 eV). These functional groups could act as specific nucleation sites for a well-dispersed deposition of platinum clusters on the surface of carbon nanotubes. The morphology change of nanotubes from oxidation has been studied by TEM[86]. As the boiling time of nanotubes in nitric acid increased,

the shorter and straighter tubes were obtained. It was suggested that the oxidation took place at the stress concentrated end sites or at curvature points.

A very simple method was developed to determine the acid content and total functional sites of nitric acid purified SWNTs[87] besides the method that measure the total CO_2 and CO evolution from purified SWNTs heated above 1200K[88]. The total functional sites (including carboxylic acids, lactones and phenols), could be determined by titration with NaOH, while the carboxylic acid groups could be individually determined by titration with $NaHCO_3$.

Direct chemical functionalization of the side walls using addition reactions, e. g. direct fluorination and subsequent nucleophilic substitution[89] have been reported to date. A similar study on the direct reaction of single wall nanotube side wall was conducted by Hoolzinger et al.[90] The [2+1] cycloaddition of nitrene, alkyl azidoformate, nucleophilic addition of carbene, dipyridyl imidazolidene, and photoinduced free radical addition, perfluorinated alkyl, were carried out under the corresponding reaction conditions, resulting in successful side wall functionalization of SNWT. The electronic, optical and physical properties of SNWT were changed by grafting functional groups.

The functionalization based on the 1, 3-dipolar cycloaddition of azomethine yields, generated by condensation of an α-amino acid and an aldehyde, was conducted on various SNWTs.[91] The solubility of the functionized SWNT were improved significantly, for example, the solubility of functionalized SWNT was close to 50 mg/ml without sonication.

Highly purified single-wall carbon nanotubes (SWNTs) were fluorinated to form "fluorotubes", which were then solvated as individual tubes in various alcohol solvents via ultrasonication.[92] The solvation of individual fluorotubes was verified by dispersing the tubes on a mica substrate and examining them with atomic force microscope (AFM). As high as five percent of carbon in the SWNT can be functionalized. Elemental analysis of the tubes revealed that light sonication in alcohol solvents does not remove significant amounts of fluorine. The solvated fluorotubes can react with sodium methoxide to yield methoxylated SWNTs. The Figure 1.9 and 1.10 shows the scheme of SWNT end cap and side wall chemistry

1.10 SWNT Characterizations

There are many methods used for SWNT characterization. These include Raman spectroscopy, UV-vis spectroscopy, atomic microscopy (AFM), transmittance electron microscopy (TEM), scanning tunneling microscopy (STM), scanning electron microscopy (SEM), X-ray photonelectron spectroscopy (XPS), infra-red spectroscopy, etc. Some of these monitor changes in the electronic properties, while others monitor changes in the chemical structure.

Raman spectroscopy is a powerful technique for characterizing SWNT. From Raman study, the diameter, diameter distribution, defects, load transfer state as well as the electronic state of SWNT can be evaluated. Raman scattering by SWNT has been experimentally shown to be a resonant process associated with allowed optical transitions (AOT) between spikes in the 1D electronic density of states (named van Hove singularities), which fall in the visible and near-infrared regions (Figure 1.11).
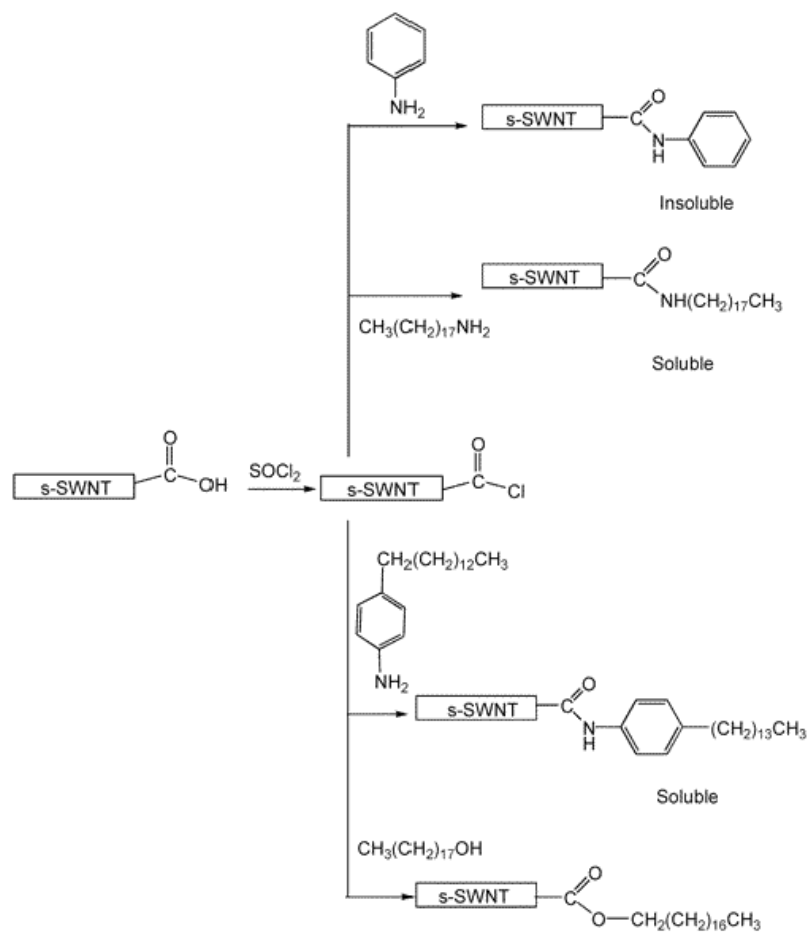
Figure1.9 Scheme of various end cap SWNT chemistries.[93]
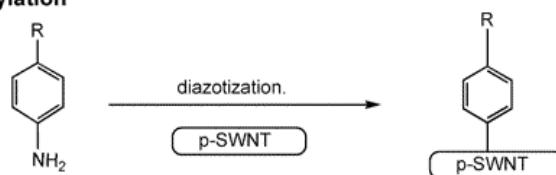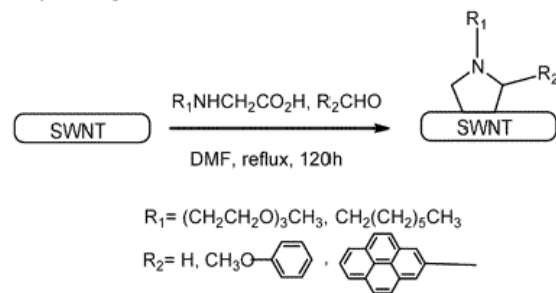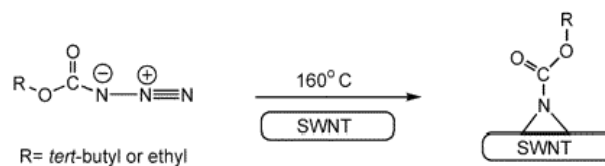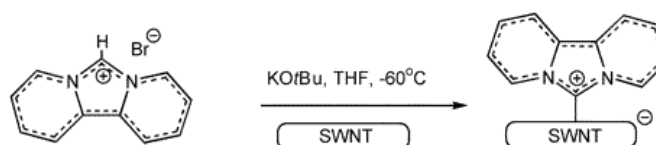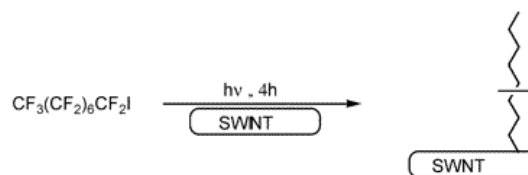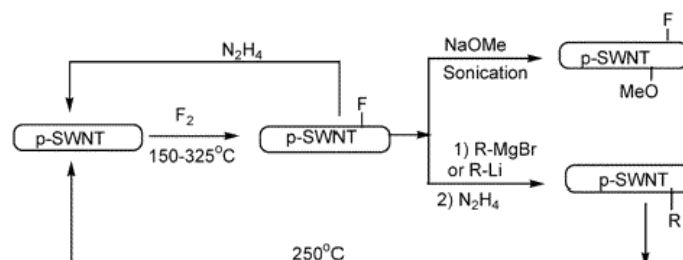
Figure 1.10 Scheme of various side wall SWNT chemistries.[93]
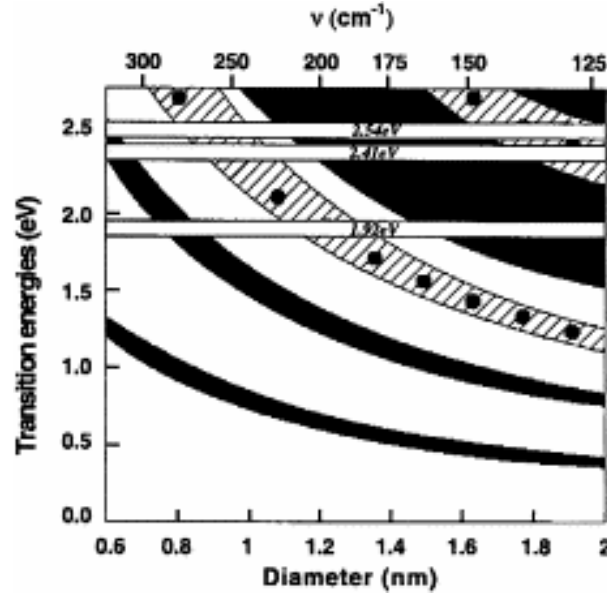
Figure 1.11. Allowed optical transitions calculated in the zone folding scheme for SWNT with various diameters and helicities.[95]

The energies of the van Hove transitions are found to depend both on the diameter and metallic or semi-conducting character of the tubes.[94, 95] When subjected to different lasers as the excitation source, tubes will respond differently.

The Figure 1.12 is the full range Raman spectrum of a single wall carbon nanotube. In this spectrum four important features are listed as: radial breathing mode (RBM), the disorder induced D-band, the tangential G-band (derived from the graphite like in-plane mode) and G* band (overtone of D band).

The spectrum in the range of 150 to 350 cm^{-1} is the RBM, and is influenced by the diameter of the nanotubes. Several calculations have related the diameter of the tube with radial breath frequency of Raman spectrum mathematically.[96]

$$d = 224/\omega_{RBM}$$
$$or \hspace{4cm} (1\text{-}5)$$
$$d = 248/\omega_{RBM}$$

35
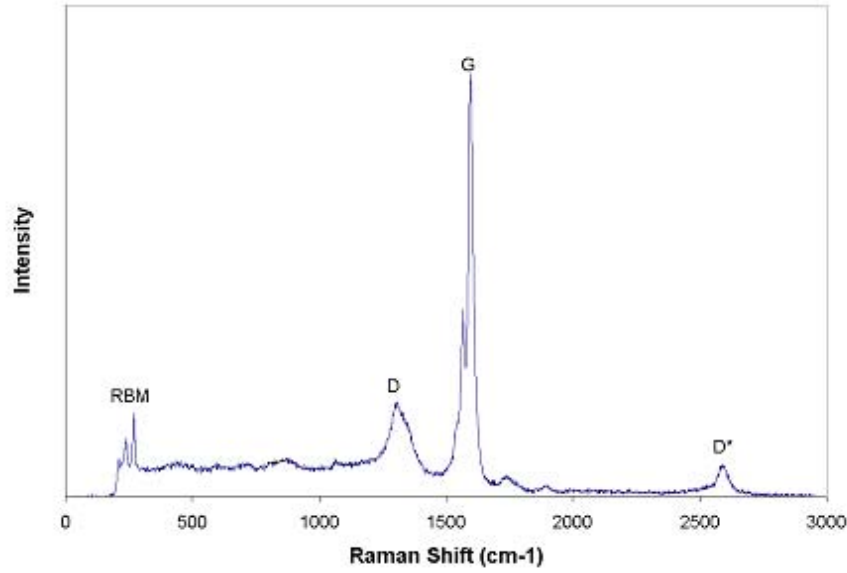
Figure 1.12 Raman spectrum of single wall carbon nanotubes.

However, most of the tubes self-assemble into bundles and radial modes are very sensitive to the nanotube packing. Calculating the RBM frequency considering the van der Waals interactions between the tubes, the following equation was given:[97]

$$d = 232/(\omega_{RBM} - 6.5) \qquad (1\text{-}6)$$

By separating the contributions of different diameter tubes to the radial breathing intensity, the diameter distribution of the nanotube can be obtained.

The Raman spectrum in the range of 1250 to 1450 cm^{-1} is called D band, which is due to the defect on the nanotube. This band can be used to monitor the structure perfection of the nanotubes. Also it can be used to qualitatively characterize the chemical functionalization of the tube. Side wall functionalization damages the tube, increasing the D band intensity. The feature in the range of 2500 to 2900 cm^{-1} also originates from the defect. It is the second order overtone of D band. It is widely used to monitor the load transfer between SWNT and the matrix.

The most important aspect of the G-band is the characteristic Raman lineshape, which differs in accordance with whether the nanotube is semi-conducting or metallic. This intrinsic property allows one to readily distinguish between metallic and semi-conducting nanotubes. In case of semi-conducting tube, two Lorentzian features dominate the lineshape but in case of metallic tube, one Lorentzian is replaced by Breit–Wigner–Fano line. Based on the sensitivity of the G-band to the electronic energy state, the position of G-band can be used to monitor the energy state change due to environment. For example, the thermal energy input to the SWNT can lead to the shift of the D-band; the pressure applied on the SWNT will lead the shift of D-band; most importantly, the chemical environment change, such as the doping effect, will also induce the D-band position change.

As we mentioned earlier, AFM can be used to experimentally measure the mechanical properties of isolated individual SWNT or SWNT bundle. In addition, AFM is also used to directly image the SWNT, allowing for diameter of SWNT determination. [98] Figure 1.13 shows the AFM image of individual SWNT.
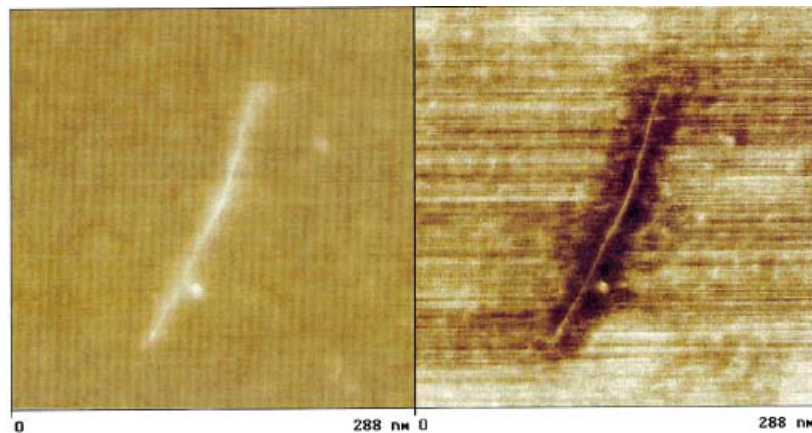
Figure 1.13 AFM image of individual SNWT.[98]

TEM is also used to measure the mechanical properties and to directly image the SWNT.[99] Figure 1.14 is the typical TEM image of SWNT bundle. STM is not only able to get the high-resolution image of SWNT to reveal its atomic structure, but also able to study the electronic structure change of SWNT (Figure 1.16). It is a precise instrument to correlate the electronic properties change with respect to the environment change.
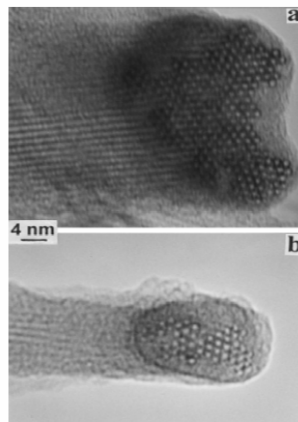
Figure 1.14 TEM Image of SWNT Bundles[99]
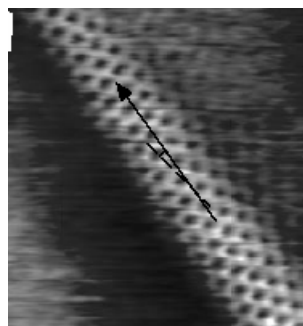
Figure 1.15 STM images of SWNT on the surface of a rope. [100, 101]

The energy of van Hove transition in SWNT is comparable to light energy in UV-vis range. So, UV-vis spectroscopy is another useful method to characterize the changes of electronic properties. For example, due to functionalization, the electronic structure of the original SWNT is damaged. The UV-vis spectrum of the chemically modified SWNT becomes featureless contrary to the fine pattern in the original tube. Also, because the transition energy is different in individual SWNT and in SWNT bundle, in small bundles and large bundles, the UV-vis spectrum can be a standard tool for the qualitative assessment of SWNT dispersion, as shown in Figure 1.16.
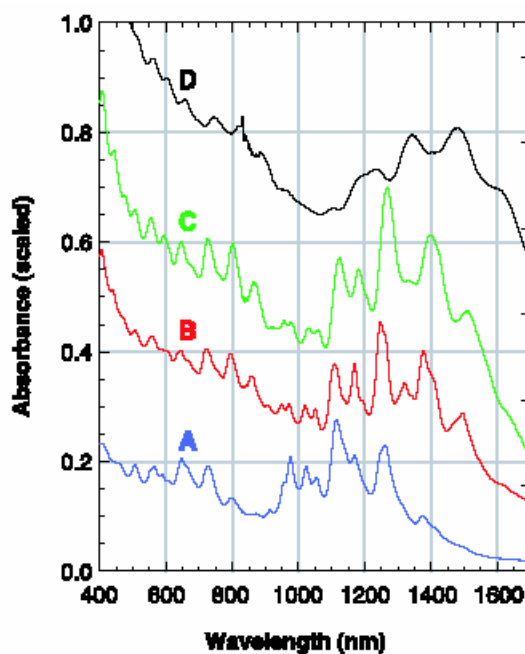
Figure 1.16 UV-vis spectrum of SWNT dispersion.

Figure 1.16 is the absorption spectra of SWNT in SDS-D$_2$O suspension. The top trace D is typical of tubes prepared in suspension without centrifugation. The broadened and redshifted absorption features show that most nanotubes in the sample are aggregated in small bundles. Trace C is from individual SDS micelle coated

39

nanotubes after addition of PVP. Traces B and A are from samples of individual

nanotubes separated and solubilized by SDS micelles.[102]

Neutron and light scattering techniques for wave vectors Q in the range 10^{-4} –

10^{-1} A^{-1} (corresponding to length scales 1–1000 nm) are ideal for investigating the

structure of SWNTs in suspension based on the scattering intensity's power law

dependence on wave vector q:[103]

$$I_s \sim q^{-D} \hspace{3cm} (1\text{-}7)$$

q = $4\pi\sin(\theta/2)/\lambda$, D is fractal dimension. The morphology of fractal can be indicated

by D value. The fractal dimension is 1 for rods, 2 for disks, and 3 for sphere.

The investigation of small angle neutron scattering on SWNT suspensions in

D_2O provided strong evidence for individual SWNTs and very small bundles in

suspension rigid rods like behavior. Crossover in the power law of Q-dependence of

scattered intensity I from -1 to approximately -2 at low Q was observed, suggesting

that these isolated tubes and small bundles may form a loose three-dimensional

network. On the contrary, suspensions agglomerates of SWNTs do not exhibit the

scattering behavior characteristic of isolated rigid rods.[104]. On the other hand, recent

studies of SWNTs in suspension and in polymer composites exhibited power law

dependence with exponents in the range -2 to -3; which suggest the configurations of

nanotubes in such suspensions and composites are random coil or non-rigid rod-like

structures.[105] In Dale W. Schaefer et al.'s paper, it was found that SWNTs exist as

entangled network instead of rigid rods in polyelectrolyte dispersion based on small-

angle (SAXS) and ultra-small angle X-ray (USAXS) scattering.[106] Light scattering

has also been used to determine the length of SWNT. Both radius and extinction

coefficients of SWNT have no effect on normalized scattering intensity, which indicate that the average length of SWNTs can be determined without consideration of radius and absorption coefficient. Through the comparison of simulation and experimental results, the SWNT length could be deduced.[107] Light scattering can also be used to predict the in-plane elastic properties (Young's modulus) of SWNT.[108]

1.11 SWNT Applications

The applications of single wall carbon nanotubes are mostly related to three unique features, namely, small dimensions, as well as electronic and mechanical properties. Following Iijima's discovery, there is strong feeling in the research community that carbon nanotubes would be ideal molecular-level composite reinforcements in polymeric, ceramic, or metal matrices due to their light weight, potentially outstanding mechanical properties, and excellent thermal conductivity in the axial direction. As we know, nanotubes are atomically smooth and have nearly the same diameters and aspect ratios (length/diameter) as polymer chains and single wall carbon nanotubes are almost always organized into aggregates, which behave differently in response to load, as compared to individual nanotubes. 5 wt% percent of SWNT enhanced the tensile strength of PVA film by 70%.[109] Some other successful examples can also be obtained in case of epoxy,[110] polyimide,[111] and PMMA[112] matrices. In addition to structural composite applications, other unique properties of SWNT are being incorporated into polymer matrix. Recently, poly (m-phenylenevinylene-co-2,5-dioctoxyp- phenylenevinylene) (PPV), filled with SWNTs has shown large increase in electrical conductivity (by nearly eight orders of

magnitude) compared to the pristine polymer.[113] 2% SWNT loading is found to monotonically increase resistance to indentation (Vickers hardness) by up to 3.5 times and 1% SWNT loading doubled the thermal conductivity.[114] There are other less-explored areas where nanotube-polymer composites could be useful. For example, nanotube filled polymers could be useful in electro magnetic interference (EMI)[115] shielding applications where carbon fibers have been used extensively.

Carbon nanotubes are being considered for energy production and storage. It has been pointed out that compared to conventional carbon electrodes, the electron transfer kinetics in nanotubes is faster. This makes carbon nanotubes a better candidate for carbon electrodes in fuel cells. Also, the catalyst particle required for oxygen reduction reaction in fuel cell can be selectively filled into the carbon nanotubes, which makes carbon nanotubes based fuel cell more efficient.[116] The research on the SWNT based rechargeable battery indicate that SWNT can improve the battery performance, with high energy capacity, fast charging time and long cycle time.[117] It has been speculated that a higher Li capacity may be obtained in carbon nanotubes if all the interstitial sites are accessible for Li intercalation.

Materials with high hydrogen storage capacity are desirable for energy storage applications. Because of their cylindrical and hollow geometry, and nanometer-scale diameters, it has been predicted that the carbon nanotubes can store liquid and gas in the inner cores through capillary effect.[118] Upon cutting (opening) the nanotubes by an oxidation process, the amount of absorbed H_2 molecules increased to 4–5wt%. A Temperature-Programmed Desorption (TPD) study on SWNT-containing material (0.1–0.2wt% SWNT) estimates a gravimetric storage density of 5–10wt% SWNT.[119]

It is believed that hydrogen is first adsorbed on the outer surface of the crystalline ropes.

Because of the high electrochemically accessible surface area of porous nanotube arrays, combined with their high electronic conductivity and useful mechanical properties, these materials are attractive as electrodes for devices that use electrochemical double-layer charge injection. Examples include "supercapacitors,"[120] which have giant capacitances in comparison with those of ordinary dielectric-based capacitors, and electromechanical actuators that may eventually be used in robots. Supercapacitors with carbon nanotube electrodes can have a capacitance of 300 F/g[121] and a power density of 20 kW/kg at an energy density of about 7 W-hour/kg for SWNT electrodes.[122, 123]

Industrial and academic research activity on electronic devices have focused principally on using SWNTs as field emission electron sources[124] for flat panel displays.[125] Recently, a 4.5 inch diode-type field emission display has been fabricated by Samsung with SWNT stripes on the cathode and phosphor-coated ITO stripes on the anode running orthogonally to the cathode stripes.[126] The advantages of nanotubes over liquid crystal displays are low power consumption, high brightness, wide viewing angle, fast response rate, and a wide operating temperature range.

Nano-size electronic device is currently an active research field. For example, nanotube field effect transistors (NT-FETs) gating has been achieved by applying a voltage to a submerged gate beneath a SWNT, which is contacted at opposite nanotube ends by metal source and drain leads.[127] Research toward nanoscopic NT-FETs aims to replace the source-drain channel structure with a nanotube. A more

radical approach is to construct entire electronic circuit from interconnected nanotubes.

The small and uniform dimensions of the nanotubes produce some interesting applications. With extremely small sizes, high conductivity, high mechanical strength and flexibility, nanotubes may ultimately become indispensable in their use as nanoprobes. Since nanotubes are conducting, they can be used in STM, AFM[128] instruments as well as other scanning probe instruments, such as an electrostatic force microscope. Functionalized nanotubes were used as AFM tips to perform local chemistry, to measure binding forces between protein-ligand pairs and for imaging chemically patterned substrates. The advantage of the nanotube tip is its slenderness and the possibility to image features in narrow, deep crevices and improve resolution. Nanoscopic tweezers have been made that are driven by the electrostatic interaction between two nanotubes on a probe tip.[129]

Since nanotube tips can be selectively modified chemically through the attachment of functional groups, they can also be used as molecular sensor, with potential applications in chemistry and biology. Open nanotubes with the attachment of acidic functionalities have been used for chemical and biological discrimination on surfaces. [130]

Since nanotubes have relatively straight and narrow channels in their cores, it was speculated from the beginning that it might be possible to fill these cavities with foreign materials to fabricate one-dimensional nanowires. The materials used to fill SWNT include metal halide, KI[131], $LnCl_3$[132], $ZrCl_4$, $AgCl_xI_{1-x}$,[133] etc, metal oxide, CrO_3[134], Sb_2O_3[135], etc. SWNT filling can be realized in high temperature in the

presence of metals. SWNT filling can also be synthesized *in situ*, during the growth of nanotubes in an electric arc or by laser ablation. During the electric arc formation of carbon species, encapsulated nanotubular structures are created in abundance. Nanocomposite structures based on carbon nanotubes can also be built by coating nanotubes uniformly with organic or inorganic structures. These unique composites are expected to have interesting mechanical and electrical properties due to a combination of dimensional effects and interface properties.

1.12 SWNT Polymer Composites

In general, the thermal transport properties of polymeric materials are not good, which limits their application where fast heat dissipation is required. The high thermal conductivity as well as the large aspect ratio makes SWNTs a good candidate for thermal management material in polymer/SWNT composites. Choi et al. observed that thermal conductivity is anomalously greater than theoretical predictions and is nonlinear with nanotube loadings in the nanotube-oil dispersion system.[136] In comparison with other nanostructured materials dispersed in fluids, the nanotubes provide the highest thermal conductivity enhancement due to their unique structure. A modified conventional model for thermal conductivity has been studied by Nan et al.[137]

$$\frac{k_e}{k_m} = \frac{3 + 2f\left[\beta_x\left(1 - L_x\right) + \beta_z\left(1 - L_z\right)\right]}{3 - f\left(2\beta_x L_x + \beta_z L_z\right)}$$

Here:

$$\beta_x = \frac{k_x - k_m}{k_m + L_x\left(k_c - k_m\right)},$$

$$\beta_z = \frac{k_z - k_m}{k_m + L_z\left(k_c - k_m\right)},$$ (1-8)

$$L_x = \frac{p^2}{2\left(p^2 - 1\right)} - \frac{p}{2\left(p^2 - 1\right)^{3/2}}\cosh^{-1}p,$$

$$L_z = 1 - 2L_x$$

Here, k_e is the effective thermal conductivity of composite; k_m is the thermal conductivity of matrix; k_x and k_z are thermal conductivity of the carbon nanotubes along transverse and longitudinal axes, respectively; f is the volume fraction of nanotube; L_x and L_z are geometrical factors dependent on the nanotube aspect ratio p; the k_c is the thermal conductivity of nanotubes. Since the large aspect ratio of nanotube (>100) and the high thermal conductivity of nanotube (both transverse and longitudinal), the equation can be simplified as follow:

$$\frac{k_e}{k_m} = \frac{3 + fk_c / k_m}{3 - 2f}$$ (1-9)

SWNTs have been shown to improve the thermal transport properties of an industrial epoxy. Samples loaded with 1 wt% unpurified SWNT showed a 70% increase in thermal conductivity at 40 K, rising to 125% at room temperature.[138] Electrical conductivity data showed a percolation threshold between 0.1 and 0.2 wt% SWNT loading. The Vickers hardness rose monotonically with SWNT loading up to a factor of 3.5 at 2 wt%. These results suggest that with incorporation of SWNT not only

thermal transport property but also mechanical properties of epoxy composites improve. The similar system has been further studied showing the relationship between the thermal conductivity of composite with the temperature.[139] The orientation effect of SWNT on the thermal conductivity has been studied. The results show that without SWNT orientation thermal conductivity increased by up to 300% with 3 wt % SWNT loading. The thermal conductivity is further enhanced by another 10% by magnetic field alignment at 25 T.[140] In SWNT composites, the phonon mismatch at the boundaries of the nanotube and epoxy matrix results in high thermal boundary resistance and the phonon mode of SWNT is affected by surrounding epoxy matrix, which suppresses the efficiency of SWNT as a thermal conducting filler.

Generally, the electrical conductivity of an engineering plastic is below 10^{-10} S/m. Due to relatively high electric conductivity as well as excellent mechanical properties, SWNT can be used as a filler to improve the conductivity of composite materials without damaging other intrinsic properties of the matrix. The conduction mechanism for SWNT in the composite is though the percolation of SWNT. When the concentration of SWNT reaches the percolation level, the conductivity of composite will increase sharply. The analytic model used to predict the percolation volume fraction has been developed and applied in the polymer/SWNT composite field.

$$V_{SWNT} = \frac{4}{3}\pi r^2 + \pi l r^2$$

$$V_{ex} = \frac{32}{3}\pi r^3 + 8\pi l r^2 + 4l^2 r \langle \sin(\gamma) \rangle$$

$$\rho_c \propto (V_{ex})^{-1} \qquad\qquad\qquad (1\text{-}10)$$

$$V_c = \rho_c V_{SWNT}$$

$$Then:$$

$$\phi_c = \frac{\rho_c V_{SWNT}}{V_{total}}$$

Here, l and r are length and diameter of SWNT respectively; V_{SWNT} is the volume of SWNT; V_{ex} is the exclusive volume of SWNT, which is defined as the region of space into which the center of another SWNT may not penetrate; <sinγ> describes the orientation of SWNT; γ is the angle between two SWNT, in the perfectly orientated case γ = 0°, and for random orientation γ = 45°; ρ_c is the critical number density of SWNT at percolation; ϕ_c is the volume fraction at the percolation.[141]

SWNTs were well dispersed in polystyrene (PS) or polycarbonate (PC) matrices assisted by Poly (phenylenethylene) (PPE).[115] The composite films made from such dispersion show very low percolation volume fraction and good electric conductivity. The percolation threshold ranged from 0.05 to 0.1wt%. Further increasing the SWNT loading, the electrical conductivity increases to 10^2 S/m. These composite films can find applications in electrostatic painting or electrostatic dissipation. In the homogenously dispersed SWNT/epoxy composite film,[142] as the concentration of SWNT increases from 0.01 to 0.21 wt%, the conductivity of composite shows clear percolation behavior. The percolation concentration is determined to be 0.074 wt%. Using PMMA as the matrix polymer, the electrical

conductivity of PMMA/SWNT composite film with or without SWNT orientation are characterized. The results show that the conductivity significantly decreases with the SWNT orientation.[112] This can be explained by SWNT network forming ability difference in these two cases. Alkoxysilane terminated amide acid (ASTAA) polymer and SWNT composite shows percolation level at 0.05 wt%.[143] In Sandler's work, percolation threshold was observed at 0.0025 wt% MWNT loading, with t = 1.2 in the power law equation.[144] SWNT can also be used to convert insulating nanoceramics to metallically conducting composites. The conductivity of these composites increases with increasing SWNT content. The conductivity of dense SWNT/Al_2O_3 nanocomposites increased to 3345 S/m at 15 vol % SWNT at room temperature. This is an increase of 13 orders of magnitude over pure alumina.[145]

The excellent results are obtained from polyvinyl (9-carbazole) (PVK) or Polyvinyl alcohol (PVA) carbon nanotube composite in form of film and fiber.[146] In all cases significant increase in both Young's modulus and hardness are observed. For PVK based composite the Young's modulus and hardness increased by 200% and 100% respectively. Similar result is obtained in the case of carbon nanotube epoxy composite. The hardness increased 20% on loading 2 wt% tubes. But the strength is reduced in this composite, the reason may be due to the structural inhomogeneity and/ or the existence of weak interface between the nanotube and matrix.[147] Isotropic SWNT/epoxy sample has been characterized. It was found that the Young's modulus of this sample linearly increased with the SWNT loading. The PC/SWNT composite can be produced through melt extrusion. Well dispersed SWNT in PC matrix is obtained.[148] SWNT improves the mechanical performance of PVA film, increasing

both the tensile strength and modulus.[109] The most successful achievement in case of mechanical reinforcement of polymer matrix by SWNTs has recently been reported by Mamedov et al[149] in the multilayered polymer SWNT composite thin film made by layer-by-layer assembly. The SWNTs load was as high as 50 wt%. After subsequent crosslinking, the exceptionally strong tensile strength can be obtained, which is approaching that of hard ceramics. Here, chemically modified SWNTs were used and the polyelectrolytes poly (ethyleneimine) (PEI, positive charged) and poly (acrylic acid) (PAA, negative charged) were used. PEI was used for its NH and NH_2 group in main chain and branches, which provided crosslinking point for carbonyl group in SWNTs and PAA. It is thought that the LBL technical has prevented phase segregation in making polymer SWNT thin films.

As the nanotubes are distributed randomly in the composite film, composite modulus can be predicted using Halpin-Tsai equation.

The general Halpin-Tsai equation is expressed as following equation:

$$E_{random} = \frac{3}{8}E_{11} + \frac{5}{8}E_{22} \qquad (1\text{-}11)$$

$$E_{11} = \frac{1 + 2\left(\dfrac{l_f}{d_f}\right)\eta_L V_F}{1 - \eta_L V_f}E_m \qquad (1\text{-}12)$$

$$E_{22} = \frac{1 + 2\eta_T V_f}{1 - \eta_T V_f}E_m \qquad (1\text{-}13)$$

Here, V_f, l_f and d_f are volume fraction, length and diameter of filler, respectively.

For nanotube reinforced polymer composite:

$$E_c = \left[\frac{3}{8} \frac{1 + 2\left(\dfrac{l_{NT}}{d_{NT}}\right)\eta_L V_{NT}}{1 - \eta_L V_{NT}} + \frac{5}{8} \frac{1 + 2\eta_T V_{NT}}{1 - \eta_T V_{NT}} \right] E_M \qquad (1\text{-}14)$$

$$\eta_L = \frac{\left(\dfrac{E_{NT}}{E_M}\right) - 1}{\left(\dfrac{E_{NT}}{E_M}\right) + 2\left(\dfrac{l_{NT}}{d_{NT}}\right)} \qquad (1\text{-}15)$$

$$\eta_T = \frac{\left(\dfrac{E_{NT}}{E_M}\right) - 1}{\left[\dfrac{E_{NT}}{E_M}\right] + 2} \qquad (1\text{-}16)$$

Here, E_{11} is longitudinal modulus; E_{22} is transverse modulus; E_c, E_{NT} and E_M are the moduli of composite, nanotube and matrix respectively; V_{NT} is nanotube fraction; L_{NT} and D_{NT} are length and diameter of nanotube respectively.[150]

Normally, in composite fiber, the SWNT has high orientation. The orientation of SWNT in composite is expected to improve the mechanical performance of the composites, especially the Young's modulus. The correlation between the orientation of SWNT and Modulus of the composite has been studied by Liu et al.[151] The result indicates increasing orientation of SWNT, the modulus of composite increase slowly at first, then rapid increase is obtained in the high orientation region. Several methods have been used to introduce orientation of nanotube into the polymer composite, such as mechanical stretching[152], magnetic field,[153] electric force etc. After mechanical stretching, SWNTs alignment in PVA/SWNT composite spun fibers can be significantly improved (with FWHMs 40% smaller). The procedure is based on the elastic deformability of swollen networks of nanotubes and adsorbed polymers. With

this procedure, the fiber mechanical properties are improved (Young's modulus and tensile strength can be increased by a factor of 4 and 2 respectively).[154] By adding 1 wt% SWNT to polypropylene, the fiber mechanical performance is enhanced. The fiber preparation is through solvent dispersion followed by melt spinning. The resulting composite fiber has 13.1 g/denier strength and 93 g/denier modulus, which are 40 % and 55 % higher than the control PP fiber.[155] The 50 % increase in tensile strength of composite fiber as presence of SWNT can be observed in poly (p-phenylene benzobisoxazole) (PBO) fiber.[156] SWNT is dispersed in isotropic petroleum pitch matrix to form nanotube composite carbon fibers with enhanced mechanical and electrical properties. The result shows that the tensile strength, modulus, and electrical conductivity of a pitch composite fiber with 5 wt% loading of purified SWNTs are enhanced by, 90%, 150%, and 340% respectively, as compared to the corresponding values in unmodified isotropic pitch fibers.[157]

Recently, super-tough PVA/SWNT composite fiber has been reported. This process consists of dispersing nanotubes in a surfactant solution, re-condensing the nanotubes in the flow of a PVA solution to form a nanotube mesh, and then collating this mesh to a nanotube fiber.[158, 159] The process is relatively simple and can produce continuous fiber. The spinning set up is shown in Figure 1.18. The appearance of as spun fiber though this method is shown in Figure 1.19. The SWNT content in this fiber is as high as 60 wt percent. The true stress of this composite fiber is near 1.6 GPa and the modulus reached 80 GPa. The elongation to break is about 100 %. More importantly, the energy to break achieve unusually high value of 570 J / gm.[160] This is several times that of the spider silk fiber (165 J/ gm), which is supposed to be the

toughest material we ever knew before. This discovery stimulates further research in SWNT/polymer composite field. More recently, the tensile strength of PVA/SWNT composite fiber near 3 GPa was reported by the same group.[161]
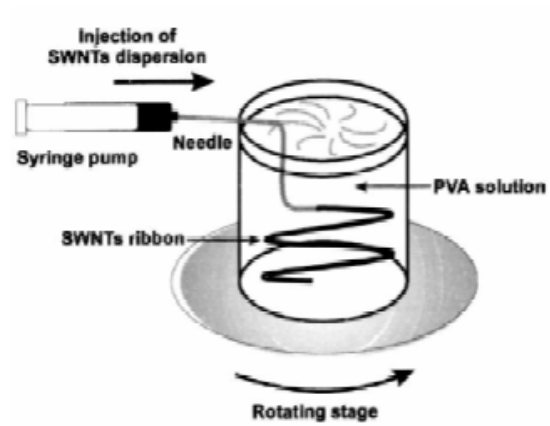
Figure 1.17 Set up of SWNT fiber spinning.[158]
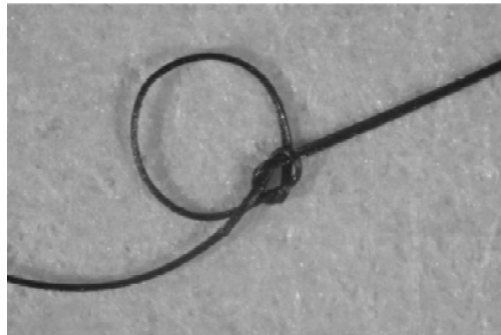
Figure 1.18 SWNT fiber.[159]

REFERENCES

[1] Kroto, H. W.; Heath, J. R.; O'Brien, S. C.; Curl, R. F. Smalley, R. E., *Nature* **1985**, *318*, 162.

[2] Iijima, S. *Nature*, **1991**, *354*, 56.

[3] Iijima, S. Ichihashi T., *Nature*, **1993**, *363*, 603.

[4] Bethune, D. S; Klang, C. H.; de Vries, M. S.; Gorman, G.; Savoy, R. Vazquez, J.; Beyers, R. *Nature*, **1993**, *363*, 605.

[5] Bacon, R. *J. Appl. Phys*. **1960**, *31*, 283.

[6] Wong, S.; Joselevich, E.; Wooley, A.; Cheung, C.; Lieber, C. *Nature*, **1998**, *394*, 52.

[7] Dillion, A. C.; Jones, K. M.; Bekkedahl, T. A.; Kiang, C. H.; Bethune, D. S. *Nature*, **1997**, *386*, 377.

[8] Shenderova, O. A.; Zhirnov, V. V.; Brenner, D. W. *Critical Reviews in Solid State and Materials Science* **2002**, *27*, 227.

[9] Osawa E., *Kagaku*, **1970**, *25*, 854.

[10] Kroto, H. W.; Heath, J. R.; O'Brien, S. C.; Curl, R. F.; Smalley, R. H. *Nature* **1985**, *318*, 162.

[11] Satio, R.; Dresselhaus, G.; Dresselhaus, M. S. Physical properties of Carbon Nanotubes, Imperial College Press, London, 1998

[12] Dresselhaus, M. S.; Dresselhaus, G.; Saito,R. *Carbon* **1995**, *33*, 883.

[13] Guo, T.; Nikolaev, P.; Thess, A.; Colbert, D.T.; Smalley, R.E. *Chem. Phys. Lett*. **1995**, *243*, 49.

[14] Yacamàn, M. J.; Yoshida, M. M.; Rendon, L.; Santiesteban, J. G. *Appl. Phys. Lett*. **1993**, *62,* 202.

[15] Kong, J.; Soh, H. T.; Cassell, A. M.; Quate, C. F.; Dai H. *Nature*, **1998**, *395*, 878.

[16] Journet, C.; Bernier, P. *Appl. Phys. A* **1998**, *67*, 1.

[17] Fields, C. L.; Pitts, J. R.; Mischler, D.; Bingham, C.; Lewandowski, A.; Schulz, D. L.; Bekkedahl, T. A.; Jones, K. M.; Heben, M. J. Proceedings of the 8th International

Symposium on Solar Thermal Concentrating Technologies (Köln, Germany: October 6-11, 1996)

[18] Hsu, W. K.; Terrones, M.; Hare, J.P.; Terrones, H.; Kroto, H.W.; Walton, D.R.M. *Chem. Phys. Lett*. **1996**, *262*, 161.

[19] Li, Y. L.; Yu, Y. D.; Liang, Y. J. *Mater. Res*. **1997**, *12*, 1678.

[20] Kuznetsov, V. L.; Usoltseva, A. N.; Chuvilin, A. L. *Phys. Rev. B* **2001**, 64, 235401.

[21] Liu, J.; Rinzler, A. G.; Dai, H.; Hafner, J. H.; Bradley, R. K.; Boul, P. J.; Lu, A.; Iverson, T.; Shelimov, K.; Huffman, C.B.; Rodriguez-Macias, F.; Shon, Y.-S.; Lee T.R.; Colbert, D.T.; Smalley, R.E. *Science* **1998**, *280*, 1253.

[22] Durjardin, E.; Ebbesen, T. W.; Krishnan, A.; Treacy: M. M. J. *Adv. Mater*. **1998**, *10*, 611.

[23] Vaccarini, L.; Goze, C.; Aznar, R.; Micholet, V.; Journet, C.; Bernier, P. *Synthetic. Metals*. **1999**, *103*, 2492.

[24] Zhang, M.; Yudasaka, M.; Iijima, S. *J. Phys. Chem. B* **2004**, *108*, 149.

[25] Chiang, L. W.; Brinson, B. E.; R Smalley,. E.; Margrave, J. L.; Hauge, R. H. *J. Phys. Chem. B* **2001**, *105*, 1157

[26] Bandow, S.; Asaka, S.; Zhao, X.; Ando, Y. Appl. Phys. A 1998, 67, 23.

[27] Duesberg, G. S.; Muster, J.; Krstic, V.; Burghard, S M.. Appl. Phys. A 1998, 67, 117.

[28] Thess, A. et al., Science, 1996, 273, 483.

[29] Girifalco, L. A.; Hodak, M.; Lee, R. S. Phys, Rev. B, 2000, 62, 13104.

[30] Chen, Y.; Haddon, R. C.; Fang, S.; Rao, A. M.; Eklund, P. C.; Lee, W. H.; Dickey, E. C.; Grulke, E. A.; Pendergrass, J. C.; Chavan, A.; Haley, B. E.; Smalley, R. E. *J. Mater. Res*. **1998**, *13*, 2423.

[31] Lu, K. L.; Lago, R. M.; Chen, Y. K.; Green, M. L. H.; Harris, P. J. F.; Tsang, S. C. *Carbon*, **1996**, *34*, 814

[32] Moore, V. C.; Strano, M. S.; Haroz, E. H.; Hauge, R. H.; Smalley, R. E. *Nano Lett*. **2003**, *3*, 1379

[33] Matarredona, O.; Rhoads, H.;Li, Z.; Harwell, J. H.; Balzano, L.; Resasco, D. E. *J. Phys. Chem. B*, **2003**, *107*, 13357.

[34] Richard, C. *Science*, **2003**, *300*, 775.

[35] Kuznetsova, A.; Mawhinney, D. B.; Naumenko, V.; Yates Jr., J. T.; Liu, J.; and Smalley, R. E. *Chem. Phys. Lett*. **2000**, *321*, 292.

[36] Hamon, M. A.; Chen, J.; Hu, H.; Chen, Y.; Itkis, M. E.; Rao, A. M.; Eklund, P. C.; Haddon, R. C. *Adv. Mater.* **1999**, *11*, 824.

[37] Sun, Y.; Huang,W.; Lin, Y.; Fu, K.; Kitaygorodskiy, A.; Riddle, L. A.; Yu, Y. J.; Carroll, D. L. *Chem. Mater.* **2001**, *13*, 2864.

[38] Mickelson, E. T.; Chiang, I. W.; Zimmerman, J. L.; Boul, P. J.; Lozano, J.; Liu, J.; Smalley, R. E.; Hauge, R. H.; Margrave, J. L. *J. Phys. Chem.* **1999**, *103*, 4318.

[39] Zhu, J.; Kim, J.; Peng, H.; Margrave, L.; Khabashesku, V. N.; Barrera, E. V. *Nano Lett.* **2003**, *3*, 1107.

[40] Li, X-H.; Wu, B.; Huang, J.; Zhang, J.; Liu, Z.; Li, H. *Carbon*, **2002**, *41*, 1670.
[41] Huang, J.; Li, X.; Xu, J.; Li, H. *Carbon*, **2003**, *41*, 2731.

[42] Park, C.; Ounaies, Z.; Watson, K. A.; Crooks, R. E. *Chem. Phys. Lett*. **2002**, *363*, 303.

[43] Putz, K.; Mitchell, C. A.; Krishnamoorti, R.; Green, P. F. *J. Polym. Sci. B: Polym. Phys.* **2004**, *42*, 2286.

[44] O'Connell, M. J.; Boul, P.; Ericson, L. M.; Huffman, C.; Wang, Y.; Haroz, E.; Kuper, C.; Tour, J.; Ausman, K. D.; Smalley, R. E. et al., *Chem. Phys. Lett*. **2001**, *342*, 265.

[45] Star, A.; Stoddart, J. F. *Macromolecules*, **2002**, *35*, 7516.

[46] Bandyopadhyaya, R.; Nativ-Roth, E.; Regev, O.; Yerushalmi-Rozen, R. *Nano Lett.* **2002**, *2*, 25.

[47] Star, A.; Steuerman, D. W.; Heath, J. R.; Stoddart, J. F. Starched Carbon Nanotubes. *Angew. Chem., Int. Ed.* **2002**, *41*, 2508.

[48] Stéphan, C. et al, *Synthetic Metals*, **2000**, *108*, 139.

[49] Ruoff, R. S.; Lorents, D. C. Carbon 1995, 33, 925.

[50] Krishnan, A, Dujardin, E, Ebbesen, T. W.; Yianilos, P. N.; Treacy, M. M. *J. Phys Rev B* **1998,** *58*, 14013.

[51] Lu, J. P. *Phys Rev Lett* **1997**, *79*, 1297.

[52] Lier, G. V.; Alsenoy, C. V.; Doren, V. V.; Geerlings, P. *Chem Phys Lett* **2000,** *326,* 181.

[53] Goze, C.; Vaccarini, L.; Henrard, L.; Bernier, P.; Hernandez, E.; Rubio, A. *Synthetic Metals* **1999**, *103*, 2500

[54] Natsuki, T.; Tantrakarn, K.; Endo, M. *Carbon* **2004**, *42*, 39.

[55] Salvetat, J. P.; Andrew, G.; Briggs, D.; Bonard, J.; Bacsa, R. R. *Phys. Rev. Lett.* **1999**, *82*, 944.

[56] Yu, M.; Files, B. S.; Arepalli, S.; Ruoff, R. S. *Phys. Rev. Lett.* **2000**, *84*, 5552.

[57] Walters, D. A.; Ericson, L. M. *Appl. Phys. Lett.* **1999**, *74*, 3803.

[58] Yakobson, B. I.; Brabec, C. J.; Bernholc, J. *Phys. Rev. Lett.* **1996**, *76*, 2511.

[59] Zhang, P.; Lammert, P. E.; Crespi, V. H. *Phys. Rev. Lett.* **1998**, *72*, 918.

[60] Brown, S. D. M.; Corio, P.; Marucci, A.; Dresselhaus, M. S.; Pimenta, M. A. *Phys. Rev. B* **2000**, *61*, R5137.

[61] White, C. T.; Mintmire, J. W. *Nature* **1998**, *394*, 29.

[62] Thess, A. et al, *Science* **1996**, *273*, 483.

[63] Fisher, J. E.; Dai, H. D et al, *Phys. Rev. B* **1997**, *55*, R4921.

[64] Hilt, O.; Brom, H. B.; Ahlskog, M. *Phys. Rev. B* **2001**, *61*, R5129.

[65] Zhang, X. unpublished

[66] Sreekumar, T. V.; Liu, T.; Kumar, S.; Ericson, L. M.; Hauge, R. H.; Smalley, R. E. *Chem. Mater.* **2003**, *15*, 175.

[67] Andriotis, A. N.; Menon, M.; Chernozatonskii, L. *Nano Lett.* **2003**, *3*, 131.

[68] Shiraishi, M.; Ata, M. *AIP proceeding* **2002**, *633*, 251.

[69] Collins, G.P.; Zettl, A.; Bando, H.; Thess, A.; Smalley, R.E.; *Science* **1997**, 278, 100.

[70] Bonard, J.M.; Kind, H.; Stockli, T.; Nilsson, L.O. *Solid-State Electron.* **2001**, *45*, 893.

[71] Bachtold, A.; Hadley, P.; Nakanishi, T.; Dekker, C. *Science* **2001**, *294*, 1317.

[72] Shi, L.; Li, D.; Yu, C.; Jang, W.; Kim, D.; Yao, Z.; Kim, P.; Majumdar, A. *J. Heat Transfer*, **2003**, *125*, 881.

[73] Hone, J.; Whitney, M.; Zettl, A. *Synthetic Metals* **1999**, *103*, 2498.

[74] Cao, J. X.; Yan, X. H.; Xiao, Y.; Ding, J. W. *Phys. Rev. B* **2004**, *69*, 073407.

[75] Berber, S.; Kwon, Y.; Tománek, D. *Phys. Rev. Lett.* **2000**. *84*, 4613.

[76] Osman, M. A.; Srivastava, D. *Nanotechnology*, **2001**, *12*, 21.

[77] Kim, P.; Shi, L.; Majumdar, A.; Macuen, P. L. 2001, 12, 215502

[78] Hone, J.; Liaguno, M. C.; Biercuk, M. J.; Johnson, A. T.; Batlogg, B.; Benes, Z.; Fischer, J. E. *Appl. Phys. A*, **2002**, *74*, 339.

[79] Doug, B.; Mawhinney, Naumento, V.; Kuznetsova, A.; Yates, J. T. Jr. *J. Am. Chem. Soc*. **2000**, *122*, 2383.

[80] Hennrich, F.; Wellmann, R.; Malik, S.; Lebedkin, S.; Kappes, M. *Phys. Chem. Chem. Phys*. **2003**, *5*, 178.

[81] Zhao, W.; Song, C.; Pehrsson, P. E. *J. Am. Chem. Soc*. **2002**, *124*, 12418.

[82] Chen, J.; Rao, A. M.; Eklund, P. E.; Colbert, D. T.; Smalley, R. E.; and Haddon, R. C. *J. Phys. Chem. B* **2001**, 105, 2525.

[83] Bower, C.; Kleinhammes, A.; Wu, Y.; Zhou, O. *Chem. Phys. Lett*. **1998**, *288*, 481.

[84] Liu, Z.; Shen, Z.; Zhu, T.; Hou, S.; Ying, L. *Langmuir*, **2000,** 16, 3769.

[85] Yu, R. et al, *Chem. Mater*. **1998**, *10*, 718.

[86] Jia, Z.; Wang, Z.; Liang, J.; Wei, B.; Wu, D. *Carbon*, **1999**, *37*, 903.

[87] Hu, H.; Bhowmik, P.; Zhao, B.; Hamon, M. A.; Itkis, M. E.; Haddon, R. C. *Chem. Phys. Lett*. **2001**, *345*, 25.

[88] Mawhinney, D. B.; Naumenko, V.; Kuznetsova, A.; Smalley, R. E. *Chem. Phys. Lett*. **2000**, *324*, 213.

[89] Boul, P. J.; . Liu, J.; Mickelson, E. T.; Huffman, C. B.; Ericson, L. M.; Chiang, I. W.; Smith, K. A.; Colbert, D. T.; Hauge, R. H.; Margrave, J. L.; Smalley, R. E. *Chem. Phys. Lett.* **1999**, *310*, 367.

[90] Holzinger, M. et al, *Angew. Chem. Int. Ed*. **2001**, *40*, 4002.

[91] Georgakilas, V.; Kordatos, K.; Holzinger, M.; Hirsch, A. *J. Am. Chem. Soc*. **2002**, *124*, 760.

[92] Mickelson, E. T.; Chiang, I. W.; Zimmerman, J. L.; Boul, P. J.; Lozano, J.; Liu, J.; Smalley, R. E.; Hauge, R. H.; Margrave, J. L. *J. Phys. Chem.* **1999**, *103*, 4318.

[93] Niyogi, S.; Hamon, M. A.; Hu, H.; Zhao, B.; Bhowmik, P.; Sen, R.; Itkis, M. E.; Haddon, R. C. *Acc. Chem. Res*. **2002**, *35*, 1105.

[94] Wildoer, J.W.G.; Venema, L.C.; Rinzler, A.G.; Smalley, R.E.; Dekker, C. *Nature,* **1998**, *391*, 59.

[95] Kataura, H. *Synth. Metals* **1999**, *103,* 2555.

[96] Bandow, S. *Phys. Rev. Lett.* **1998**, *80*, 3779

[97] Alvarez, L.; Righi, A.; Rols, S.; Anglaret, E.; Sauvajol, J. L.; Munoz, E.; Maser, W. K.; Benito, A. M.; Martinez, M. T.; de la Fuente, G. F. *Phys. Rev. B* **2001**, *63*, 153401.

[98] Hamon, M. A. *Adv. Mater*. 1999, *11*, 834.

[99] Monthioux, M.; Smith, B.W.; Burteaux, B.; Claye, A.; Fischer, J. E.; Luzzi, D. E. *Carbon*, **2001**, *39*, 1251.

[100] Hu, J. T.; Odom, T W; Lieber, C. M. *Acc. Chem. Res*. **1999**, *32*, 435.

[101] Odom, T. W.; Huang, J. L.; Kim, P.; Lieber, C. M. *Nature* **1998**, *391*, 62.

[102] O'Connell, M. J.; M. J.; Bachilo, S. M.; Huffman, C. B.; Moore, V. C.; Strano, M. S.; Haroz, E. H.; Rialon, K. L.; Boul, P. J.; Noon, W. H.; Kittrell, C.; Ma, J.; Hauge, R. H.; Weisman, R. B.; Smalley, R. E. *Science* **2002**, *297*, 593.

[103] Schaefer, D.W. *Science* **1989**, *243*, 1023.

[104] Zhou, W.; Islam, M. F.; Wang, H.; Ho, D. L.; Yodh, A.G.; Winey, K. I.; Fischer, J. E. *Chem. Phys. Lett.* **2004**, *384,* 185.

[105] Hobbie, E. K.; *NIST/NASA Purity and Dispersion Measurement Issues Workshop on Single-Wall Carbon Nanotubes*, NIST, 27–29 May, **2003**

[106] Schaefer, D.W.; Zhao , J.; Brown, J.M.; Anderson , D. P.; Tomlin, D. W.; *Chem. Phys. Lett*. **2003**, *375*, 369.

[107] Wang, T. Light *Scattering Study on Single Wall Carbon Nanotube (SWNT) Dispersions, MS thesis*, School of Polymer, Textile and Fiber Engineering, Georgia Institute of Technology, Atlanta, GA, 30332.

[108] Bottani, C. E.; Bassi, A. L.; Beghi, M. G. *Phys. Rev.B* **2003**, *67*, 155407.

[109] Zhang, X.; Liu, T.; Sreekumar, T. V.; Kumar, S.; Moore, V. C.; Hauge, R. H.; Smalley, R. E. *Nano Lett.* **2003**, *3*, 1285.

[110] Vaccarini, L.; Desarmot, G.; Almairac, R.; Tahir, S.; Goze, C.; Bernier, P. *AIP Conference Proceedings* **2000**, *544*, 521.

[111] Ounaies, Z.; Park, C.; Wise, K. E.; Siochi, E. J.; Harrison, J. S. *Composites Science and Technology* **2003**, *63*, 1637.

[112] Du, F.; Fischer, J. E.; Winey, K. I. *J. Polym. Sci., B: Polym. Phys*. **2003**, *41*, 3333.

[113] Curran, S.; Ajayan, P. M.; Blau, W.; Carroll, D. L.; Coleman, J.; Dalton, A. B.; Davey, A. P.; McCarthy, B.; Strevens, A. *Adv.Mater*. **1998**, *10*, 1091.

[114] Biercuk, M.J et al, *Appl. Phys. Lett*. **2002**, *80*, 2767.

[115] Ramasubramaniam, R.; Chen, J.; Liu, H. *Appl. Phys. Lett*. **2003**, *83*, 2928.

[116] Lordi, V.; Yao, N.; Wei, J. *Chem. Mater*. **2001**, *13*, 733.

[117] Gao, B.; Kelinhammes, A.; Tang, X. P.; Bower, C.; Wu, Y.; Zhou, O. *Chem. Phys. Lett.* **1999**, *307*, 153.

[118] Pederson, M. B. J. *Phys. Rev. Lett*. **1992**, *69*, 2689.

[119] Dillon, A. C.; Jones, K. M.; Bekkedahl, T. A.; Kiang, C. H.; Bethune, D. S.; Heben, M. J. *Nature* **1997**, *386*, 377.

[120] An, K. H. *AIP Conference Proceedings* **2001**, *590*, 241.

[121] Liu, T.; Sreekumar, T. V.; Kumar, S.; Hauge, R. H.; Smalley, R. E. *Carbon* **2003**, *41*, 2440.

[122] An, K. H. et al., *Adv. Funct. Mater.* **2001**, *11*, 387.

[123] Niu, C.; Sickel, E. K.; Hoch, R.; May, D.; Tennent, H.; *Appl. Phys. Lett.* **1997**, *70*, 1480.

[124] de Heer, W. A.; Chatelain, A.; Ugarte, D. *Science* **1995**, *270*, 1179.

[125] Lee, N. S. *Diamond Relat. Materials* **2001**, *10*, 265.

[126] Choi, W. B. et al, *Appl. Phys. Lett.* **1999**, *75*, 399.

[127] Tans, S. *Nature* **1998**, *93*, 49.

[128] Klein, D.; Jensenius, H.; Kijne, J.; Bol, K. S.; *Single Molecules* **2002**, *3*, 160.

[129] Kim, P.; Lieber, C. M. *Science* **1999**, *286*, 2148.

[130] Wong, S. S.; Joselevich, E.; Woolley, A. T.; Cheung, C. L.; Lieber, C. M. Nature **1998**, *394*, 414.

[131] Wilson, M.; Madden P. A. *J. Am. Chem. Soc.* **2001**, *123*, 2101.

[132] Xu, C.; Sloan, J.; Brown, G. *Chem. Comm.* **2000**, 2427.

[133] Monthioux, M. *Carbon*, **2002**, *40*, 1809.

[134] Mittal, J.; Monthioux, M.; Allouche, H.; Stephan, O. *Chem. Phys. Lett.* **2001**, *339*, 311.

[135] Friedrichs, S.; Meyer, R. R.; Sloan, J. et al., *Chem. Comm.* **2001**, 929.

[136] Choi, S. U. S.; Zhang, Z. G.; Yu, W.; Lockwood, F. E.; Grulke, E. A. *Appli. Phys. Lett.* **2001**, *79*, 2251.

[137] Nan, C. W.; Shi, Z.; Lin, Y. *Chem. Phys. Lett.* **2003**, *375*, 666.

[138] Biercuk, M. J.; Llaguno, M. C.; Radosavljevic, M.; Hyun, J. K.; Johnson, A. T.; Fischer, J. E. *Appl. Phys. Lett.* **2002**, *80*, 2767.

[139] Hone, J.; Llaguno, M. C.; Biercuk, M. J.; Johnson, A. T.; Batlogg, B.; Benes, Z.; Fischer, J. E.; *Appl. Phys. A* **2002**, *74*, 339.

[140] Choi, E. S.; Brooks, J. S.; Eaton, D. L.; Al-Haik, M. S.; Hussaini, M. Y.; Garmestani, H.; Li, D.; Dahmen, K. *J. Appl. Phys.* **2003**, *94*, 6034.

[141] Ounaies, Z.; Park, C.; Wise, K. E.; Siochi E. J.; Harrison, J. S. *Comp. Sci. Tech.* **2003**, *63*, 1637.

[142] Kim, B.; Lee, J.; Yu, I. *J. Appl. Phys.* **2003**, *94*, 6724.

[143] Smith Jr, J. G.; Connel, J. W.; Delozier, D. M; Lillehei, P. T.; Watson, K. A.; Lin, Y.; Zhou, B.; Sun, Y. P. *Polymer* **2004**, *45*, 825.

[144] Sandler, J. K. W.; Kirk, J. E.; Kinloch, I. A.; Shaffer, M. S. P.; Windle, A. H. *Polymer* **2003**, *44*, 5893.

[145] Zhan, G.; Kuntz, J. D.; Garay, J. E.; Mukherjee, A. K *Appl. Phys. Lett.* **2003**, *83*, 1228

[146] Cadek, M.; Le Foulgoc, B.; Coleman, J. N.; Barron, V.; Sandler, J.; Shaffer, M. S. P.; Fonseca, A.; van Es, M.; Schulte, K.; Blau, W. J. *AIP Conference Proceedings* **2002**, *633*, 562.

[147] Lau, K.; Shi, S. *Carbon* **2002**, *40*, 2961.

[148] Sennett, M.; Welsh, E.; Wright, J. B.; Li, W. Z.; Wen, J. G.; Ren, Z. F. *Appl. Phys. A* **2003**, *76*, 111.

[149] Mamedov, A. A; Kotov, N. A.; Prato, M.; Guldi, D. M.; Wicksted, J. P.; Hirrch, A. *Nature Material* **2002**, *1*, 190.

[150] Mallick, P. K. *Fiber-Reinforced Composites*, Marcel Dekker, New York, 1993

[151] Liu, T.; Kumar, S. *Nano Lett.* **2003**, *3*, 647.

[152] Jin, L.; Bower, C.; Zhou, O. *Appl. Phys. Lett.* **1998**, *73*, 1197.

[153] Wlters, D. A.; Casavant, M. J.; Qin, X. C.; Huffman, C. B.; Boul, P. J.; Ericson, L. M.; Haroz, E. H.; O'Connell, M. J.; Smith, K.; Colbert, D. T.; Smalley, R. E. *Chem. Phys. Lett.* **2001**, *338*, 14.

[154] Vigolo, B.; Poulin, P.; Lucas, M.; Launois, P.; Bernier, P. *Appl. Phys. Lett.*, **2002**, *81*, 1210.

[155] Kearns, J. C.; Shambaugh, R. L. *J. Appl. Poly. Sci* **2002**, *86*, 2079.

[156] Kumar, S.; Dang, T. D.; Arnold, F. E.; Bhattacharyya, A. R.; Min, B. G.; Zhang, X. F.; Park, C.; Adams, W.; Hauge, R. H.; Smalley, R. H., *Macromolecules* **2002**, *35*, 9039.

[157] Andrews, R.; Jacques, D.; Rao, A.M.; Rantell, T.; Derbyshire, F.; Chen, Y.; Chen, J.; Haddon, R.C, *Appl. Phys. Lett*. **1999**, *75*, 1329.

[158] Vigolo, B.; Pénicaud, A.; Coulon, C.; Sauder, C.; Pailler R.; Journet, C. *Science* **2000**, *290*, 1331.

.

[159] Poulin, P.; Vigolo, B.; Launois, P. *Carbon* **2002**, *40*, 1741.

[160] Baughman, R. H. *Nature*, **2003**, *423*, 703.

[161] Dalton, A. B.; Collins, S.; Razal, J.; Munoz, E.; Baughman, R. H. J. *Chem. Mater*. **2004**, *14*, 1

CHAPTER 2

Single Wall Carbon Nanotubes Dispersion

2.1 Surfactant assisted SWNT dispersion

2.1.1 Introduction

Due to the van der Waal interactions, the SWNTs form bundles of about 20 to 30 nm diameters. The theoretical calculations indicate that this van der Waal force is as high as 500 – 900 meV per nanometer. The properties of SWNT bundle are different from that of individual SWNTs. For the purpose of reinforcing the matrix, in order to take full advantage of the superior SWNT mechanical properties, large interfacial area, SWNT exfoliation or at least dispersion in small diameter bundle size is essential. For making conducting SWNT composite, the large aspect ratio is the key factor to control the efficiency of SWNT. The percolation volume fraction is related to the size of SWNT. The smaller SWNT diameter will give the lower percolation level. Thus lower SWNT loading is needed. A similar phenomenon is observed in case of using SWNT as the thermal management filler for the composites. Currently, many researchers are actively working to obtain good dispersion, both using non-covalent and covalent bonding approaches. In general, physical sonication and shear mixing are used in all cases to process SWNT dispersion. From the nondestructive point of view, surfactant, polymer, as well as in situ polymerization are used to obtained homogeneous SWNT dispersion in various solvent or matrix. Enhanced dispersion of SWNT in solvent or matrix based on the chemical

modification of SWNT is a destructive approach, because it deteriorates the intrinsic properties of SWNT to a certain extent.

In this section the dispersion assisted by surfactant as well as polymer will be studied. A series of anionic, cationic, and nonionic surfactants and polymers have been studied for their ability to suspend individual single wall nanotubes. The size of the hydrophilic group of nonionic surfactant or polymer is the major factor for suspending nanotubes. With higher molecular weights, more SWNT suspension is realized because of enhanced steric stabilization with longer polymeric groups.[1] The dispersion mechanism has been studied in detail based on the sodium dodecylbenzenesulfonate (NaDDBS) and SWNT dispersion.[2] In our study, an anionic surfactant, sodium dodecyl sulfate (SDS), will be chosen to prepare aqueous SWNT dispersion. SWNT/SDS/water phase diagram has been studied by other research groups. Their results suggested that SWNT were able to form homogeneous
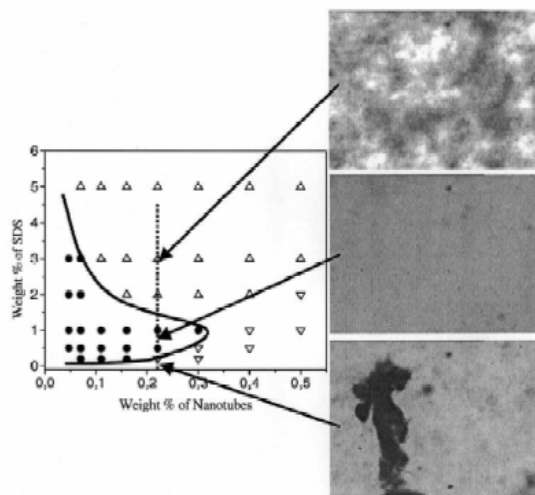
Figure 2.1 Phase diagram of SWNT/SDS/water system.[3]

dispersion with the proper ratio of SDS to SWNTs and proper concentration of SDS. The phase diagram is shown in Figure 2.1.[3]

2.1.2 Experimental

50 mg SDS (Aldrich) was prepared into 2 wt% aqueous solution at room temperature. Then 14 mg ultra purified SWNTs (CNI; lot # P0247; used without further modification; 98% purity) were put into the SDS solution. The dispersion was sonicated in bath sonicator for 72 hrs. The resulting dispersion was visually homogeneous, as shown in Figure 2.2. This dispersion was stable for several months without phase separation. Small angle X-ray diffraction, FTIR and TEM were used to study the structure of SDS/SWNT system.

200

Figure 2.2 Optical image of SWNT/SDS homogeneous dispersion.

2.1.3 Results and Discussion

Study of molecular organization of surfactant at the solid-liquid interface indicates that quaternary ammonium surfactants showed ordered structure, hemi-cylinder on crystalline hydrophobic substrates, full cylinder on mica, and sphere on amorphous

silica.[4] Sodium dodecyl sulfate was found forming the hemi-cylinder ordered structure on the graphite-solution interface.[5] It was also found that SDS formed ordered striation either perpendicular or tilted at a certain angle to the MWNT axis[6]. In order to study the organization of SDS on the SWNT surface, this dispersion was processed into a film with PVA as the matrix. This film was subsequently stretched mechanically. The small angle X-ray diffraction of this stretched SWNT/SDS/PVA film shows an interesting four-point pattern, as shown in Figure 2.3.

a

b
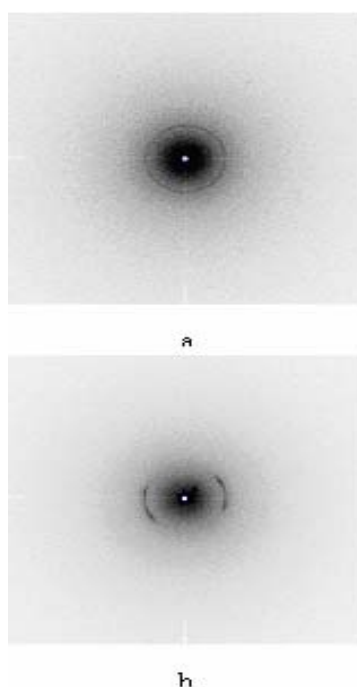
Figure 2.3 SAXD pattern of SWNT/SDS/PVA film, a) un-stretched, b) stretched

The d-spacing corresponding to these four-point spots is 3.9 nm, which is assigned to the a-axis of SDS crystal. It suggests that the SDS crystals arrange themselves in a specific manner on the surface of SWNT; the a-axis tilts at a certain angle with respect to the SWNT axis. If the SDS crystals randomly arrange on the SWNT, a two-arc pattern with the most intensive point in the equatorial direction will be observed, as in the

case of a PEO/SDS nanofiber.[7] The azimuthal integration results of SWNT/SDS/PVA films SAXD near d-spacing 3.9 nm are shown in Figure 2.4.
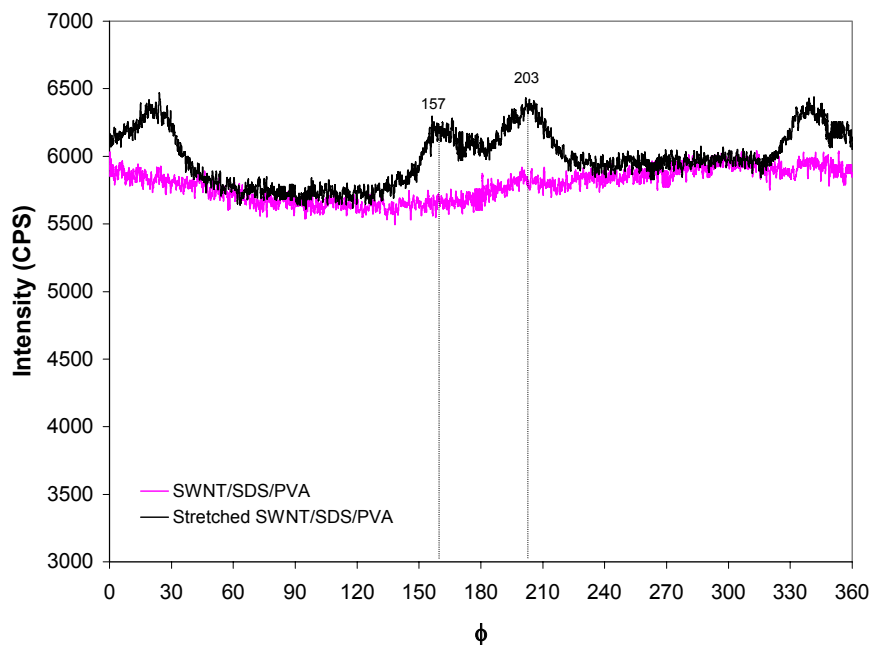
Figure 2.4 Azimuthal scan at 3.9 nm d-spacing of SWNT/SDS/PVA film SAXD pattern.

The intensity is nearly constant with angle ϕ in case of un-stretched film sample, which suggests the random orientation of SWNT within the film plane. After mechanical stretching, the SWNT is oriented along the stretching direction. The intensity profile shows four peaks along the angle ϕ, which appear around 23, 157, 203 and 337 degrees from equatorial direction, respectively. This result suggests that the SDS crystals organize themselves in ordered structure, and their a-axis is tilted about 23° with the respect to transverse SWNT axis direction. The scheme for this structure is shown in Figure 2.5.
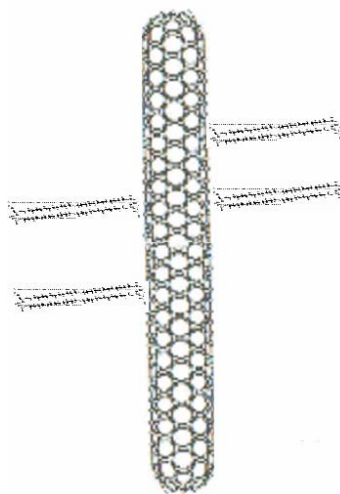
Figure 2.5 Scheme of SDS molecular arrangement on the SWNT surface.

Polarized FTIR can be used to determine molecular orientation. The vibration differences between CH_2 and SO groups in SDS provide the way to verify the self-organization of SDS with respect to SWNT. The CH_2 stretching vibration is perpendicular to the main chain of SDS, while the SO stretching vibration is along the main chain direction. So, symmetric stretch absorption peak of CH_2 located around 2860 cm^{-1} and symmetric stretch absorption peak of SO located at 1220 cm^{-1} are used to characterize the SDS self organization in stretched film.[8] The polarized FTIR spectra of Stretched SWNT/SDS/PVA film are shown in Figure 2.6. The result indicates that the intensity of CH_2 absorption peak is larger when polarizer is in the 0° direction than in 90° (The 0° of polarizer is defined as the polarizer and stretching direction parallel to each other. The 90° of polarizer is defined as the polarizer and stretching direction perpendicular to each other.). This would happen when CH_2 stretching vibration predominates in the 0 degree direction. Considering that after film stretching the a-axis of SDS crystal is at about 23° with respect to the normal
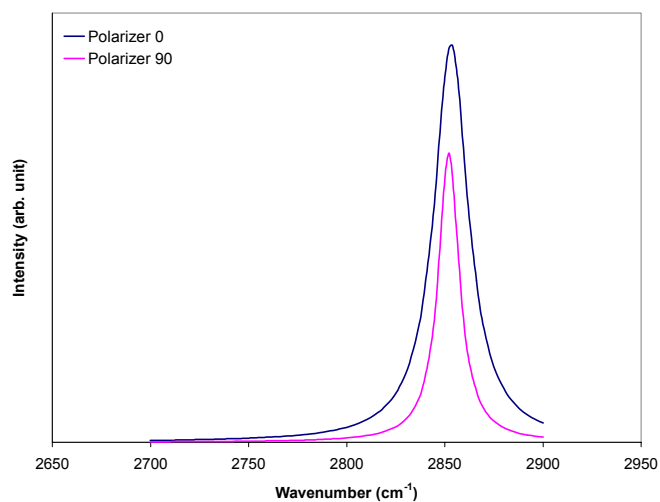
Figure 2.6 Polarized FTIR spectrum of CH_2 asymmetric stretch vibration in SDS. FTIR spectra obtained on stretched SWNT/SDS/PVA film.
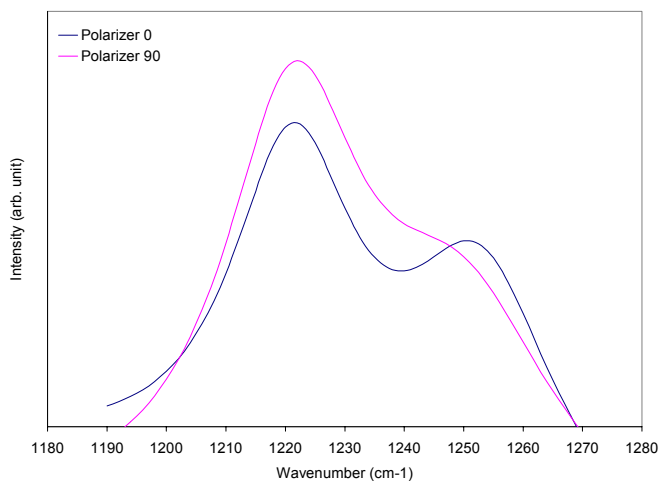
Figure 2.7 Polarized FTIR spectrum of SO stretch vibration in SDS. FTIR spectra obtained on stretched SWNT/SDS/PVA film.

SWNT axis direction and hydrocarbon chain of SDS is 14° with respect to the crystallographic direction [1 0 0],[9] the CH_2 stretching vibration does predominate along the film stretching direction. The opposite result is obtained for the SO group, as shown

in Figure 2.7 in which SO absorption peak intensity is larger at polarizer 90° direction. The polarized FTIR characterization confirms the SDS self-arrangement in an ordered form on the SWNT surface, although it doesn't explain exact configuration. From the high-resolution transmission electron microscopy characterization, the structure of SWNT/SDS can be directly imaged, as shown in Figure 2.8.

2 nm
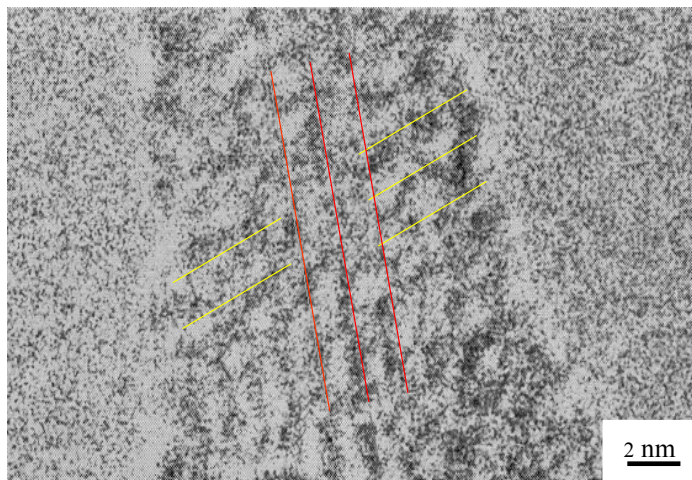
Figure 2.8 High-resolution TEM image of SWNT/SDS system: red lines show tube walls and yellow lines show SDS crystals.

A drop of this dispersion was dropped on the   SEM stub for observation. The single wall carbon nanotube bundles showed alewife shape structure (Figure 2.9), which was similar to the alewives reported from SWNT dispersion in oleum.[10] No further characterization was carried out on these alewives.

When one drop of this SWNT/SDS dispersion was dropped into PVA solutions using a glass pipette, thin films of different shapes were formed based on the concentration of PVA solution. When this dispersion was dropped into 0.1 wt%
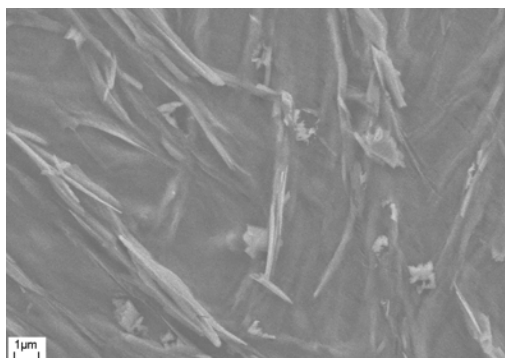
Figure 2.9 Alewife shape of SWNT in SDS aqueous dispersion.

PVA solution, the SWNT dispersion automatically spread out forming homogeneous round ultra thin film (as shown in Figure 2.10). We deposited 20 layers of such thin films together forming a thicker film. The thickness thin film was about 200 nm based on the overall measurement of the thickness of stacked film. When the SWNT dispersion was dropped into a 5 wt% PVA solution, a star shaped film was formed instead of a circular film. Also, the film formed in 5 wt% PVA solution was thicker than that formed in 0.1 wt% PVA solution. The edge of this film was composed of twigs unlike a uniform edge in 0.1 wt% PVA solution. The films formed in PVA solutions between 0.1 and 5 wt% showed intermediate shapes and thickness. The surface tension of SWNT / SDS aqueous dispersion is lower than that of PVA solution. The decrease in the interfacial tension between the PVA solution and air is the driving force for the SWNT / SDS dispersion to spread out. The tendency of PVA replacing SDS or the tendency of SDS to dissolve in water is thought to be the reason for the formation SWNT/PVA thin film. The viscosity

differences among various concentration of PVA solution is thought to be the major

factor contributing to the shape and thickness of SWNT / PVA films.
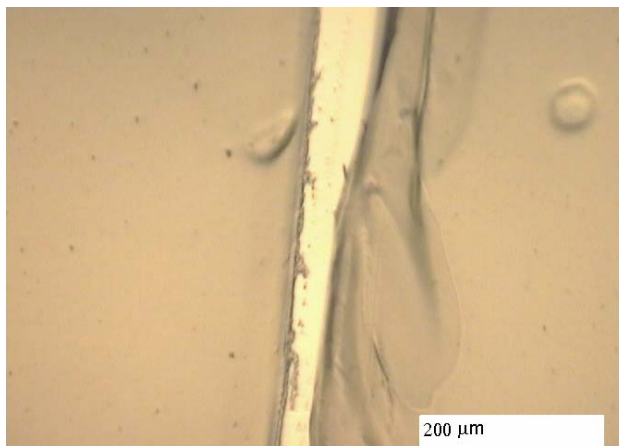
Figure 2.10 Ultra thin film forming through dropping SWNT/SDS aqueous dispersion into PVA solution.

2.2 Polymer Assisted SWNT Dispersion

From reinforcement point of view, surfactant assistant SWNT dispersion is not

the best option, because the small residual surfactant molecules in the matrix will weaken

the reinforcing efficiency of SWNT. For making polymer/SWNT reinforced composites,

polymer assisted SWNT homogeneous dispersion is the best choice. Polymer assisted

SWNT dispersions have been studied by several research groups. It has been found that

small amount of PVP, PPE, and PmPV incorporated with SWNT can render

homogeneous dispersion. In our study, PVA was chosen to make dispersion with SWNT

in water, DMSO, or water/DMSO mixed solvent systems. For comparison, in these

solvent systems, the dispersions with or without the presence of PVA were prepared.

Typically, the dispersion was prepared as follows: 1) disperse SWNT in the solvent and

sonicate for 24 hrs, 2) stop the sonication, 3) shear mix the dispersion using heavy-duty mixer for 72 hrs, 4) for those dispersions containing PVA, PVA solution was add to the dispersion prior to step 3. The resulting dispersions show that in the presence of PVA the dispersion quality is much better than those without PVA. The optical micrographs of these dispersions are shown in Figure 2.11.
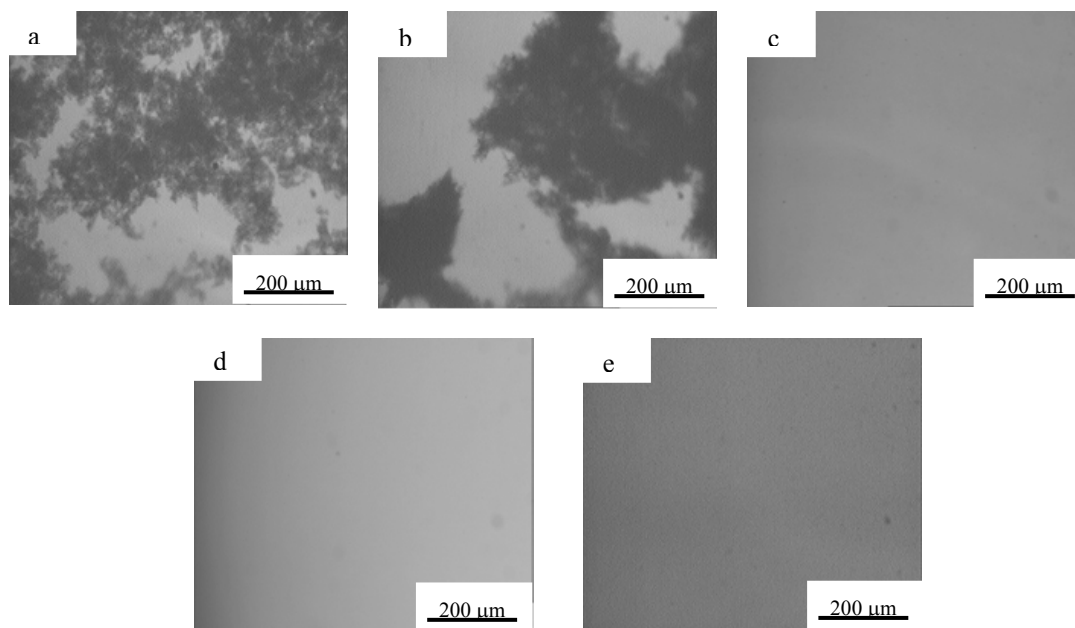
Figure 2.11 Optical micrographs of SWNT dispersions: a) DMSO/SWNT, b) H_2O/SWNT, c) DMSO/SWNT/PVA, d) DMSO/SWNT/H_2O/PVA, e) H_2O/SWNT/PVA.

As described in 1.10, UV-vis spectroscopy is a powerful tool to qualitatively monitor the degree of dispersion. The UV-vis spectra of these dispersions (Figure 2.12) indicate that in the presence of PVA, the van Hove transition peaks of SWNT are clearly observed, but it is not the case for the dispersion systems without PVA. This suggests that

a homogeneous dispersion containing small size SWNT bundles was obtained in PVA containing systems. The mechanism of PVA assisted dispersion is not clear at the current stage. But since PVA can be used as an emulsion stabilizer[11], it can be concluded that the PVA works in a similar manner as surfactant. It exposes its hydrophobic main chain to the SWNT and extends its hydrophilic OH group towards the solvent. In such a manner, the physical screening effect of PVA prevents the re-aggregation of SWNT bundles once they are broken down by physical force, sonication or shearing. .
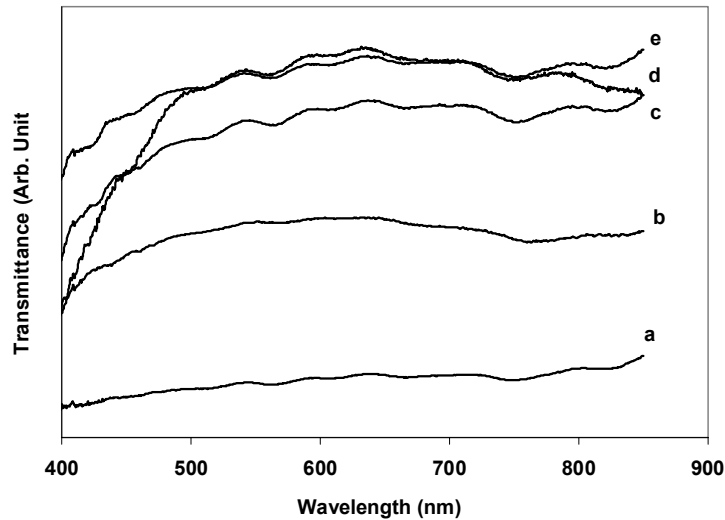
Figure 2.12 UV-vis spectra of various SWNT dispersions. a) DMSO/SWNT, b) H_2O/SWNT, c) SWNT/H_2O/PVA, d) DMSO/SWNT/PVA, e) DMSO/SWNT/H_2O/PVA.

2.3 Quantitative characterization of SWNT dispersion

2.3.1 Introduction

Due to high electrical conductivity, SWNTs can be used as conducting filler to improve the electrical performance of various matrices, such as polymer, ceramic, etc. Depending on the conductivity, these materials can find applications either in

electrostatic dissipation, electrical printing and electromagnetic interference shielding. Except for the doping or tunneling functional conducting filler, general conducting mechanism for conducting filler is the formation of a network path. Once these paths have been formed, the conductivity of the composite increases. Percolation theory is used to describe that there is a critical concentration or percolation threshold at which a conductive path is formed in the composite causing the material to convert from a capacitor to a conductor. A great deal of research has been done to investigate the electrical conductivity of polymer/SWNT composites, especially their percolation behavior. Z. Ounaiesa, et al. prepared polyimide/SWNT composite through in situ polymerization under sonication.[12] The SWNT used in their study was produced by laser ablation at Rice University. 0.05 vol % percolation volume fraction was observed in this system. J-M. Beniot et al. prepared PMMA/ SWNT (produced by arc discharge) through 1) sonicating PMMA and SWNT in toluene and 2) drop-casting thin film on glass substrate. In their studies, 0.33 vol.% percolation volume fraction was obtained.[13] Epoxy and SWNT (HiPCO^{TM}) composite film was made through ultrasonicating epoxy, SWNT, and DMF dispersion. The percolation volume fraction for this system was found to be between 0.1 and 0.2 vol.%.[14] Homogeneous poly (phenylene ethynylene) (PPE), SWNT and chloroform dispersion was obtained by vigorous shaking or with mild bath sonication for a short period. With assistance of the PPE/SWNT dispersion, homogeneous carbon nanotube/polymer (PC, PS, etc.) composites were fabricated using noncovalently functionalized, soluble single wall carbon nanotubes. These composites show dramatic improvements in the electrical conductivity with very low percolation threshold, ~0.05–

0.1 wt% of SWNT loading[15]. At even high SWNT loading, the electrical conductivity can reach several tens of S/m, which can find lots of potential applications (Figure 2.13).
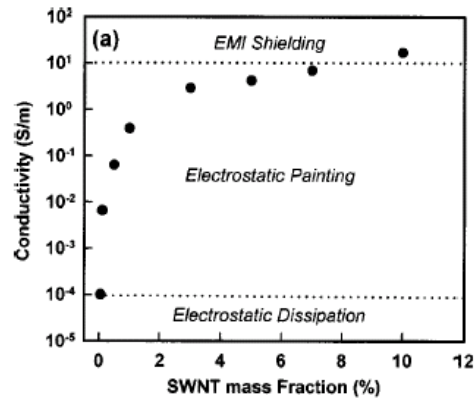
Figure 2.13 Conductivity vs SWNT loading for PPE-SWNT/PS composite.[15]

Several other groups have also reported an increase in the electrical conductivity for SWNT/ polymer composites. For example, Barraza et al[16] reported an increase of the electrical conductivity of an SWNT/polystyrene composite from 10^{-14} S/ m at 4% nanotube loading to 10^{-4} S/m at 8.5% nanotube loading, corresponding to a threshold of approximately 6%. Du et al found percolation at 2 vol% for unaligned SWNT in PMMA matrix.[17] Besides the systems mentioned above, the percolation behavior of SWNT in various matrices has been studied, such as Gum Arabic[18], poly (3-octythiophene) (P3OT)[19], alkoxysilane terminated amide acid polymer,[20] and ceramics.[21]

The reported SWNT electrical percolation levels are inconsistent among different research groups, even for the same polymer system. The reasons may be: 1) different types of SWNT, which are tubes produced by laser ablation, arc discharge or the HiPCO process; 2) dispersion prepared through different sonication power and time; 3) different

polymer matrices; and 4) different solvents. However, the basic conclusion is that the dispersion quality and the degree of SWNT exfoliation within the polymer matrix affect the electrical percolation threshold. The conducting filler percolation level within the matrix is controlled by the geometry of the conducting filler[22, 23]. In SWNT dispersion preparation, different sonication time and power will result in SWNT bundles of varying length and diameter. In the different polymer and solvent systems, SWNT bundle size may also be different. The SWNT geometric factor is the key factor for controlling the percolation volume fraction. Therefore, a method has been developed to assess the SWNT dispersion quality by monitoring the conductivity change in a given SWNT dispersion system. Z. Ounaiesa et al. have summarized the relation of SWNT geometric size with the percolation volume fraction.[12]

The nanotubes are modeled as capped cylinders of radius r and length l, in the limit of very high aspect ratio ($r/l<<1$). The volume of these nanotubes (V_{cyl}) is expressed as:

$$V_{cyl} = \frac{4}{3}\pi r^3 + \pi l r^2 \qquad (2\text{-}1)$$

The excluded volume of an object is defined as the region of space into which the center of another similar object may not penetrate. For capped cylinders, this volume (V_{ex}) is expressed as:

$$V_{ex} = \frac{32}{3}\pi r^3 + 8\pi l r^2 + 4l^2 r\langle\sin(\lambda)\rangle \qquad (2\text{-}2)$$

where the $<\sin(\lambda)>$ term describes the degree of alignment of the rods, λ being the angle between two rods. This term ranges from 45 degree for the isotropic samples of interest here to 0 degree for aligned samples. For isotropic suspensions of nanotubes, it has been predicted that the percolation threshold (ρ_c) (i.e. the critical number density of capped cylinders at percolation) scales as the inverse of the excluded volume:

$$\rho_c \propto \left(V_{ex}\right)^{-1} \tag{2-3}$$

This proportionality becomes exact in the limit of $r/l <<0$. Therefore, the total volume of capped cylinders (V_c), at percolation is:

$$V_c = \rho_c V_{cyl} \tag{2-4}$$

Dividing by the total volume of the sample cell yields the volume fraction at percolation (ϕ_c):

$$\phi_c = \rho_c V_{cyl} / V_{tot} \tag{2-5}$$

The Table 2.1 shows the calculated percolation volume percentage as the function of diameter and length.

Table 2.1 Theoretical prediction of percolation volume fraction as a function of SWNT length and SWNT bundle diameter.

D (nm)		L (nm)	Vc (%)		L (nm)	Vc (%)		L (nm)	Vc (%)
1		200	0.2751		500	0.1112926		1000	0.05586
3		200	0.79543		500	0.32888712		1000	0.16631
5		200	1.27929		500	0.5400651		1000	0.2751
7		200	1.7303		500	0.7450978		1000	0.38227
9		200	2.15157		500	0.9442415		1000	0.48786
11		200	2.54587		500	1.13773852		1000	0.59189
13		200	2.91563		500	1.32581816		1000	0.6944
15		200	3.26298		500	1.50869757		1000	0.79543
17		200	3.58983		500	1.68658252		1000	0.89499
19		200	3.89789		500	1.85966815		1000	0.99314

D = SWNT bundle diameter

L = SWNT bundle length

V_c = Percolation volume fraction percentage

The percolation behavior is supposed to be observed in a series of volume fraction SWNT dispersions or SWNT/polymer composite. Then the conductivity of the dispersion should dramatically increases as described by the following equation:

$$\sigma_c \propto (\phi - \phi_c)^{\beta} \qquad\qquad (2\text{-}6)$$

After curve fitting the experimental data near the percolation volume fraction range, the critical volume fraction can be obtained. Introducing this percolation volume fraction into

the geometry-percolation equation, the aspect ratio of individual SWNT or SWNT bundle can be estimated. Furthermore, if either the diameter or the length is known, the other parameter can be calculated.

2.3.2 Experimental

In order to obtain quantitative information on SWNT dispersion in the polymer matrix, a set of PVA/SWNT films with SWNT weight fraction ranging from 0.0005 to 0.1 were prepared. The SWNT used in this work was received from CNI (lot # P0247) and used without further modification. Based on TGA, the purity of this SWNT was about 98%. Polyvinyl alcohol (PVA) was received from Kuraray Specialities Europe GMBH with degree of hydrolysis 98% and molecular weight of 200,000 g/mol. DMSO was purchased from Fisher Scientific. 70 mg SWNT was dispersed in 50 ml DMSO and sonicated in bath sonicator. Meanwhile, 0.7 g PVA was dissolved into 20 ml DMSO at 95 °C. After 24 hour sonication of SWNT/DMSO dispersion, PVA solution was gradually added into this dispersion. At the same time, rigorous shear mixing and bath sonication was applied on the dispersion. Sonication was stopped after 36 hours, but mixing continued for another 84 hours. 4 wt% PVA solution was prepared for diluting the SWNT/PVA dispersion. The 10 ml original PVA/SWNT dispersion with 100 mg PVA and 10 mg SWNT solid content was poured into 5 cm diameter teflon petri dish. This dispersion formed into a film after vacuum drying at 50 °C for 5 days. PVA solution with 100 mg solid contend was added into 10 ml original dispersion to make SWNT/ PVA film with 5 wt% SWNT. The mixed PVA solution and PVA/SWNT dispersion were

sheared using a stirrer for 30 minutes before vacuum drying. In a similar way, films with other SWNT concentrations (1%, 0.5%, 0.1%, 0.05% and 0.01%) were prepared.

2.3.3 Results and Discussion

Four-probe sourcemeter was used to measure the conductivities of these PVA/SWNT composite films. The relationship between the composite conductivity and SWNT concentration in the film is shown in Figure 2.14.
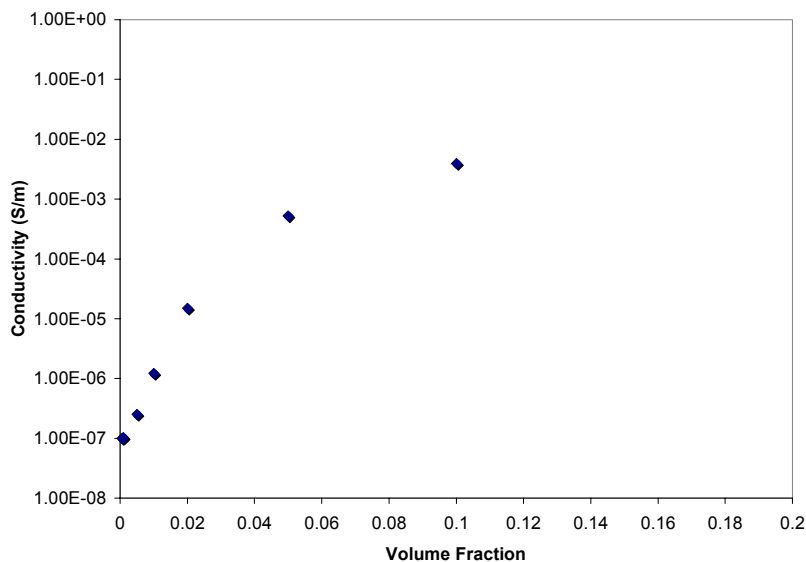
Figure 2.14 Percolation behavior of PVA/SWNT composite films.

The conductivity showed percolation behavior around 2 wt%. The equations 2-1 to 2-6 are used to describe the conductivity change with respect to conducting filler volume fraction. Here the SWNT density is assumed to be 1.3 g/cm^3. Since the PVA density is also around 1.3 g/cm^3, the SWNT volume fraction is regarded equal to weight fraction in the composite films. After curve fitting equation (2-6) with the experimental data, the exponential constant β is estimated to be 2.17, which is comparable to the result

in the literature.[13] The critical percolation volume fraction is estimated to be 1.75 v%. The length of HiPCO[TM] SWNT is around 200 nm after sonication.[24] So, with the SWNT percolation threshold of 1.75 v% and 200 nm in length, the theoretical bundle diameter of the SWNT is determined to be about 7 nm (Table 2.1). In order to verify the reliability of SWNT bundle size predicted based on the percolation theory, transmission electron microscope has been done on this dispersion. Small drop of diluted SWNT/PVA dispersion was cast into an ultra thin film on the micro grid. Jeol-100 model transmission electron microscope was used in the bright field imaging mode at operation voltage 100 KV. The TEM image of the SWNT bundle is shown in Figure 2.15. The diameters of the SWNT bundles were estimated to be about 7 nm, which is quite consistent with the result from the percolation prediction.
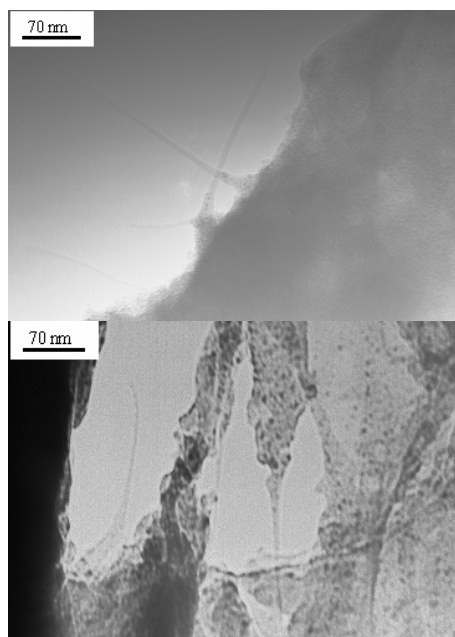
Figure 2.15 Transmission electron microscope studies of PVA/SWNT dispersion.

REFERENCES

[1] Moore, V. C.; Strano, M. S.; Haroz, E. H.; Hauge, R. H.; Smalley, R. E. *Nano Lett*. **2003**, *3*, 1379.

[2] Matarredona, O.; Rhoads, H.; Li, Z.; Harwell, J. H.; Balzano, L.; Resasco, D. E. *J. Phys. Chem. B* **2003**, *107*, 13357.

[3] Poulin, P.; Vigolo, B.; Launois, P. *Carbon* **2002,** *40*, 1741.

[4] Manne, S.; Gaub, H. E. *Science* **1995**, *270*, 1480.

[5] Wanless, E. J.; Ducker, W. A. *J. Phys. Chem*. **1996**, *100*, 3207.

[6] Richard, C. *Science* **2003**, *300*, 775.

[7] Dror, Y.; Salalha, W.; Kalfin, R. L.; Cohen, Y.; Yarin, A. L.; Zussman, E. *Langmuir* **2003**, *19*, 7012.

[8] Amalvy, J. I.; Soria, D. B. *Progress in Organic Coatings* **1996**, *28*, 279.

[9] Smith, L. A.; Hammond, R. B.; Roberts, K. J.; Machin, D.; Mcleod, G. *J. Molecular Structure* **2000**, *554*, 173.

[10] Ramesh, S.; Ericson, L. M.; Davis, V. A.; Saini, R. K.; Kittrell, C.; Pasquali, M.; Billups, W. E.; Adams, W. W.; Hauge, R. H.; Smalley, R. E, *J. Phys. Chem. B* **2004**, *108*, 8794.

[11] Sakurada, I. *Polyvinyl Alcohol Fibers*, Marcel Dekker Inc. New York 1985

[12] Ounaies, Z.; Park, C.; Wiseb, K. E.; Siochi, E. J.; Harrison, J. S. *Composites Science and Technology* **2003**, *63*, 1637.

[13] Beniot, J. M.; Corraze, B.; Lefrant, S.; Blau, W. J.; Bernier, P.; Chauvet, O. *Synthetic Metals* **2001**, *121*, 1215.

[14] Biercuk, M. J.; Llaguno, M. C.; Radosavljevic, M.; Hyun, J. K.; Johnsond, A. T. *Appl. Phy. Lett*. **2002**, *80*, 2767.

[15] Ramasubramaniama, R.; Chen, J.; Liu, H. *Appl. Phys. Lett*. **2003**, *83*, 2928

[16] Barraza, H. J.; Pompeo, F.; Orear, E. A.; Resasco, D. E. *Nano Lett*. **2002**, *2*, 797.

[17] Du, F,; Fisher, J. E.; Winey, K. I. *J. Polym. Sci. B* **2003**, *41*, 3333.

[18] Grunlan, J. C.; Mehrabi, A. R.; Bannon, M. V.; Bahr, J. L. *Adv. Mater*. **2004**, *16*, 150.

[19] Kymakis, E.; Alexandou, I.; Amaratunga, G. A.; *Synthetic. Metals* **2002**, *127*, 59.

[20] Smith, J. G.; Connell, J. W.; Delozier, D. M ; Lillehei, P. T.; Watson, K. A.; Lin, Y.; Zhou, B.; Sun, Y. P. *Polymer* **2004**, 45, 825.

[21] Rul, S.; Lefevre-schlick, F.; Capria, E.; Laurent, C.; Peigney, A. *Acta Materialia* **2004**, *52*, 1061

[22] Munson-McGee, S. H. *Phys. Rev. B* **1991**, *43*, 3331.

[23] Garboczi, E. J.; Snyder, K. A.; Douglas, J. F.; Thorpe, M. F. *Phys. Rev. E* **1995**, *52, 819.

[24] O'Connell, M. J.; Boul, P.; Ericson, L. M.; Huffman, C.; Wang, Y.; Haroz, E.; Kuper, C.; Tour, J.; Ausman, K. D.; Smalley, R. E. *Chem. Phys. Lett.* **2001**, *342*, 265.

CHAPTER 3

Poly (vinyl alcohol) /SWNT Composite Film

3.1 Introduction

Exceptional mechanical and electrical properties of single wall carbon nanotubes (SWNTs) as well as their high aspect ratio and low density make them an ideal candidate for developing functional and structural polymer/SWNT composites[1]. To achieve full reinforcing potential of SWNTs, they must be well dispersed and exhibit good interfacial strength with the matrix. Also, considering the fact that the shear modulus of large diameter SWNT ropes is relatively low[2] (shear modulus of 20 nm diameter ropes is about 1 GPa and that for the 4 nm diameter ropes it is about 6 GPa), SWNT exfoliation is also important in processing composites with good mechanical properties. In addition, in oriented systems (e.g. fibers), to achieve high modulus, SWNT orientation is also important.[3] Petroleum pitch[4], PMMA[5], PBO[6], and polypropylene[7] are examples of matrix systems where SWNTs have been dispersed successfully, and the oriented composite fibers with improved mechanical properties have been processed. To preserve SWNT dispersion, a layer-by-layer (LBL) deposition method was reported for processing isotropic polymer/SWNT composites.[8] Super tough PVA/SWNT fibers[9], processed with the aid of surfactant, containing 60 wt% SWNT have also been reported. In chapter 2, the SWNT homogeneous dispersion has been studied. In this chapter, the polymer/SWNT

composite keeps the homogeneous SWNT dispersion and enhanced mechanical performance will be studied. This chapter presents PVA/PVP/SDS/SWNT composite films exhibiting good nanotube dispersion and load transfer from polymer matrix to the carbon nanotubes.

3.2 Experiment

Poly (vinyl alcohol) (from Aldrich, molecular weight range 124,000 - 186,000 g/mole, 99+% hydrolyzed) was dissolved in distilled water at 90 °C (to give 1 wt% solution) and subsequently cooled down to room temperature. The HiPco SWNT aqueous dispersion assisted by sodium dodecyl sulfate (SDS), and poly (vinyl pyrrolidone) (PVP) was prepared according to the previously published procedure.[10] SWNTs were dispersed in SDS aqueous (1 wt%) solution followed by homogenization, ultra-sonication, and ultra-centrifugation. To the decanted supernatant, 0.1 wt% concentration of PVP-40 (molecular weight 40,000 g/mole) was added, and the mixture was incubated at 50 °C for 12h. Then residual SDS and PVP were removed by cycling through a tangential flow filtration system with a 100,000 g/mole molecular weight cut-off polyethersulfone membrane. In this process, individual nanotubes or bundles containing few nanotubes are covered by SDS and PVP. The association between PVP and SWNT is reported to be quite robust, resulting in the disappearance of the NMR signal for the wrapped PVP polymer, due to a combination of factors.[10] SWNT, SDS, and PVP concentrations in the dispersion were about 45, 16, and 75 mg/liter. Appropriate amount of PVP/SDS/SWNT aqueous dispersion was mixed with PVA solution at room temperature to give the desired 1

and 5 wt% SWNT concentration with respect to the PVA weight. The mixture was mildly sonicated (Branson water bath sonicator by Smithkline company, model number B-22-4, 125 Watts) for 1 hour at room temperature and subsequently transferred into a rotary evaporator at 40 ºC for partial water evaporation to give a concentrated PVA/PVP/SDS/SWNT. The sample containing 5 wt% SWNT (with respect to the PVA weight) has approximate composition of PVA/PVP/SDS/SWNT in the ratio of 100:8:2:5. Therefore, an aqueous control solution of PVA/PVP/SDS in the similar weight ratio was also made.

The PVA and PVA/PVP/SDS solutions, as well as PVA/PVP/SDS/SWNT dispersions were poured into Teflon Petri dishes and kept in vacuum at 60 °C for film formation until weight reached an equilibrium value. Thickness of the resulting film was about 30 μm. Tensile tests were conducted at room temperature using a Rheometric Scientific solids analyzer (RSA III) at an extension rate of 0.05 mm/s using 10 mm gage length on 2 mm wide films. Five samples were tested in each case. For tensile tests vacuum oven dried samples were conditioned in the laboratory environment (23 ºC and 35% relative humidity) for 24 hours before testing as PVA and PVP exhibit high degree of moisture sensitivity. Raman spectroscopy was done using 785 nm excitation wavelength and 1.5 mW beam power on Holoprobe Research Raman microscope made by Kaiser Optical System Inc. Raman spectroscopy was collected on films held at the desired strain in a tension frame. UV-visible spectroscopy was performed on SEE 1100 Microspectrometer.

3.3 Results and Discussion

No nanotube aggregates were observed in the optical micrograph of PVA/PVP/SDS/SWNT film (Figure 3.1). PVA is miscible with PVP in all composition range.[11] This behavior is expected to help in achieving good dispersion of the PVP wrapped nanotubes in PVA.
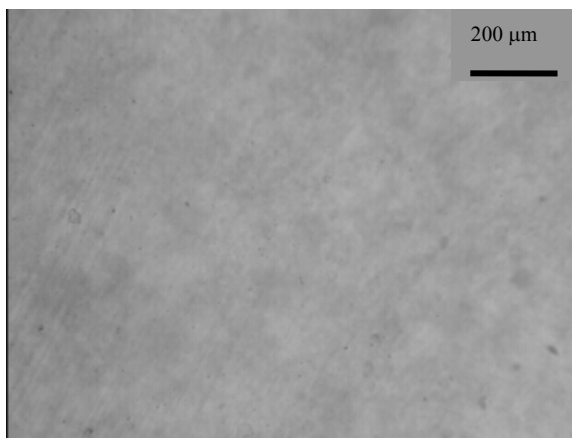
Figure 3.1 Optical micrograph of PVA/PVP/SDS/SWNT composite film containing 1 wt% SWNTs.

The UV-Visible spectrum of PVP/SDS/SWNT aqueous dispersion (Figure 3.2a) shows relatively sharp SWNT van Hove transitions[12]. The good resolved optical absorption spectrum was believed coming from the individual or small bundle of nanotubes by free from the perturbation of surrounding tubes and surfaces. Otherwise, the broadening and emerging absorption peaks would appear due to interactions between bundled tubes in side-by-side contact[13]. The individual dispersion of SWNTs was also verified by AFM. These optical absorption peaks are associated with interband transitions, which are governed by the pairs of van Hove

singularities of one dimension SWNT. Furthermore, these interband transitions are closely related to the diameter of SWNT. [14] The first and second van Hove transitions of semiconducting tube are in the range of 800 to 1400 nm and 550 to 900 nm, respectively, and the first van Hove transition of metallic tube is in the range between 400 and 600 nm as shown in Figure 3.2.[13] Based on the theoretical prediction, $E = ka_{c-c}\gamma_0 / d$, the SWNTs' diameters were calculated out to be in the range of 0.8 to 1.18 nm. Here, E is transition energy, a_{c-c} is the nearest-neighbor carbon-carbon distance, 0.144 nm, γ_0 is the nearest-neighbor carbon-carbon interaction energy, 2.9 eV[15], d is the diameter of SWNT and k is constant 2, 4, 8, 6, and 12 for 1st, 2nd and 3rd van Hove transitions in semiconducting tubes and 1st and 2nd van Hove transitions in metallic tubes, respectively[16]. This result was consistent with that obtained from theoretical calculation based on Raman RBM (Radial Breathing Mode) frequency of SWNTs in composite films[17, 18], which gave SWNTs diameters range between 0.88 and 1.16 nm, $v(cm^{-1}) = 223.75(cm^{-1} \cdot nm)/ d(nm) + 15(cm^{-1})$. On the other hand, broadened van Hove transitions, which have the same peak positions as that for the aqueous dispersion, are observed in PVA/PVP/SDS/SWNT (1 and 5 wt% SWNT, Figures 3.2b and c, respectively) films. Van Hove transitions for a PVA/SWNT (1 wt% SWNT, Figure 3.2d) film prepared without SDS not only exhibit broadening but also are red shifted by about 50 meV with respect to PVP/SDS/SWNT aqueous dispersion and PVA/PVP/SDS/SWNT films. The 50 meV shift is reported to be a result of SDS coating[13, 19], and no further shift is obtained with the addition of PVP and PVA.
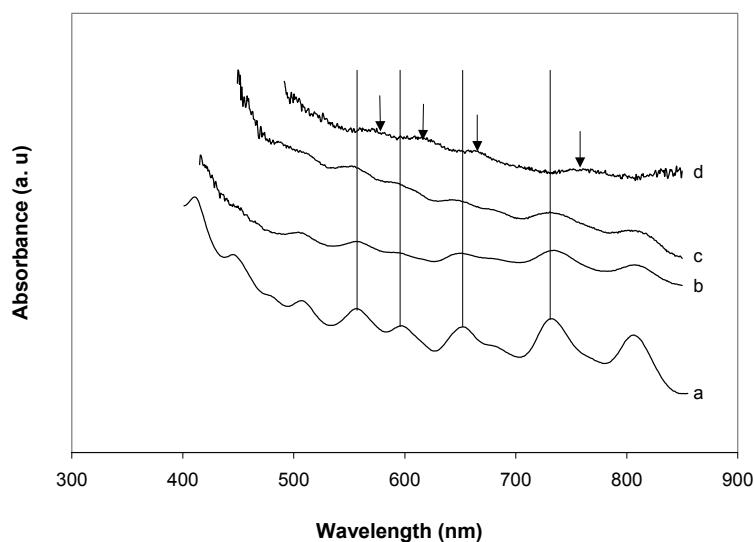
Figure 3.2 UV-visible spectra of the aqueous dispersion and of various composite films; (a) PVP/SDS/SWNT aqueous dispersion, (b) PVA/PVP/SDS/SWNT film (1 wt% SWNT), (c) PVA/PVP/SDS/SWNT film (5 wt%), and (d) PVA/SWNT film (1 wt%).

The typical stress-strain curves for PVA, PVA/PVP/SDS, and PVA/PVP/SDS/SWNT films are given in Figure 3.3 and their mechanical properties are listed in Table 3.1. Compared to the PVA, tensile yield strength of PVA/PVP/SDS/SWNT film, containing only 5 wt% SWNT increases by 78% from 83 MPa to 148 MPa, and the Young's modulus increases by 110% from 1.9 GPa to 4 GPa. Tensile strength of PVA/PVP/SDS/SWNT film is much higher than that of the PVA/PVP/SDS film. All films were tested after being conditioned in the laboratory environment (23 ºC and 35% relative humidity) for 24 hours. Moisture contents of the

films at these conditions are also listed in Table 1.

Table 3.1 Tensile properties of various films.

	Tensile yield strength (MPa)	Tensile modulus (GPa)	Elongation to break (%)	Moisture content (wt%)
PVA	83 ± 6	1.9 ± 0.2	45 ± 7	3
PVA/PVP/SDS	50 ± 4	2.5 ± 0.2	207 ± 10	5
PVA/PVP/SDS/SWNT (5 wt% SWNT)	148 ± 5	4.0 ± 0.2	48 ± 5	4

Figure 3.3 Stress-strain curves for various films. PVA/PVP/SDS/SWNT film contains 5 wt% SWNT.

Based on the enthalpy of melting, PVA crystallinity in PVA/PVP/SDS/SWNT film containing 5 wt% SWNTs is 13% lower compared to that for the pure PVA film and 7% lower compared to that for the PVA/PVP/SDS film. Therefore the increased modulus and strength in the nanotube containing film is not attributed to changes in crystallinity.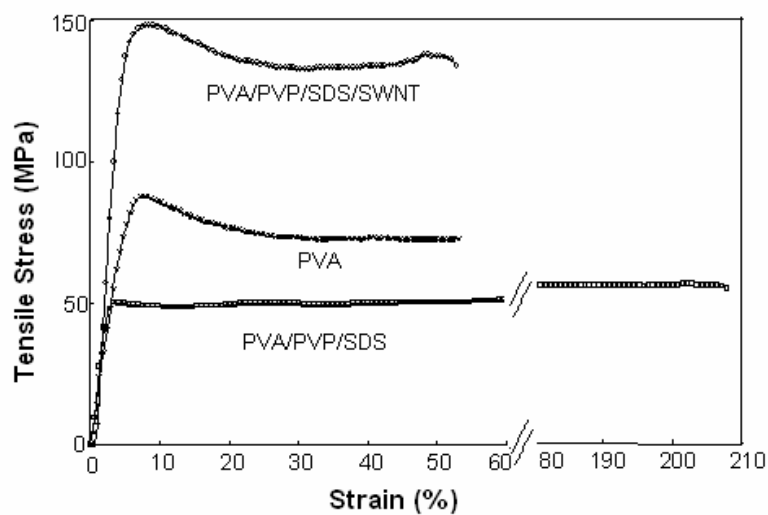 PVA/PVP/SDS/SWNT film did not dissolve in boiling water even after 8 hours, while PVA and PVA/PVP/SDS films dissolved within 30 minutes.

The deformation induced SWNT orientation[20] was also determined. The results show that the Herman's orientation factor[21] for the SWNT increased monotonically from 0 to 0.22 corresponding to 0 to 44 % strain. It should be pointed out that the films reported in this study have not been subjected to any post-processing treatment. Annealing and drawing will result in increased crystallinity and orientation, further improving mechanical properties.

The D^* Raman band of SWNT at ~2600 cm^{-1} has been used to monitor the load transfer from polymer matrix to SWNT[22,23,24]. A study of the fine structure of this band has recently been reported[25]. The D* band position as a function of strain for the PVA/PVP/SDS/SWNT composite film containing 5 wt% nanotubes is presented in Figure 3.4 and 3.5. The curve of the D* band shift versus strain is similar to the stress-strain curve for the corresponding composite film. This confirms that there is excellent load transfer between PVA matrix and the PVP wrapped SWNTs. Considering that the band structure of nanotubes can be dramatically altered with mechanical strain/stress[26] and that the effect is a function of the tube type (metallic or semi-conducting)[27], the shift in D* with stress may find applications in a variety of sensors.
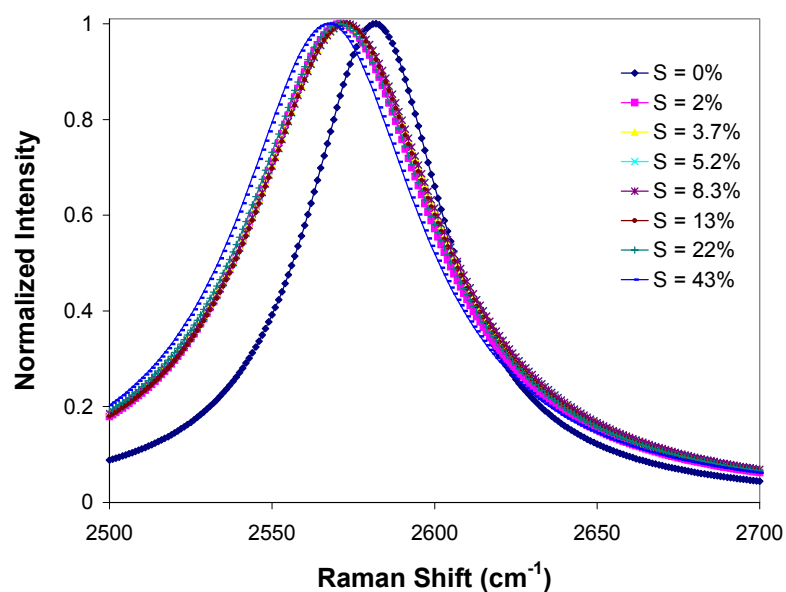
Figure 3.4 Raman D* band peak position under various strain for PVA/PVP/SDS/SWNT composite films containing 5 wt% SWNT.
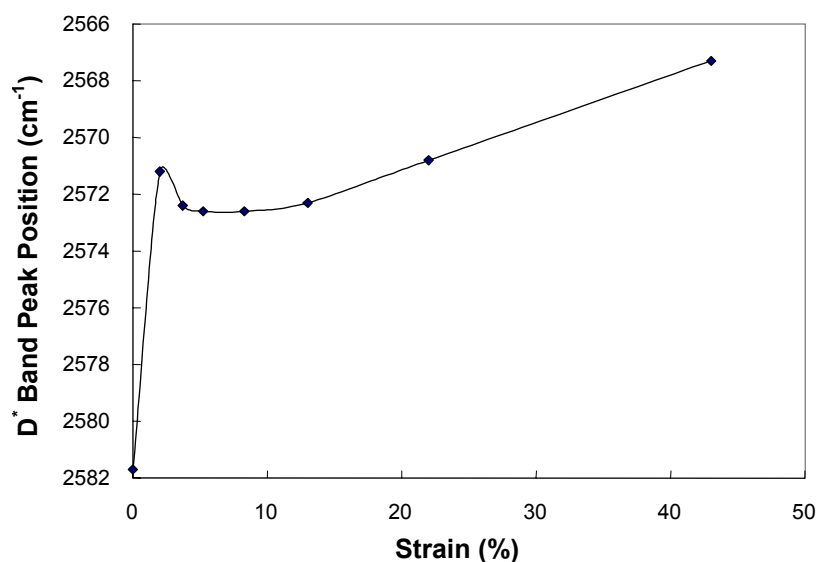
Figure 3.5 Raman D* band peak position as a function of strain for PVA/PVP/SDS/SWNT composite films containing 5 Wt% SWNT. Excitation laser wavelength is 785 nm and the laser power is 1.5 mw.

Halpin-Tsai equation has been successfully used to predict the modulus of polymer/carbon nanotube composites[28, 29]. Considering the random distribution of carbon nanotubes in the polymer matrix, the modified Halpin-Tsai equation is written as[30]:

$$E_c = \left[\frac{3}{8} \frac{1 + 2(l_{NT}/D_{NT})\eta_L V_{NT}}{1 - \eta_L V_{NT}} + \frac{5}{8} \frac{1 + 2\eta_T V_{NT}}{1 - \eta_T V_{NT}} \right] E_P$$

$$\eta_L = \frac{(E_{NT}/E_P) - 1}{E_{NT}/E_P + 2(l_{NT}/D_{NT})} \qquad (3.1)$$

$$\eta_T = \frac{(E_{NT}/E_P) - 1}{E_{NT}/E_P + 2}$$

where E_c, E_{NT}, and E_p are the tensile moduli of composite, nanotube, and polymer matrix, and l_{NT}, D_{NT} and V_{NT} are the length, diameter and volume fraction of nanotubes in the composite, respectively. Aspect ratio (l_{NT}/D_{NT}) of the reinforcing nanotubes can be estimated if E_c, E_{NT}, E_p and V_{NT} are known. Modulus of the 5 wt% PVA/PVP/SDS/SWNT composite film (E_c) and that for the control PVA film (E_p) are listed in Table 3.1. Axial modulus of the SWNTs[1] (E_{NT}) is 640 GPa, and the density of PVA matrix[31] and that for the SWNT reinforcement can be taken as 1.3 g/cm^3. Using these values, aspect ratio of the reinforcing SWNTs in PVA/PVP/SDS/SWNT is calculated to be ~32. Thus, based on the average length of PVP wrapped SWNTs measured from atomic force microscopy of ~ 170 nm[10], diameter of the reinforcing SWNT ropes is calculated to be ~5 nm. However from light scattering, length of nanotubes in the PVP/SDS/SWNT aqueous dispersion was measured to be in the 600 to 700 nm range[32]. Thus based on the Halpin-Tsai aspect ratio of 32, rope diameter can be calculated as about 20 nm. Scanning electron microscopy (Figure 3.6) shows

that rope diameter in the PVA/PVP/SDS/SWNT composite film is as large as 30 nm and length is of the order of micrometers. UV-Visible spectra of the PVP/SDS/SWNT aqueous dispersion (Figure 3.2a) gives clear evidence of individual tubes or bundles of few tubes. SEM observation of relatively large diameter (30 nm) and long length (in the order of micrometers) bundles suggests that SWNT ropes covered with PVP and SDS do aggregate during composite film processing. The high resolution SEM image of the fracture surface of the PVA/SWNT film indicated that the SWNTs was wetted by PVA to a certain extent, and somehow the SWNT bundles interlocked with each other forming a network. The tensile load was transferred to SWNT bundles leading to the breaking of SWNT bundles instead of pull-out. The failed bundles were observed over the cracks in fracture surface of PVA/SWNT composite film.
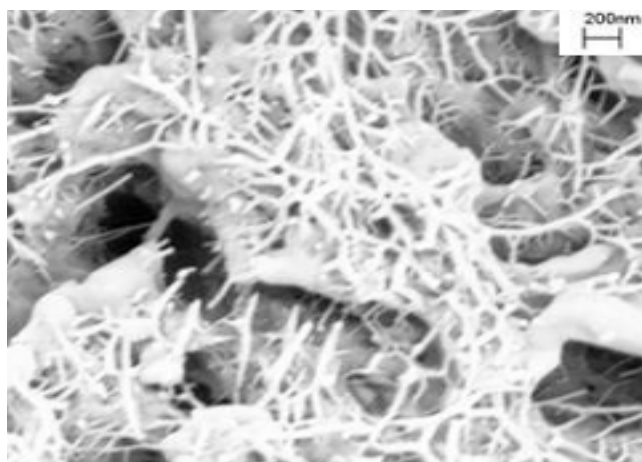

Figure 3.6. Scanning electron micrograph of PVA/PVP/SDS/SWNT composite film.

REFERENCES

[1] Baughman, R., *Science*, **2002**, 297:787.

[2] Salvetat, J-P.; Briggs, G. A. D.; Bonard, J-M.; Bacsa, R. R.; Kulik, A. J.; Stockli, T.; Burnham, N. A.; Forro, L. *Phys. Rev. Letts*. **1999**, 82, 944

[3] Liu, T.; Kumar, S. *Nano Letters*, **2003**, 3, 647

[4] Andrews, R.; Jacques, D.; Rao, A. M.; Rantell, T.; Derbyshire, F.; Chen, Y.; Chen, J.; Haddon, R. C. *Appl. Phys. Lett*. **1999,** 75, 1329

[5] Haggenmueller, R.; Gommans, H. H.; Rinzler, A. G.; Fischer, J. E.; Winey, K. I. *Chem. Phys. Lett*. **2000**, 330, 219

[6] Kumar, S.; Dang, T. D.; Arnold, F. E.; Bhattacharyya, A. R.; Min, B. G.; Zhang, X.; Vaia, R. A.; Park, C.; Adams, W. W.; Smalley,R. H. Ramesh,S.; Willis, P. A. *Macromolecules*, **2002**, 35, 9039

[7] Kearns J. C.; Shambaugh, R. L. *J. Appl. Polym. Sci.* **2002**, 86, 2079.

[8] Mamedov, A. A.; Kotov, N. A.; Prato, M.; Guldi, D. M.; Wicksted, J. P.; Hirsch, A. *Nature Materials*, **2002**, 1, 190

[9] Dalton, A. B.; Collins, S.; Munoz, E.; Rajal, J. M.; Ebron, V. H.; Ferraris, J. P.; Coleman, J. N.; Kim, B. G.; Baughman, R. H.; *Nature*, **2003**, *423*, 703.

[10] O'Connell, M. J.; Boul, P.; Ericson, L. M.; Huffman, C.; Wang, Y.; Haroz, E.; Kuper, C.; Tour, J.; Ausman, K. D.; Smalley, R. E. *Chem. Phys. Lett*. **2001**, 342, 265.

[11] Cassu, S. N.; Felisberti, M. I. *Polymer*, **1997**, 38, 3907

[12] Rao, A. M.; Richter, E.; Bandow, S.; Chase, B.; Eklund, P. C.; Williams, K. A.; Fang, S.; Subbaswamy, K. R.; Menon, M.; Thess, A.; Smalley, R .E.; Dresselhaus, G.; Dresselhaus, M. S. *Science*, **1997**, *275*, 187

[13] O'Connell, M. J.; Bachilo, S. M.; Huffman, C. B.; Moore, V. C.; Strano, M. S.; Haroz, E. H.; Rialon, K. L.; Boul, P. J.; Noon, W. H.; Kittrell, C.; Ma, J.; Hauge, R. H.; Weisman, R. B.; Smalley, R. E. *Science*, **2002**, *297*, 593

[14] Rao, A. M.; Richter, E.; Bandow, S.; Chase, B.; Eklund, P. C.; Williams, K. A;. Fang, S.; Subbaswamy, K. R.; Menon, M.; Thess, A.; Smalley, R .E.; Dresselhaus, G.; Dresselhaus, M. S. *Science*, **1997**, *275*, 187

[15] Brown, S. D. M.; Corio, P.; Marucci, A;. Dresselhaus, M. S.; Pimenta, M. A.; Kneipp, K. *Phys. Rev. B* **2000**, *61*, R5137

[16] White, C. T.; Mintmire, J. W. *Nature*, **1998**, *394*, 29

[17] Satio, R.; Takeya, T.; Kimura, T.; Dresselhaus, G. M.; Dresselhauls, S. *Phys. Rev. B*, **1998**, *57*, 4145

[18] Yu, Z.; Brus, L. *J. Phys. Chem. B*, **2001**, *105*, 1123

[19] Hagen, A.; Hertel, T. *Nano Letters*, **2003**, 3, 383

[20] Liu, T.; Kumar, S. To be published in Chemical Physics Letters.

[21] Samuels, R. J. *Structured Polymer Properties: The Identification, Interpretation, and Application of Crystalline Polymer Structure*, John Wiley & Sons, New York, 1974

[22] Ajayan, P. M.; Schadler, L. S.; Giannaris, C.; and Rubio, A. *Adv. Mater.* **2000**, *12*, 750

[23] Wood, J. R.; Zhao, Q.; Wagner, H. D. *Composites A*, **2001**, *32*, 391

[24] Frogley, M. D.; Zhao, Q.; Wagner, H. D. *Phys. Rev. B*, **2002**, *65*, 113413

[25] Zolyomi, V.; Kurti, J.; Gruneis, J.; Kuzmany, H. *Phys. Rev. Lett.* **2003**, 90, 157401.

[26] Minot, E.D.; Yaish, Y.; Sazonova, V.; Park, J. Y.; Brink, M.; McEuen, P. L. *Phys. Rev. Lett.* **2003**, 90, 156401.

[27] Cao, J.; Wang, Q.; Dai, H. J. *Phys. Rev. Let.* **2003**, 90, 157601.

[28] Qian, D.; Dickey, E. C.; Andrews, R.; Rantell, T. *Appl. Phys. Lett.* **2000**, *76*, 2868

[29] Cadek, M.; Coleman, J. N.; Barron, V.; Hedicke, K.; Blau, W. J. *Appl. Phys. Lett.*, **2002**, 81, 5123

[30] Mallick, P. K. *Fiber-Reinforced Composites*, Marcel Dekker, New York, **1993**, 91-130

[31] Finch C. A., *Polyvinyl alcohol – development*, John Wiley & Sons Ltd, Chichester, England, **1992**

[32] Wang, T, unpublished results.

CHAPTER 4

Gel Spinning of PVA/SWNT Composite Fiber

4.1 Introduction

For those working in engineering polymers, incorporating the high strength and modulus SWNT into polymer matrix remains most attractive. Although some polymer/SWNT composites, such as PBO[1], PAN[2] and PI[3] with improved mechanical properties have been made, SWNT dispersion and exfoliation in most polymer matrices remain a challenge. SWNT can be dispersed using surfactants,[4, 5] for example SDS, NaDDBS and Triton-X 100, etc. However, the remaining surfactant in the polymer matrix will also influence the final mechanical properties of the composites. Therefore, to improve mechanical properties, polymer assisted dispersion is desirable. Polyvinyl alcohol (PVA) is a useful water-soluble polymer, either in fiber or film form. PVA fiber (vylon[TM]) is widely used as textile or construction material due to its relatively high tensile strength and modulus. Recently PVA/ SWNT composite fiber was successfully processed using water and SDS.[6] Normally, PVA fiber with several hundred MPa tensile strength and about 10 GPa Young's modulus is produced using the traditional solution spinning technology.[7] In the 1970's, the new gel-spinning concept was applied to PVA[8]. The gel-spun PVA fiber has much higher tensile strength and modulus than the traditional solution spun PVA fiber. Moreover, during the heat-draw process, PVA gel fiber can be drawn to very

high draw ratio. As discussed in chapter 2, PVA can assist SWNT being dispersed in aqueous and various organic solvent. So, preparation of PVA/SWNT composite direct from PVA/SWNT dispersion is on of the focuses in our studies. This chapter presents the preparation of good SWNT/PVA dispersion in DMSO/H_2O solvent, and the structure and properties of the resulting gel-spun fiber.

4.2 Experiment

SWNT used in this work was received from CNI (lot # P0247) and used without further modification. Based on TGA, the purity of this SWNT was about 98%. Polyvinyl alcohol (PVA) was received from Kuraray Specialities Europe GMBH with degree of hydrolysis 98% and molecular weight about 200,000 g/mol. DMSO was purchased from Fisher Scientific. Methanol used in this work was USP grade. Fiber spinning was done using syringe pump and syringe needle. 60 mg SWNT was dispersed in 10 ml DMSO and sonicated in bath sonicator. Meanwhile, 2 g PVA was dissolved into 30 ml DMSO and 10 ml water mixed solvent around 100 °C. After 24 hour sonication of SWNT/DMSO dispersion, PVA solution was gradually added into this dispersion. At the same time, rigorous shear mixing and bath sonication was applied on the dispersion. Sonication was stopped after 48 hours, but mixing continued for another 24 hours. The optically homogeneous PVA/SWNT dispersion thus obtained was ready for gel spinning. The PVA/SWNT/DMSO/H_2O dispersion was injected into dry ice cooled methanol coagulation bath (maintained at -25 ± 5°C) through 20 gauge needle. This dispersion immediately formed gel once it went into the coagulation bath. Gel fiber was continuously collected on a fiber take-

up unit. The gel spinning set-up is shown in Figure 4.1. The gel fiber was kept emerged in methanol bath for two days and dried in the vacuum oven at 70 °C for three days before drawing on a hot plate at 200 °C.
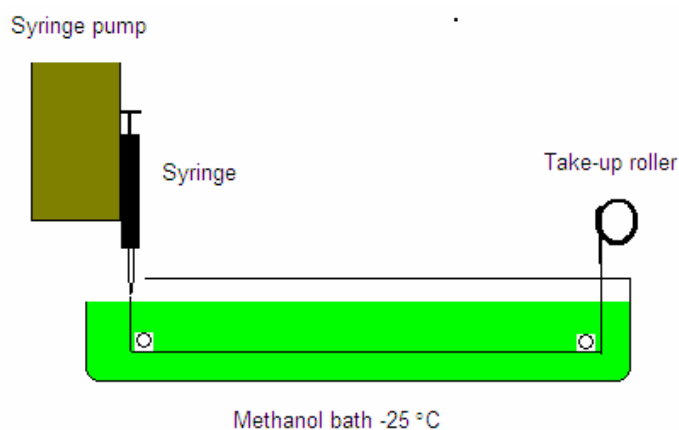
Figure 4.1. Set-up for PVA gel spinning.

4.3 Results and Discussion

Generally, homogenous aqueous SWNT dispersions have been prepared with the aid of surfactant and the weight of surfactant is generally higher than that of SWNT.[9] The existence of such large amount of surfactant is not good for making polymer SWNT composites, especially for the improvement of mechanical properties. From this point, the polymer assisted SWNT dispersion is desirable. In previous studies, PVP was thought to wrap around the SWNT, which rendered certain solubility of SWNT in the aqueous solution. Garden starch could also render SWNT readily soluble in water.[10] Hyperbranched Polymer, like polymer poly{(m-phenylenevinylene)-co-[(2,5-dioctoxy-p-phenylene)vinylene]} (PmPV), help dissolution of SWNT in $CHCl_3$[11]. Polymers mentioned above have the suitable

chemical compatibility and configuration to wrap SWNT, then provide SWNT solubility in certain solvents. In the current work, DMSO / water solvent mixture has been used. Although there are several solvents, such as phenol[12], ethylene glycol[13] and N-methylmorpholine-N-oxide (NMMO)[14] have also been used for this purpose, DMSO is the one widely chosen in PVA gel study.[15, 16] DMSO is one of the better solvents for SWNT.[17] For comparing dispersion quality, DMSO/SWNT, DMSO/SWNT/H$_2$O, DMSO/SWNT/PVA, DMSO/SWNT/H$_2$O/PVA and SWNT/H$_2$O/PVA dispersions were prepared according to the above mentioned procedure. With the presence of PVA, the optical quality of dispersion is much better than those without PVA as shown in Figure 2.11. Qualitatively, SWNT dispersion is slightly better in DMSO systems than in aqueous systems (Figure 2.11c and 2.11e), which is due to better SWNT solubility in DMSO than in water. UV-vis spectra of these dispersions were also recorded (Figure 2.12). The absorption peaks in 400 – 600 nm range are associated with first pair van Hove transitions from the metallic tubes. The absorption peaks in the range of 550 – 850 nm are due to second pair van Hove singularity in semi-conducting SWNTs. Sharpness of the UV-vis absorption peak is qualitatively related to the bundle size of SWNT.[18] For large bundle diameters, the peaks broaden and merge with each other due to inter-tube side-by-side van der Waals interactions[19]. As seen in Figure 2.12, the dispersions d and f are almost featureless, suggesting that the SWNT bundle size in these two dispersions must be rather large, which is consistent with optical microscopy observation. On the other hand, the dispersions with PVA, a, b and c, show relatively well-resolved van Hove transition absorption peaks. Sample d is PVP wrapped SWNT in aqueous solution,

which is composed of small size SWNT bundles and individual nanotubes[20]. Through the characterization by UV-vis spectroscopy, we can observe that PVA can assist in SWNT dispersion in water, DMSO or similar solvent systems. This method, however, is qualitative and does not give quantitative information on SWNT bundle diameter. In SDS assisted SWNT aqueous dispersion, sonication first breaks down the bundle size. If sonication stops, these bundles tend to aggregate. If SDS is introduced in the dispersion, then hydrophobic tails of SDS surround the individual SWNT or SWNT bundle. Thus, the SDS layers surrounding SWNT prevent SNWT aggregation. Although SDS may cover SWNT in various manners[21], its basic function is physical screen. PEO-grafted-SWNT forms similar micelle structure with SWNT as the core and PEO expanded in CH_3Cl solution[22]. So, the reason that PVA can assist in the dispersion of SWNT is similar to SDS. After 24 hours sonication, the size of SWNT bundle is broken down, and at this time PVA solution is added into the dispersion with PVA exposing its main chain to SWNT and hydroxyl groups towards to the solvent. During this process, the SWNT is physically screened from each other by the surrounding PVA molecules. The DMSO/SWNT/H_2O/PVA dispersion is stable for several months without visible phase separation.

The concept of producing high performance fibers from flexible polymers is based on arresting polymer orientation and preventing chain folding by gel spinning, which induces crystallization and minimizes chain entanglements. High mechanical drawability is the key for obtaining high orientation. In order to obtain high drawability, entanglement control between the chains is crucial. Certain degree of entanglement is needed to endure the force during drawing, but too much

entanglement would reduce drawability. In the other words, the concentration of the polymer solution should be near critical concentration theoretically. But in reality, the concentration is chosen much higher than the critical concentration, as fibers can't be drawn near the critical concentration. For gel spinning of PVA or other polymers, crystallization induced gelation is the key step in the process. These crystals act as physical crosslinks for mechanical drawing. For good drawability, the crystal size should be as small as possible. So, the criterion for selection of solvent is that the solvent shall not be a good solvent, but not a very poor solvent, either. In our current work, DMSO and water mixture was chosen. To understand the effect of SWNT on the PVA/SWNT composite fiber, all the process parameters are set identical in both cases, including PVA solution concentration, injection speed, take-up speed, coagulation bath temperature, heat treatment temperature and draw ratio.

For comparison, the PVA and PVA/SWNT (PVA to SWNT weight ratio being 100 to 3) gel fibers are both drawn six times their original length during the heat-treatment process. The mechanical properties of these gel-spun fibers are characterized on RSA III solid analyzer with elongation rate 0.05 mm/s (Figure 4.2 and Table 4.1). The standard paper tab was used in the test (gauge length 2.54 cm). Diameters of these fibers were determined by laser scattering method. As we can see from Table 4.1, with 3 wt% SWNT, the gel spun PVA/SWNT composite fiber tensile strength is 22% higher than the control PVA gel spun fiber, increasing form 0.9 GPa to 1.1 GPa under our gel spinning conditions. Also, the Young's modulus increases by 40% from 25.6 GPa to 35.8 GPa.

Table 4.1. Mechanical properties of PVA and PVA/SWNT gel-spun fibers

	Diameter (μm)	Tensile Strength (GPa)	Modulus (GPa)	Elongation (%)
PVA	26.5 ± 1.6	0.9 ± 0.1	25.6 ± 2.6	7.5 ± 1.6
PVA/SWNT (3 wt%)	27.0 ± 2.0	1.1 ± 0.2	35.8 ± 3.5	8.8 ± 1.7
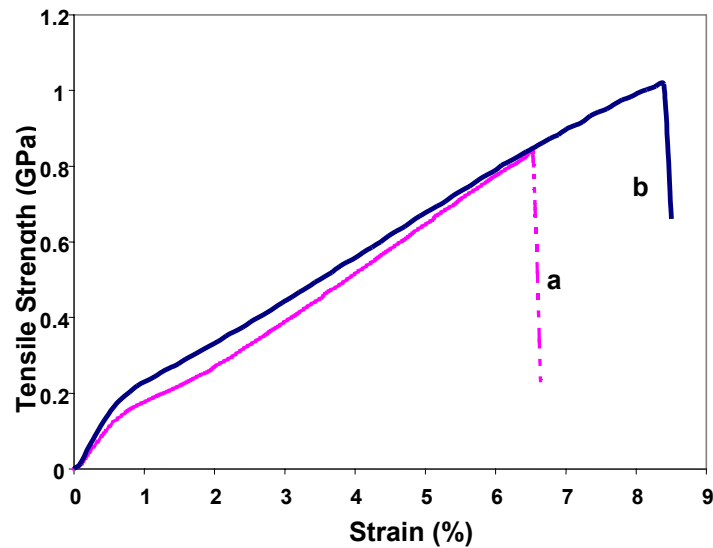
Figure 4.2 Strain-stress curves for (A) PVA and (B) PVA/SWNT gel-Spun fibers.

In general, the tensile modulus reflects the average of the structure, but tensile strength is more related to the weakest point in the structure. Among the high performance flexible polymer fibers, the weakest point is expected to be within the amorphous region, such as the chain ends, defects and not highly oriented chains, etc. So, if there is a way to overcome these disadvantages, the mechanical performance of such fibers will increase. The effect of the extent of SWNT orientation on the

modulus of composite has been studied theoretically[23]. Carbon nanotube orientation can be achieved by magnetic field,[24] or by mechanical stretching.[25] In current work, mechanical drawing has been used to introduce SWNT orientation in composite fiber by taking advantage of the very high drawability of the gel-spun PVA fiber. Either physical entanglements or molecular interactions between SWNT and PVA are assumed to provide drawing induced SWNT orientation. Polarized Raman spectroscopy is used to study the SWNT orientation.[26] As we can see from Figure 4.3, the orientation increases with increasing draw ratio. The Hermans orientation factor of SWNT at the draw ratio 6 is estimated to be 0.8. So, the high orientation of SWNT is believed to be the reason that PVA/SWNT composite fiber has superior modulus.
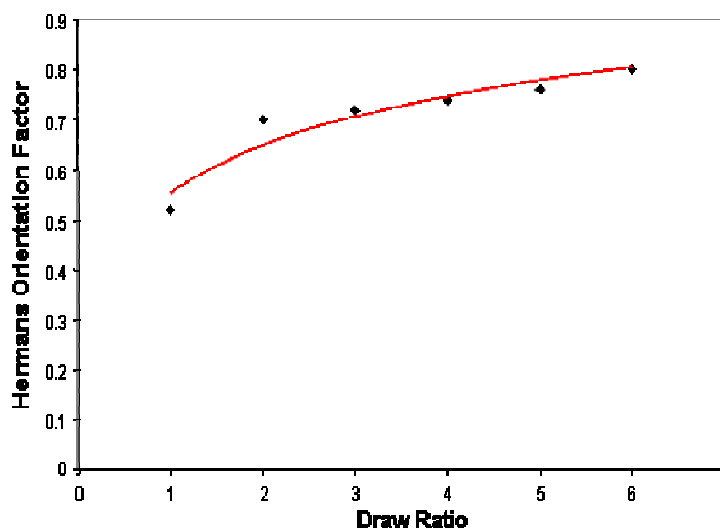
Figure 4.3 Orientation of SWNT in PVA/SWNT fiber as a function of draw ratio.

Both the crystallinity and crystal orientation of PVA and PVA/SWNT gel-spun fiber are characterized by wide-angle x-ray diffraction (Figure 4.4).
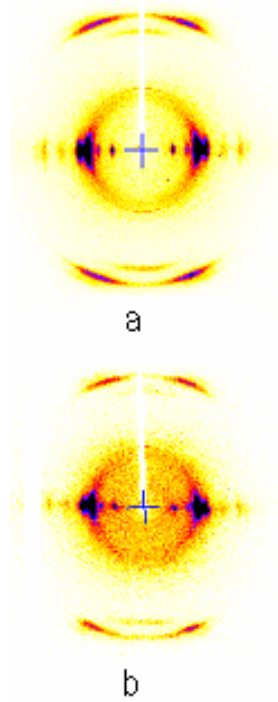
Figure 4.4 WAXD Of PVA (a) and PVA/SWNT (b) gel-spun fiber.

The degree of orientation of PVA crystal is determined using the following equation:

$f_{010} = (3 < \cos^2 \phi > -1)/2$. The $<\cos^2 \theta>$ is calculated through equation 4-1 after

azimuthal integration of diffraction pattern.

$$< \cos^2 \phi_{hkl}, z >= \frac{\int\limits_{0}^{\pi/2} I(\phi)\sin(\phi)\cos^2(\phi)d\phi}{\int\limits_{0}^{\pi/2} I(\phi)\sin(\phi)d\phi} \qquad (4\text{-}1)$$

It was found that the PVA crystals are highly oriented in fiber direction in both the

PVA and PVA/SWNT gel-spun fibers with the Herman's orientation factor as high as

0.65. The crystallinity and crystal size can be obtained from the radial scans. It was

found that crystallinity of PVA in PVA fiber is 60%, while that in PVA/SWNT fiber

was 53%. Therefore, crystallinity and crystal orientation are not the major factors that govern the mechanical performance of PVA/SWNT gel-spun fiber. Since the weak portion of PVA gel spun fiber is its amorphous region, there must be some improvement in mechanical performance in the amorphous regions in the presence of SWNT in order to get reinforced composite fiber. The dynamic mechanical analysis (DMA) has been done on the gel-spun fibers. The frequency/temperature sweep mode was chosen. The 50 MPa initial static stress and 0.05% dynamic strain was applied. During the testing, the static force adjusted itself to be 20% larger than dynamic force based on living tracking dynamic force. Figure 4.5 shows temperature ramp curve at 1 Hz frequency.
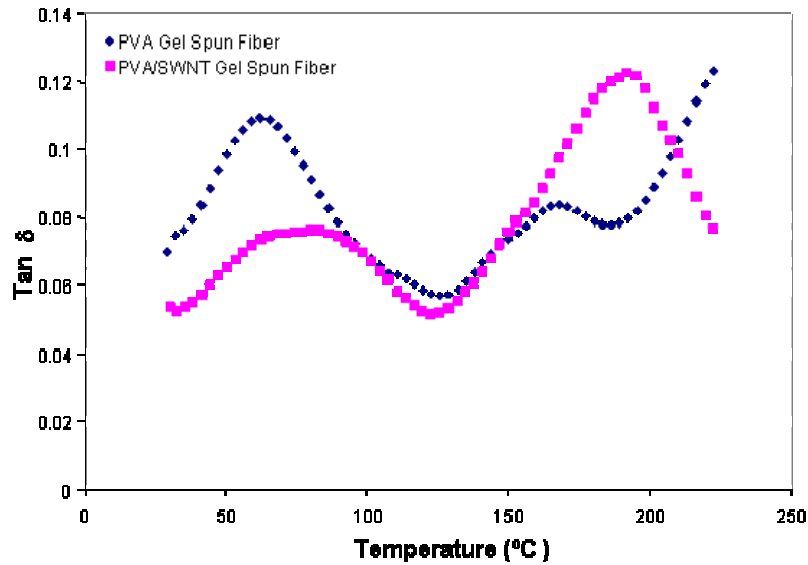

Figure 4.5 Dynamic mechanical characterization of PVA and PVA/SWNT gel-spun fibers.

The glass transition temperature peak of PVA in composite fiber is broadened and shifted upward compared to the pure PVA gel-spun control fiber. In the control sample, the glass transition peak is located at 62 °C, while in composite fiber, the high end of the transition peak shifts to 86 °C. This suggests the interaction between PVA and SWNT in amorphous region. Due to the interaction, the PVA molecular movement is restricted near the SWNT. So, it leads to higher glass transition temperature. Because of the existence of interaction between SWNT and PVA, the fiber tensile strength is improved. In Figure 4.5, the transition peak around 170 °C is attributed to sub-crystal transition[27]. There is a noticeable up-shift of this transition temperature in composite fiber compared to the control sample, which may suggest that something happens in the crystal region. In previous study, nanotubes were found nucleate PVA and PP[28, 29]. It was also found out that PVA crystal size was smaller near the inorganic filler (MMT) surface than in bulk phase[30].

Table 4.2. Structural parameters in PVA and PVA/SWNT gel-spun fiber

	PVA	PVA/SWNT
h k l	Crystal size (A)	Crystal size (A)
1 0 0	84	79
0 0 2	85	68
0 1 0	69	73
Crystallinity (WAXD)	60%	53%
PVA crystal orientation factor	0.65	0.65
SWNT orientation factor		0.8

Table 4.2 lists the crystal sizes of PVA in both control and composite fibers determined from WAXD using Scherrer equation. It is noticed that crystal sizes in (1 0 0) and (0 0 2) crystal plane direction decrease, while it slightly increases in the (0 1 0) direction. Recall that b axis is composed of main chains of PVA molecules and the PVA molecules expose their main chains to surface of SWNT for stabilizing during the dispersion. The PVA is in a more order structure in the main chain direction due to the presence of SWNT. In such a case, the crystal size will increase. It can be imagined that the PVA crystallizes on the surface of SWNTs and these SWNTs intercalate PVA crystals. In this case, the amorphous region is reinforced by SWNT between the crystals. Finally, the tensile strength of composite fiber is improved by the presence of SWNT. It should be pointed out that in this study all the process parameters for both the PVA and PVA/SWNT fibers are the same. However, the maximum achievable draw ratio in PVA/SWNT fiber is nearly eight times the original length, and the highest tensile strength and modulus are 1.5 and 50 GPa, respectively.

Figure 4.6 shows the cross section image of PVA/SWNT composite fiber. Under low magnification, it is found that the core part of composite fiber is not compact, which implies that the coagulation in the outer layer is faster than inside the fiber. At high magnification, 20 nm diameter ropes are observed on the fracture surface. These ropes appear well bonded and covered by the PVA molecules by comparing the contrast of filler and bulk PVA. No holes are found in the fracture surface, which means no pull-out of SWNT from the polymer matrix. The interaction between SWNT and PVA suggested by dynamic mechanical analysis is in agreement

with the SEM observation. Moreover, to study the solubility of these fibers, the PVA and PVA/SWNT gel-spun fibers are boiled in the water for an hour without stirring. The PVA fiber swells and breaks into small piece, but PVA/SWNT fiber only swells and keeps the original fiber shape.
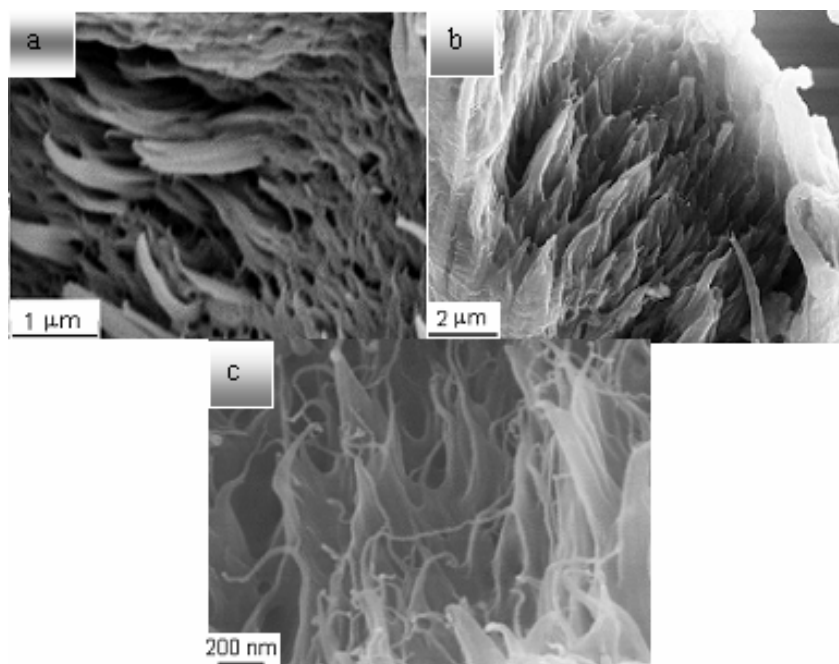
Figure 4.6. Scanning electron micrographs of fractured cross-sections of PVA and PVA/SWNT gel-spun fibers, A) low resolution PVA fiber, B) low resolution PVA/SWNT fiber, C) high resolution PVA/SWNT fiber.

In summary, due to the presence of PVA, SWNTs can be well dispersed in DMSO as well as in DMSO/H$_2$O mixed solvent. The PVA/SWNT dispersion is successfully spun into composite fiber through gel spinning. Compared to the control PVA gel-spun fiber, composite fiber exhibits improved tensile properties. This work

only focuses on comparing PVA and PVA/SWNT fibers processed under the identical conditions. However, due to the presence of SWNT, the manufacturing condition (such as concentration of PVA, coagulation bath temperature, heat-draw temperature, etc.) can be optimized to further maximize the mechanical properties of the composite fiber. DMA, X-ray diffraction and SEM characterization suggest that SWNT influences the properties of amorphous as well as the crystalline regions of PVA in composite fiber.

REFERENCES

[1] Kumar, S.; Dang, T. D.; Arnold, F. E.; Bhattacharyya, A. R.; Min, B. G.; Zhang, X.; Vaia, R.A.; Park, C.; Adams, W. W.; Hauge, R. H.; Smalley, R. E.; Ramesh, S.; Willis, P. A. *Macromolecules* **2002**, *35,* 9039

[2] Sreekumar, T. V.; Liu, T.; Min, B. G.; Guo, H.; Kumar, S.; Hauge, R. H.; Smalley, R. E, *Adv. Mater*. **2004**, *16*, 58

[3] Park, C.; Ounaies, Z.; Watson, K. A.; Crooks, R. E.; Smith, J.; Lowther, S. E.; Connell, J. W.; Siochi, E. J.; Harrison, J. S.; Clair, T. L. *Chem. Phys. Lett*. **2002**, *364*, 303

[4] Matarredona, O.; Rhoads, H.; Li, Z.; Harwell, J. H.; Balzano, L.; Resasco, D. E, *J. Phys. Chem. B* **2003**, *107*, 13357

[5] Moore, V. C.; Strano, M. S.; Haroz, E. H.; Hauge, R. H.; Smalley, R. E.; Schmidt, J.; Talmon, Y. *Nano Lett*. **2003**, *3*, 1379

[6] Dalton, A. B.; Collins, S.; Munoz, E.; Razal, J. M.; Ebron, V. H.; Ferraris, J. P.; Coleman, J. N.; Kim, B. G., *Nature* **2003**, *423*, 703

[7] Sakurada, I. *Polyvinyl Alcohol Fibers*, New York: M. Dekker, 1985

[8] Kikutani, T. *J. Appl. Polym. Sci*. **2002**, *83*, 559

[9] Poulin, P.; Vigolo, B.; Launois, P. *Carbon* **2002**, *40*, 1741

[10] Star, A.; Steuerman, D. W.; Heath, J. R.; Stoddart, F. J. *Angew. Chem. Int. Ed.* **2002**, *41,* 2508

[11] Star, A.; Stoddart, J. F., *Macromolecules* **2002**, *35*, 7516

[12] Yamaura, K.; Suzuki, M.; Yamamoto, M.; Shimada, R.; Tanigami, T. *J. Appl. Polym. Sci*. **1995**, *58*, 1787

[13] Hong, P.; Chou, C.; Chuang, W. *J. Appl. Polym. Sci.* **2001**, *79*, 1113

[14] Nagashima, N.; Matsuzawa, S.; Okazaki, M. *J. Appl. Polym. Sci.* **1996**, *62*, 1551

[15] Yamaura, K.; Kumakura, R. *J. Appl. Polym. Sci.* **2000**, *77*, 2872

[16] Suzuki, M.; Tanigami, T.; Matsuzawa, S.; Yamaura, K. *J. Appl. Polym. Sci.* **2002**, *86,* 1970

[17] Ausman, K. D.; Piner, R.; Lourie, O.; Ruoff, R. S.; Korobov, M. *J. Phys. Chem. B*, **2000**, *104*, 8911

[18] O'Connell, M. J.; Bachilo, S. M.; Huffman, C. B.; Moore, V. C.; Strano, M. S.; Haroz, E. H.; Rialon, K. L.; Boul, P. J.; Noon, W. H.; Kittrell, C.; Ma, J.; Hauge, R. H.; Weisman, R. B.; Smalley, R. E. *Science*, **2002**, *297*, 593

[19] Reich, S.; Thomsen, C.; Ordejon, P. *Phys. Rev. B* **2002**, *65*, 155411

[20] Zhang, X.; Liu, T.; Sreekumar, T. V.; Kumar, S.; Moore, V. C.; Hauge, R. H.; Smalley, R. E. *Nano Lett.*, **2003**, *3*, 1285

[21] Richard, C.; Balavoine, F.; Schultz, P.; Ebbesen, T. W.; Mioskowski, C. *Science*, **2003**, *300*, 775

[22] Sano, M.; Kamino, A.; Okamura, J.; Shinkai, S. *Langmuir*, **2001**, *17*, 5125

[23] Liu, T.; Kumar, S. *Nano Lett.* **2003**, *3*, 647

[24] Kimura, T.; Ago, H.; *Adv. Mater*. **2003**, *14*, 1380

[25] Jin, L.; Bower, C.; Zhou, O. *Appl. Phys. Lett.* **1998**, *73*, 1197

[26] Liu, T.; Kumar, S.; *Chem. Phys. Lett*. **2003**, *378*, 257

[27] Park, J. S.; Park, J. W.; Ruckenstein, E. *J. Appl. Polym. Sci*. **2001**, *82*, 1816

[28] Cadek, M.; Coleman, J. N.; Barron, V.; Hedicke, K.; Blau,W. *J Appl. Phys. Lett*. **2003**, *81*, 5123

[29] Bhattacharyya, A. R.; Sreekumar, T. V.; Liu, T.; Kumar, S.; Ericson, L. M.; Hauge, R. H.; Smalley, R. E. *Polymer*, **2003**, *44*, 2373

[30] Strawhecker K. E.; Manias, E. *Macromolecules*, **2001**, *34*, 8475

CHAPTER 5

Properties and Structure of Nitric Acid Oxidized Single Wall Carbon

Nanotube Films

5.1 Introduction

Carbon nanotube films (bucky paper) are often made by filtration of carbon nanotube dispersion. Electrical conductivity,[1] field emission properties,[2] gas permeability[3], and electronic properties of bucky paper have been studied. While the tensile strength and modulus of SWNT are as high as 37 GPa and 640 GPa[4], these values for the typical bucky paper are ~10 MPa and ~1.2 GPa[5], respectively. Tensile strength of SWNT films processed from oleum was 30 MPa.[6] On the other hand, modulus and tensile strength of SWNT fiber as high as 40 GPa and 230 MPa, respectively[7], have been reported. To improve the mechanical properties of the SWNT bulk products, covalent crosslinking of SWNTs has been proposed.[8, 9, 10] Oxidation of SWNT is one possible way to achieve crosslinking. Functional groups such as carboxylic acid, quinone,[11] phenol[12], ester[13], amide[14], and zwitterions[15] have been reported on the oxidized SWNTs. Oxidation can also occur during SWNT purification with HNO_3[16] or HCl[13]. It is understood that oxidation occurs at end caps and at the defect sites.[17] Besides HNO_3 and HCl, other agents used to oxidize SWNT include O_3[18], H_2SO_4 combined with H_2O_2 or HNO_3.[11] The presence of polycyclic aromatic amorphous carbon has been reported in the oxidized SWNT[19]. Small

diameter SWNTs have been reported to be destroyed during nitric acid treatment[20], and the formation of continuous phase morphology has been observed in HNO$_3$ purified SWNTs, which is attributed to amorphous carbon formed by the decomposition of SWNTs[21]. This chapter presents structure and properties of SWNT film processed from aqueous dispersions at various nitric acid concentrations. The structural changes have been monitored using infra-red spectroscopy, Raman spectroscopy, scanning electron microscopy, and X-ray diffraction.

5.2 Experimental Section

100 mg purified[22] HiPCO SWNTs were dispersed in 100 ml distilled water and sonicated for 2 hours using Fisher Scientific bath sonicator. Then nitric acid was added to the dispersion to reach 3M, 6M or 10M acid concentration. The dispersion was then sonicated for 2 hours, refluxed for 2 hours, and subsequently sonicated for another 20 minutes. The dispersion was filtered through PTFE membrane (Gelman Laboratory, pore diameter 1μm) and repeatedly washed with distilled water. The resulting SWNT film was easily peeled off from the PTFE membrane. The control SWNT film was formed by filtering the aqueous SWNT dispersion without nitric acid that has been sonicated for 4 hours. The films were dried at 70 °C in vacuum and heat-treated in air at 200 °C for 2 hrs.

The tensile and dynamic mechanical properties of the SWNT films were determined using Rheometric Scientific analyzer, RSAIII. Tensile tests were conducted on 1 mm wide and 0.06 mm thick samples at a gauge length of 10 mm at a strain rate of 0.5 % / s and the tensile test data are summarized in Table 5.1. A

minimum of 3 samples were tested in tension in each case. Dynamic mechanical properties as a function of temperature were determined at 10 Hz and 0.1% dynamic strain on sample sized L × W × T = 7 × 1.3 × 0.063 mm. During the dynamic test, static force adjusted itself to be 40% larger than dynamic force. In plane dc electrical conductivity of the films was measured by four-probe method. The FTIR studies of the oxidized SWNTs were conducted on a Perkin-Elmer Spectrum One FTIR microscope.

Structural changes have also been studied on films heat-treated in nitrogen for 2 minutes at 900 °C. Scanning electron microscopy has been done on uncoated films using LEO 1530 SEM. Raman spectroscopy was done on Holoprobe Research 785 Raman Microscope using 785 nm incident laser wavelength. X-ray diffraction studies on the films were done on Rigaku R-AXIS IV^{++} equipped with an image plate and data analysis was done using Jade software.

5.3 Results and Discussion

The film tensile strength increased from 10 MPa to 74 MPa, and the tensile modulus increased from 0.8 GPa to 5.0 GPa when the nitric acid concentration increased from control to 10M. While the film mechanical properties improved with nitric acid treatment, in plane dc electrical conductivity decreased from 3×10^4 S/m to 1.2×10^4 S/m These values are comparable to the bucky paper dc electrical conductivity reported in the literature,[23,24,25,26] which is in the range of 2×10^4 to 4×10^4 S/m (Table 5.1). Somewhat lower conductivity in the nitric acid treated samples

is a result of SWNT functionalization leading to imperfections, resulting in reduced

conjugation length and defects.

Table 5.1 Mechanical and electrical properties of various SWNT films

	Tensile Strength (MPa)	Modulus (GPa)	Elongation (%)	Conductivity (S / m)
Control SWNT film	10 ± 2	0.8 ± 0.1	5.6 ± 0.3	3.0×10^4
3M HNO$_3$ SWNT film	16 ± 1	1.4 ± 0.1	1.4 ± 0.2	2.3×10^4
6M HNO$_3$ SWNT film	71 ± 5	2.9 ± 0.2	3.4 ± 0.2	2.4×10^4
10M HNO$_3$ SWNT film	74 ± 2	5.0 ± 0.2	3.0 ± 0.1	1.2×10^4

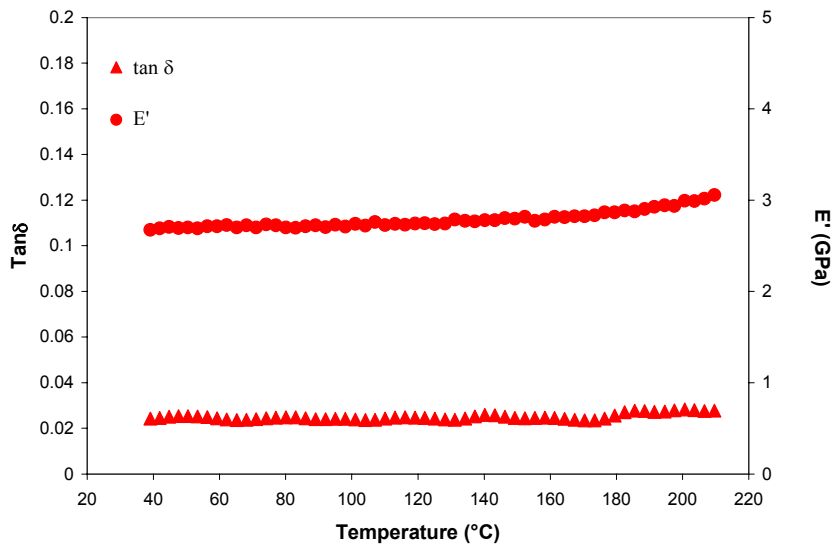The storage modulus of SWNT films was fairly constant (Figure 5.1) in the

Figure 5.1 Dynamic mechanical behavior of SWNT film processed from 6

molar nitric acid treatment.

measured temperature range (there is slight up turn above 150 ºC) and the Tan δ value is very low (~0.02), suggesting that these films are fairly elastic in this temperature range.

Chemical modification of carbon nanotube using acid treatment has been widely studied using FTIR.[11,12,13,14,27]. FTIR spectra of 6M nitric acid treated SWNT and 6M nitric acid treated SWNT after repeated KOH and distilled water washing are shown in Figure 5.2.
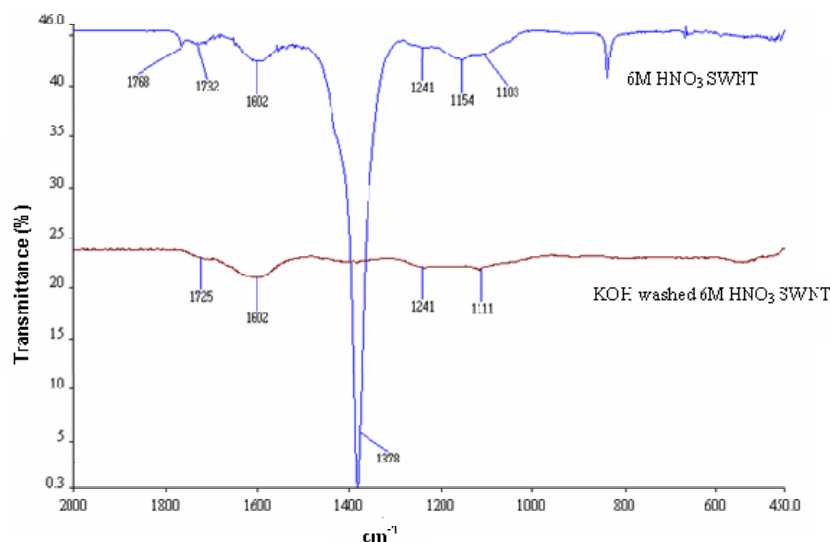
Figure 5.2 FTIR spectra of 6M HNO$_3$ treated SWNT with and without KOH wash.

The strong infra-red absorption at 1378 cm^{-1} on nitric acid treated nanotubes has generally been left unassigned in the literature[18,27,28] However, this peak was documented as arising from nitrate groups[29] in nitric acid oxidized carbon fiber[30]. After washing with KOH solution, this peak, as well as the peak around 833 cm^{-1} (OH out-of-plane torsion[29]) disappears, which confirms that the peak at 1378 cm^{-1} is due to intercalated nitric acid in SWNT bundles.[31] The peaks at 1725, 1241 and 1111 cm^{-1} in

KOH washed, HNO$_3$ treated SWNT sample suggests the possibility of functionalization of SWNT in addition to the presence of the degraded by-products not removed by the KOH wash. The disappearance of the peak at 1768 and 1154 cm^{-1} may be due to the hydrolysis of lactone, ester or anhydrate group.

Carbon nanotubes embedded in the continuous amorphous phase has previously been observed using high resolution TEM studies after nitric and sulfuric acid treatment[19]. Similar continuous morphological structure has also been reported in nitric acid treated nanotubes (SWNT or MWNT) and is attributed to the formation of amorphous carbon resulting from nanotube decomposition[32]. The scanning electron micrographs of the films processed in 3 molar acid show the presence of nanotube
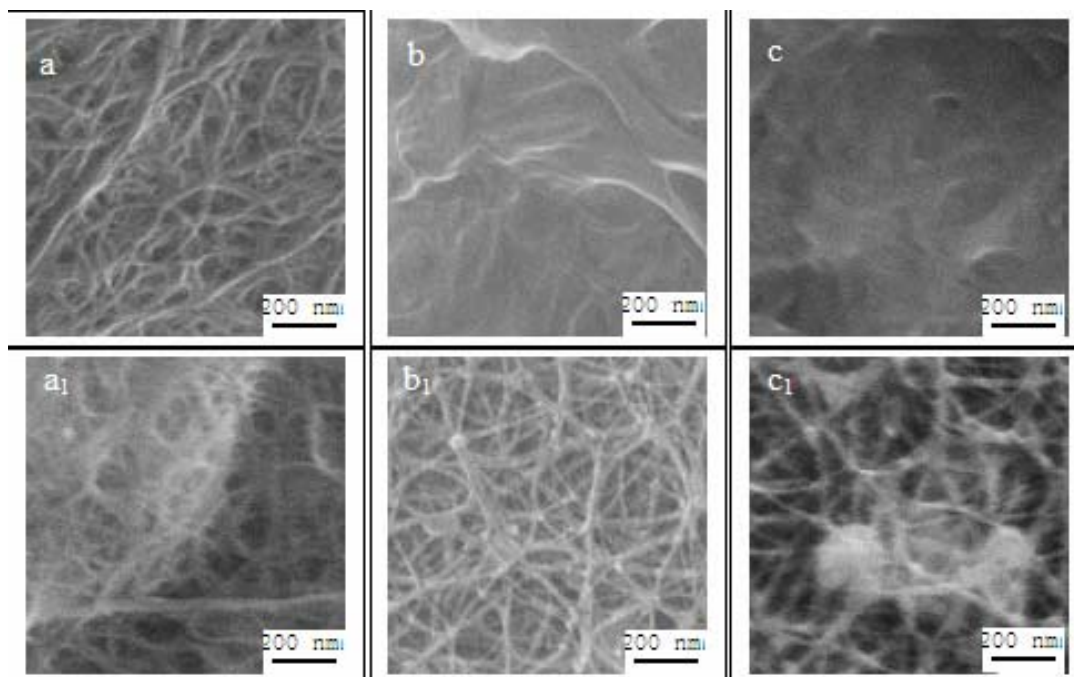

Figure 5.3 SEM images of films processed from (a) 3 M, (b) 6 M, and (c) 10 M nitric acid. The (a1), (b1), and (c1) photographs are for films heat-treated at 900°c in nitrogen

ropes. However the ropes are not seen on the film surface, when processed from 6 and 10 molar acid (Figure 5.3). On the other hand, the nanotube ropes can be clearly seen in films heat-treated at 900 ^{o}C. The embedded nanotube bundles can be observed, after the amorphous carbon has been stripped off during the 900 ºC heat-treatment process. These observations suggest that the nitric acid treated film has a composite structure, with the nanotube ropes embedded in the amorphous carbon matrix formed by the decomposition of the relatively smaller diameter SWNTs. The fracture morphology of the 6M film (Figure 5.4) shows the layered structure as well as the presence of the nanotube ropes. Layered structure was also observed in the SWNT films processed from oleum[6].
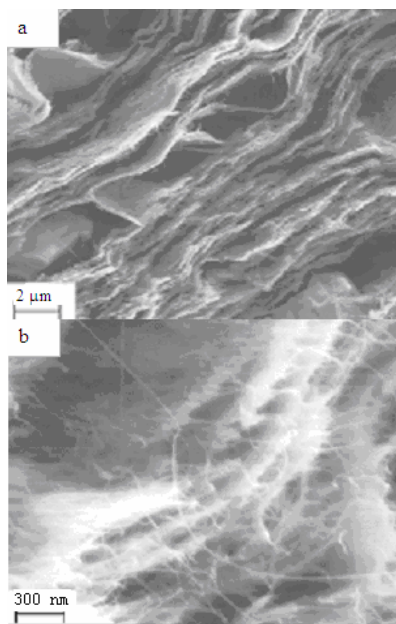

Figure 5.4 (a) low and (b) high magnification SEM images of the SWNT films processed from 6 M nitric acid treatment.

It has been reported that the most important parameter that determines the chemical oxidation attack of the nanotubes, is their diameter: Small diameter tubes, due to the stress induced by the curvature, are first attacked and destroyed. Some reactivity is also reported for the larger diameter metallic nanotubes.[33] Radial Raman breathing mode has been widely used for SWNT diameter determination. Raman spectra of various films processed from nitric acid for which properties are reported in Table 5.1 exhibit complete suppression of RBM (not shown). Therefore all the films were further heat-treated in a thermogravimetric analyzer at 20 ºC/minute to 900 ºC and held at 900 ºC for two minutes in nitrogen. Raman spectra for the 900 ºC heat-treated films in the range of 150 to 350 cm^{-1} are shown in Figure 5.5. This figure shows that in the control film, the dominant RBM is at about 267 cm^{-1}, while with increasing nitric acid concentration, the dominant RBM shifts to lower frequency, suggesting the survival of the larger diameter tubes.
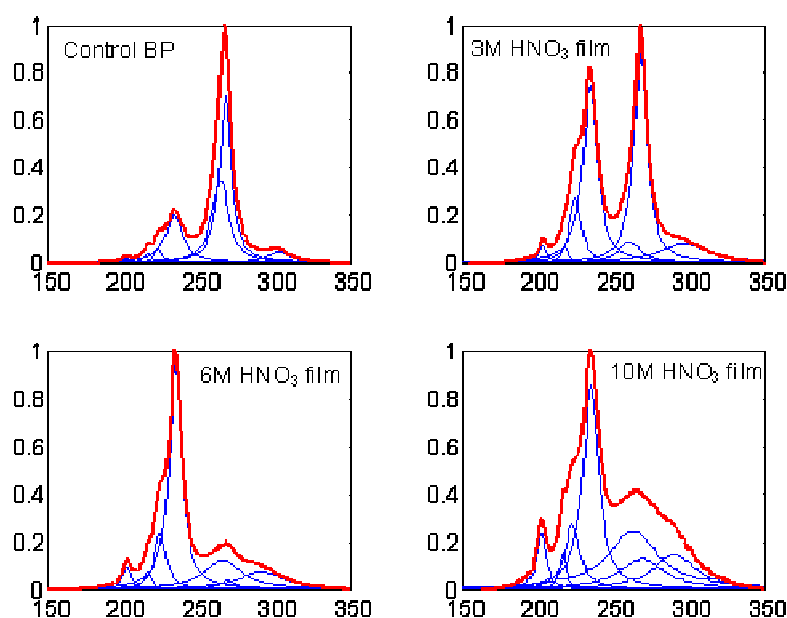

Figure 5.5 Radial breathing mode Raman band of HNO$_3$ films

To quantify the change in SWNT diameter distribution resulting from the oxidative treatment, spectra in Figure 5.5 have been resolved using Lorentz line shape peak fitting routine. Using 785 nm incident laser wavelength, six different diameters in the range of 0.88 – 1.19 nm were identified in these films. Metallic SWNTs are not observed using 785 nm laser, thus our analysis of the chemical reactivity of SWNTs with respect to the diameter is limited to the semi-conducting tubes.

It is noted that the RBM bands for HNO_3 films up-shift by $1 - 3$ cm^{-1} compared to the corresponding peaks in the control film (film processed without nitric acid). The diameters were calculated[34] based on the RBM band peak position of the control film using the empirical equation $\omega_{RBM} = 238/d^{0.93}$. For each sample, the relative fraction of the SWNT of a given diameter is determined by taking the ratio of the area of the corresponding peak to the sum of the area. As represented by the square symbols in Figure 5.6, one can see that the relative fractions of small diameter SWNTs (0.88 and 0.89 nm) significantly decreased with increasing nitric acid concentration. The percentage of these small diameter tubes decreased from 70% in the control film to less than 20% in 10 M samples, confirming the selective degradation of the small diameter SWNTs by HNO_3. As a result, the relative fraction of the large diameter SWNTs (1.19 and 1.11 nm) increased monotonically with nitric acid concentration.

The subtle chemical reactivity of SWNTs with respect to their diameter is further demonstrated by the relative population changes of 1.02 and 1.07 nm diameter SWNTs. Relative fraction of 1.07 nm diameter tubes leveled off from 6 M to 10 M HNO_3, however, the 1.02 nm diameter SWNTs fraction decreased when nitric acid

concentration increased from 6 M to 10 M. This suggests that the 1.07 nm diameter tubes have higher resistance to oxidative degradation than the 1.02 nm diameter tubes. Though the diameter difference between these two tubes is only 5%, there is a measurable difference between their oxidative resistances. In Figure 5.6, the circle symbol represents the relative fractions of SWNT with identified diameters in a 6 M HNO_3 film sample, which was subjected to more severe heat-treatment (900 ^{0}C for 30 minutes and 700 ^{0}C for 4.5 hrs in N_2). Excellent agreement in the relative populations of SWNTs at these two different heat-treatment levels, suggests no nanotube degradation under these heat-treatment conditions.
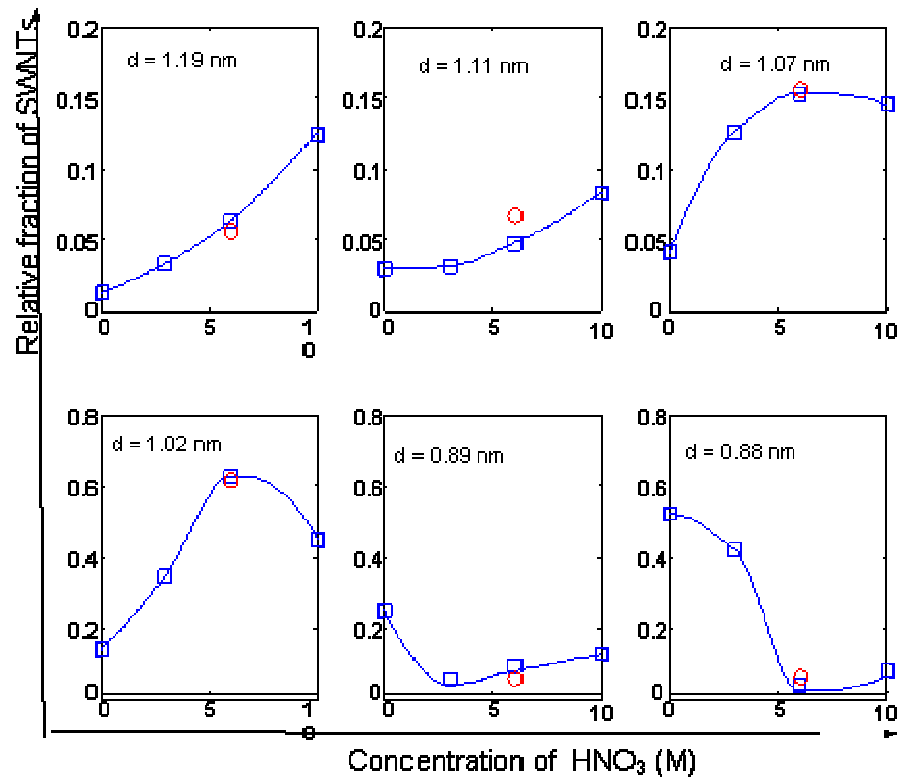

Figure 5.6 Relative fractional changes of different diameter SWNTs as a function of HNO_3 concentration.

To further understand the structural changes in SWNT under nitric acid oxidation, X-ray diffraction studies (Figure 5.7) have been carried out on the as-prepared and heat-treated films. Control film has diffraction peaks at 7.63 and 13.10 degree 2θ angles, two broad peaks at ~19 and 24 degrees and one at 43.5 degree. The first two peaks d-spacing values are 1.157 and 0.675 nm, which corresponds to (1, 0) and (1, 1) planes of the 2D hexagonal lattice of the ordered SWNT bundle[35, 36]. Taking 0.34 nm as the inter-tube distance in a SWNT bundle, the mean diameter of these HiPco SWNTs was estimated to be 0.987 nm. Extensive X-ray reports on different types of carbonaceous materials[37,38,39,40] lead to assignment of the 19 degree peak with d-space of 4.6 Å to the γ - band of carbon, which is due to partially ordered packing of aliphatic carbon structures. X-ray studies on various carbon materials suggest that the 24 degree peak is due to the (0, 0, 2) plane (d spacing 3.7 Å) of the turbostratic graphitic layer, arising from the oxidative degradation of SWNT. Each layer is considered as a polycyclic aromatic molecule, on the edge of which are the most of the functional groups identified by the infra-red spectroscopy. The strong peak at 43.5 degrees (d-spacing 0.0208 nm) is due to {1, 1, 0} reflection of the α - Fe body centered cubic lattice structure coming from the residual catalytic impurity. Diffraction from (1, 0) and (1, 1) peaks is depressed in nitric acid treated films (Figure 5.7a), while the amorphous peaks become more prominent. Upon heat treatment, SWNT (1, 0) and (1, 1) peaks show significant recovery in the 3 molar film. Less but noticeable recovery was observed in the 6 M and 10 M films (Figure 5.7b inset shows amplified intensity).
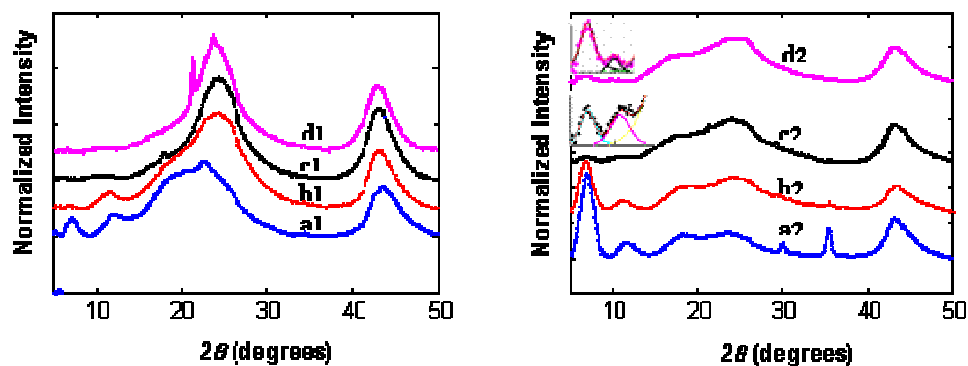
Figure 5.7 X-Ray diffraction of SWNT film heat-treated at 200 ºC (left) and 900 ºC (right). a1, a2: control film (0 molar HNO_3); b1, b2: 3M HNO_3 film; c1, c2: 6M HNO_3 film; d1, d2: 10M HNO_3 film.

The (1, 0) and (1, 1) d-spacing values increase with HNO_3 concentration (Figure 5.8). If we assume that the inter-tube distance is a constant at 3.4 Å, increase in d-spacing implies increased mean SWNT diameter. This result is consistent with the Raman scattering measurement, which shows smaller diameter SWNT tubes are much easier to be attacked by HNO_3. To rationalize the results obtained from X-ray diffraction, it is necessary to assume that individual tubes with relatively uniform diameter distribution form the ordered SWNT bundle. The SWNT bundle formed by small diameter individual tubes is much easier subjected to destruction by HNO_3. The intensity of the peak arising from oxidative degradation at 3.7 Å, increases with HNO_3 concentration. Also the different increasing rate of (1, 0) and (1, 1) d-spacing with increasing nitric acid concentration can be noticed, which may be due to the distortion of SWNTs 2-D hexagon lattice.
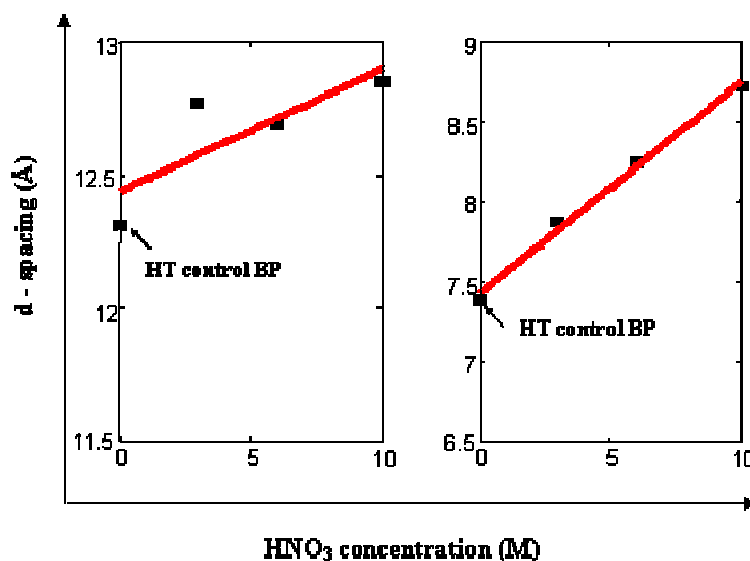
Figure 5.8 d-spacing of SWNT diffraction peaks in films processed from nitric acid. Diffraction plane (1, 0) (left) and (1, 1) (right).

FTIR, Raman, SEM and X-ray studies have already demonstrated that the nitric acid treatment creates functional groups, defects and polycyclic aromatic materials. TGA results show that the maximum residue is obtained in case of the control bucky paper (80%) and the residue is monotonously reduced with increase in nitric acid concentration. The more concentrated acid treatment, and the more damages on tube, more loss during TGA heating process.

In summary, the mechanical properties of SWNT film can be significantly improved by nitric acid oxidation. The tensile strength and modulus values as high as 74 MPa and 5 GPa, which is comparable to the values for engineering plastics, have been achieved, while the electrical conductivity of these films is in the order of 10^4 S/m, which is comparable to the electrical conductivity of the most electrically conducting polymer. These films also demonstrate stable mechanical performance in

a large temperature range (measured up to 200 °C), suggesting applications in areas requiring mechanical in such a temperature range. The results also suggest that the small diameter SWNTs are the first ones to be damaged by the nitric acid. Morphological examination of these films suggests the presence of SWNT ropes embedded in the polycyclic aromatic material formed from the degradation of the small diameter tubes and is consistent with observed changes in porosity[41].

REFERENCES

[1] Bae, D. J.; Kim, K. S.; Park, Y. S.; Suh, E. K.; An, K. H.; Moon, J.; Lim, S. C.; Park, S. H.; Jeong, Y. H.; Lee, Y. H. *Phys. Rev. B* **2001**, *64*, 233401.

[2] Knapp, W.; Schleussner, D. *J. Vac. Sci. Technol. B* **2003**, *21,* 557.

[3] Cooper, S. M.; Chuang, H. F.; Cinke, M.; Cruden, B. A.; Meyyappan, M. *Nano Lett.* **2003**, *3*, 189.

[4] Baughman, R.; Zakhidov, A. A.; de Heer, W. A. *Science,* **2002**, *297*, 787.

[5] Baughman, R.; Cui, C.; Zakhidov, A. A.; Iqbal, Z; Barisci, J. N.; Spinks, G. M.; Wallace, G. G.; Mazzoldi, A.; De R. D.; Rinzler, A. G.; Jaschinski, O.; Roth, S.; Kertesz, M., *Science* **1999**, *284*, 1340.

[6] Sreekumar, T. V.; Liu, T.; Kumar, S.; Ericson, L. M.; Hauge, R. H.; Smalley, R. E. *Chem. Mater.* **2003**, *15*, 175.

[7] Vigolo, B.; Poulin, P.; Lucas, M.; Launois, P.; Bernier, P. *Appl. Phys. Lett.* **2002**, *81*, 1210.

[8] Galvert, P. *Nature* **1999**, *399*, 210.

[9] Holzinger, M.; Steinmetz, J.; Samaille, D.; Glerup, M.; Paillet, M.; Bernier, P.; Ley, L.; Graupner, R. *Carbon*, **2004**, in press.

[10] Kis A.; Csanyi G.; Salvetat J. P.; Lee T. N.; Couteau E.; Kulik A. J.; Benoit W.; Brugger J.; Forro L. *Nature Mater.* **2004**, *3*, 153.

[11] Kuznetsova, A.; Mawhinney, D. B.; Naumenko, V.; Yates Jr., J. T.; Liu, J.; Smalley, R. E. *Chem. Phys. Lett.* **2000**, *321*, 292.

[12] Yu, R.; Chen, L.; Liu, Q.; Lin, J.; Tan, K.; Ng, S. C.; Chan, H.; Xu, G.; Andy Hor, S. T. *Chem. Mater.* **1998**, *10*, 718.

[13] Sun, Y.; Huang, W.; Lin,Y.; Fu, K.; Kitaygorodskiy,A.; Riddle, L. A.; Yu,Y. J.; Carroll, D. L. *Chem. Mater.* **2001**, *13*, 2864.

[14] Hamon, M. A.; Chen, J.; Hu, H.; Chen, Y.; Itkis, M. E.; Rao, A. M.; Eklund, P. C.; Haddon, R. C. *Adv. Mater.* **1999**, *11*, 824.

[15] Chen, J.; Rao, A. M.; Lyuksyutov, S.; Itkis, M. E.; Hamon, M. A.; Hu, H.; Cohn, R. W.; Eklund, P. C.; Colbert, D. T.; Smalley, R. E.; Haddon, R. C. *J. Phys. Chem. B* **2001**, *105*, 2525.

[16] Rinzler, A. G.; Liu, J.; Dai, H.; Nikolaev, P.; Huffman, C. B.; Rodriguez-Macias, F. J.; Boul, P. J.; Lu, A. H.; Heymann, D.; Colbert, D. T.; Lee, R. S.; Fischer, J. E.; Rao, A. M.; Eklund, P. C.; Smalley, R. E.; *Appl. Phys. A* **1998**, *67*, 29.

[17] Jia, Z.; Wang, Z.; Liang, J.; Wei, B.; Wu, D. *Carbon* **1999**, *37*, 903.

[18] Mawhinney, D. B.; Naumento, V.; Kuznetsova, A.; Yates, J. T. *J. Am. Chem. Soc.* **2000**, *122*, 2383.

[19] Y. Zhang , Z. Shi , Z. Gu , S. Iijima, *Carbon* **2000**, *38*, 2055.

[20] Zhang, M.; Yudasaka, M.; Iijima, S. *J. Phys. Chem. B* **2004,** *108,* 149.

[21] Hu, H.; Zhao, B.; Itkis, M. E.; Haddon, R. C.; *J. Phys. Chem. B*, **2003**, *107*, 13838.

[22] Chiang, L. W.; Brinson, B. E.; Smalley, R. E.; Margrave, J. L.; Hauge, R. H. *J. Phys. Chem. B* **2001**, *105*, 1157.

[23] Fischer, J. E.; Dai, H.; A. Thess, R. L.; Hanjani, N. M.; Dehaas, D. L.; Smalley, R. E. *Phys. Rev. B* **1997**, *55*, 4921.

[24] Bozhko, A. D.; Sklovsky, D. E.; Nalimova, V. A.; Rinzler, A.G.; Smalley, R. E.; Fischer, J. E. *Appl. Phys. A* **1998**, *67*, 75.

[25] Kim, G. T.; Choi, E. S.; Kim, D. C.; Suh, D. S.; Park, Y. W.;Liu, K.; Duesberg G.; Roth, S. *Phys. Rev. B* **1998**, *58*, 16064.

[26] Kaiser, A. B.; Dusberg, G.; Roth, S. *Phys. Rev. B* **1998**, *57*, 1418.

[27] Li, Y. H.; Xu, C.; Wei, B.; Zhang. X.; Zheng, M.; Wu, D.; Ajayan, P. M. *Chem. Mater*. **2002**, *14*, 483.

[28] Zhang, J.; Zou, H.; Qing, Q.; Yang, Y.; Li, Q.; Liu, Z.; Guo, X.; Du, Z. *J. Phys. Chem. B* **2003,** *107,* 3712.

[29] Ortega, I. K.; Escribano, R; Fernandez, D; Herrero, V. J.; Mate, B; Medialdea, A; Moreno, M. A. *Chem. Phys. Lett.* **2003**, *378*, 218.

[30] Zielke, U.; Huttinger, K. J.; Hoffman, W. P. *Carbon*, **1996**, *34*, 983.

[31] Bower, C.; Kleinhammes, A.; Wu, Y.; Zhou, O. *Chem. Phys. Lett*. **1998**, *288*, 481.

[32] Hu, H.; Zhao, B.; Itkis, M. E.; Haddon, R. C. *J. Phys. Chem. B*, **2003**, *107*, 13838.

[33] Menna, E.; Negra, F. D.; Fontana, M. D.; Meneghetti, M. *Phys. Rev. B,* **2003**, *68*, 193412.

[34] Rols, S.; Righi, A.; Alvarez, L.; Anglaret, E.; Almairac, R.; Journet, C.; Bernier, P.; Sauvajol, J. L.; Benito, A. M.; Maser, W. K.; Munoz, E.; Martinez, M. T.; de la Fuente, G. F.; Girard, A.; Ameline, J. C. *Euro. Phys. J. B,* **2000**, *18*, 201.

[35] Thess, A.; Lee, R.; Nikolaev, P.; Dai, H.; Petit, P.; Robert, J.; Xu, C.; Lee, Y. H.; Kim, S. G.; Rinzler, A. G.; Colber, D. T.; Scuseria, G. E.; Tomanck, D.; Fisher, J. E.; Smalley, R. E. *Science*, **1996**, *273*, 483.

[36] Journet, C.; Maser, W. K.; Bernier, P.; Loiseau, A.; Lamy de la Chapelle, M.; Lefrant, S.; Deniard, P.; Lee, R.; Fisher, J. E. *Nature*, **1997**, *388*, 756.

[37] Yen, T. F.; Erdman, J. G.; Pollack, S. S. *Anal. Chem.,* **1961**, *33*, 1587.

[38] Ruland, W. *Chemistry and Physics of Carbon*, Vol. 4, Ed. Walker, Philip L., MARCEL DEKKER, INC., New York, **1968**.

[39] Ergun, S. *Chemistry and Physics of Carbon*, Vol., 3, Ed. Walker, Philip L., MARCEL DEKKER, INC., New York, **1968.**

[40] Lu, L.; Sahajwalla, V.; Kong, C.; Harris, D. *Carbon*, **2001**, *39*, 1821.

[41] Hu, Y.; Ruckenstein, E. *Ind. Eng. Chem. Res*. **2004**, *43*, 708.

CONCLUSIONS and RECOMMENDATIONS

Conclusions

Single wall carbon nanotubes have good mechanical, electrical and thermal properties with large aspect ratio and they are light-weight, which makes them ideal candidate of filler material for polymers and other matrix materials. But due to van der Waals intertube bonding, dispersion and exfoliation large SWNT bundles into small size bundles or individual tubes is challenging. In order to circumvent this problem, surfactant is used to assist SWNT dispersion in the aqueous system. Sodium dodecyl sulfate (SDS) is a frequently used surfactant in SWNT dispersion system. Through the SAXD, FTIR and TEM studies, it has been shown that SDS crystals arrange themselves in an ordered manner on the surface of SWNTs. Surfactant-like polymer, PVA, can also help the homogeneous dispersion of SWNTs in aqueous and organic solvent systems.

Currently quantitative estimation of SWNT dispersion is not feasible except by using TEM or AFM techniques, which are quite time consuming. In this study, it has been shown that the state of the dispersion can be quantified based on the electrical percolation theory.

Poly (vinyl alcohol) (PVA) composite films containing well dispersed, poly (vinyl pyrrolidone) (PVP) and sodium dodecyl sulfate (SDS) covered single wall carbon nanotubes (SWNT) exhibit significant improvement in tensile strength and modulus as compared to the control PVA and PVA/PVP/SDS films. Tensile yield

strength increased from 83 and 50 to 148 MPa and Young's modulus increase from 1.9 and 2.5 to 4.0 GPa, respectively. The evidence of load transfer to the nanotubes in the composite film has been obtained from the shift in the Raman SWNT D* band peak position.

Single wall carbon nanotubes (SWNT), polyvinyl alcohol (PVA), dimethyl sulfoxide (DMSO) and H_2O homogeneous dispersion has been prepared using stirring and sonication. This dispersion was extruded into fiber via gel spinning. The mechanical performance of PVA / SWNT (3wt%) composite fiber was superior to that of the control PVA gel-spun fiber. The tensile strength of composite fiber increased by 22% compared to the control PVA gel-spun fiber from 0.9 GPa to 1.1 GPa. Also, the Young's modulus increased by 40% from 25.6 GPa to 35.8 GPa. Dynamic mechanical properties and X-ray diffraction studies suggest that the SWNT influenced the properties of both amorphous as well as crystalline regions of PVA in the composite fiber. The mechanical stretching induced SWNT orientation is thought to be one of the factors responsible for improving mechanical performance of PVA/SWNT composite fiber. The SWNT Hermans orientation factor is calculated to be 0.8 in gel-spun fibers.

The mechanical properties of SWNT film can be significantly improved by nitric acid oxidation. The tensile strength and modulus values as high as 74 MPa and 5 GPa, which are comparable to the values for engineering plastics, have been achieved. The electrical conductivity of these films is of the order of 10^4 S/m, which is comparable to the electrical conductivity of the most electrically conducting polymers. These films also demonstrate stable mechanical performance in the large

temperature range (measured up to 200 °C). The results also suggest that the small diameter SWNTs are the first one to be damaged by the nitric acid. Morphological examination of these films suggests the presence of SWNT ropes embedded in the polycyclic aromatic material formed from the degradation of the small diameter tubes.

Recommendations for future work

For reinforcing various matrices with SWNT, three requirements have to be satisfied: 1) dispersion and exfoliation of SWNT bundles; 2) load transfer from polymer to the nanotubes; and 3) SWNT orientation. In addition, the mechanism of PVA assisted SWNT dispersion should be studied. This will be helpful in identifying other polymers that can be used for achieving good SWNT dispersion. The processing parameters such as stirring time for high shear mixing, sonication power, sonication time need to be optimized for making good polymer/SWNT dispersion. The appropriately functionalized SWNT is perhaps the key to increase the interfacial bonding, and load transfer. So, the composites based on functionized SWNTs should be studied. The orientation of SWNT is important for the mechanical performance of final composite fiber. So, the efforts for further increasing the SWNT orientation in the fiber should continue.